ABSTRACT

Title of Dissertation: BIOCHEMICAL AND BIOLOGICAL CHARACTERIZATION OF THREE DNA REPAIR ENZYMES IN *DEINOCOCCUS RADIODURANS*

Zheng Cao, Doctor of Philosophy, 2009

Dissertation directed by: Professor Douglas A. Julin
Department of Chemistry and Biochemistry

The Gram positive bacterium *Deinococcus radiodurans* is able to withstand acute doses of gamma rays that can cause hundreds of double-strand breaks per genome. In proposed double-stand break repair pathways, however, some important enzymes, such as helicases and nucleases in the initiation step, have not been clearly identified yet. Interestingly, the common bacterial helicase/nuclease complex RecBCD or AddAB, which functions to produce a 3' ssDNA tail in double-strand break repair initiation step in other bacteria, is not found in *D. radiodurans*.

As part of efforts to identify helicases involved in double-strand break repair, the *D. radiodurans* HelIV (encoded by locus DR1572, the *helD* gene) was characterized with both *in vivo* and *in vitro* methods. The *helD* gene is predicted to encode a helicase superfamily I protein. The *helD* mutant is moderately sensitive to methyl methanesulfonate and hydrogen peroxide but it is not sensitive to gamma rays, UV and

mitomycin C. In biochemical assays, the full length HelIV exhibited DNA unwinding activity with a 5'-3' polarity whereas the truncated HelIV without N-terminal region had no detectable helicase activity.

RecJ is the exonuclease in the RecF pathway, which is suggested to function at the initiation step in DSB repair in the absence of RecBCD. In the *in vivo* study, the *D. radiodurans recJ* gene (encoded by locus DR1126) cannot be completely removed from the chromosome, indicating the essential role of RecJ in cell growth. The heterozygous mutant displayed growth defect and higher sensitivity to gamma rays, hydrogen peroxide and UV compared to wild type *D. radiodurans*, suggesting an important role in DNA repair. The RecJ expressed in *E. coli* system was insoluble but can be purified via denaturation-refolding, and the refolded RecJ showed 5'-3' exonuclease activity.

D. radiodurans has no RecB and RecC proteins, but it has a homologue of the RecD protein. We tested whether the *D. radiodurans* RecD protein could form a complex or make transient interactions with other proteins to perform more complicated functions. The RecD conjugated protein affinity column was used to attempt to identify cellular binding partners.

BIOCHEMICAL AND BIOLOGICAL CHARACTERIZATION OF THREE DNA REPAIR ENZYMES IN *DEINOCOCCUS RADIODURANS*

By

Zheng Cao

Dissertation submitted to the Faculty of the Graduate School of the
University of Maryland, College Park, in partial fulfillment
of the requirements for the degree of
Doctor of Philosophy
2009

Advisory Committee:
Professor Douglas Julin, Chair/Advisor
Professor Dorothy Beckett
Professor Jeffrey DeStefano
Professor Jason Kahn
Professor Steven Rokita

Acknowledgement

My four years of training as a Ph. D. graduate student in the Department of Chemistry and Biochemistry at University of Maryland is about to finish. I would like to express my gratitude, from the bottom of my heart, to everyone who helped me to complete the degree.

First of all, I would like to thank our department and the University of Maryland for giving me such a wonderful opportunity to study here. Great people and convenient facilities helped me get through all the hard time in my study and life. Second, I would like to thank all of my committee professors: Dr. Dorothy Beckett, Dr. Jason Kahn and Dr. Steven Rokita. They have given me a lot of valuable advice and guidance in the past four years. I also would like to thank Dr. Jeffrey DeStefano for accommodating my request and taking the time to serve as the dean's representative for my defense. Most importantly, I would like to thank Dr. Douglas Julin, my advisor, for teaching me not only knowledge but also the wisdom and attitude toward science and life, from which I will benefit a lot in the rest of my life.

In addition, I would like to thank my two labmates: Will Shadrick and Charlie Mueller. Their selfless and brotherhood-like help made my stay in Dr. Julin's lab enjoyable and memorable.

Last but not least, I would like to thank my wife and my family, especially my grandparents. Without their support, I would not be able to reach this far in my study.

Table of Contents

List of Tables

List of Figures

List of Abbreviations

ATP	Adenosine triphosphate
BER	Base excision repair
BLAST	Basic local alignment search tool
BSA	Bovine serum albumin
Cam	Chloramphenicol
DMSO	Dimethyl sulfoxide
DIG	Digoxygenin
dNTP	Deoxyribonucleic acid triphosphate
DSB	Double-strand break
dsDNA	Double-stranded DNA
DTT	Dithiothreitol
EDTA	Ethylenediaminetetracetic acid
ESDSA	Extended synthesis dependent strand annealing
GST	Glutathione-S-transferase
HelIV	Helicase IV
HR	Homologous recombination
IPTG	Isopropyl-β-D-thiogalactopyranoside
IR	Ionizing radiation
LB	Luria-Bertani
MMC	Mitomycin C

MMS	Methyl methanesulfonate
NER	Nucleotide excision repair
NHEJ	Non-homologous end joining
PAGE	Polyacrylamide gel electrophoresis
PCR	Polymerase chain reaction
PAGE	Polyacrylamide gel electrophoresis
Pi	Phosphate
PMSF	Phenyl methyl sulfonyl fluoride
PVDF	Polyvinylidene fluoride
RNAP	RNA polymerase
ROS	Reactive oxygen species
RT-PCR	Real-time polymerase chain reaction
SDS	Sodium dodecyl sulfate
SSA	Single stranded annealing
SSB	Single-stranded DNA binding protein
ssDNA	Single-stranded DNA
str	Streptomycin
SUMO	Small ubiquitin-like modifier
TLC	Thin layer chromatography
TCR	Transcription coupled repair
UV	Ultraviolet

CHAPTER 1 INTRODUCTION

The Gram-positive bacterium *Deinococcus radiodurans* was first isolated in 1956 from canned ground meat that had been irradiated by 4 kGy of gamma rays, which is roughly 250 times higher than the dose required to kill *Escherichia coli* (1,2). *D. radiodurans* was found later worldwild from locations with rich nutrients such as soil, animal feces and processed meat, as well as from nutrient-poor places including room dusts and irradiated medical instrument (3). This organism belongs to a family of bacteria called *Deinococcaceae* that were isolated from diverse environments after exposure to high doses of ionizing radiation, such as Sahara desert, hot springs, Antarctica and even intestine of *Cyprinus carpio* (European carp) (4). The cells of *D. radiodurans* are pink-orange pigmented and nonmotile. It is an aerobe and grows optimally at 30°C in rich medium (2). The fact that *D. radiodurans* is naturally competent makes it somewhat easier for genetic manipulation, such as gene inactivation via transforming recombinogenic antibiotic-resistant linear DNA (2).

D. radiodurans is extraordinarily resistant to radiation, oxidative chemicals, desiccation and DNA damaging agents which can cause damage to other cellular components as well (5,6). In particular, this organism can withstand high doses of ionizing radiation (IR) and long periods of desiccation, both of which can lead to double-strand breaks (DSBs) and oxidative damage to DNA (7). For example, *D. radiodurans* can survive an acute IR dose as high as 5 kGy which introduces over a hundred DNA DSBs per genome equivalent, without loss of viability (D_{37} dose is 6 kGy) (2,8). In contrast, many other bacteria including *E. coli* can be killed with as few as two

or three DSBs occurring from radiation (D_{37} is only 30 Gy) (8,9). For most vertebrates including human, a whole-body of exposure of 10 Gy IR is lethal (10).

D. radiodurans uses RecA catalyzed homologous recombination to reconstruct chromosomes shattered by ionizing radiation, as evidenced by extreme radiation sensitivity exhibited by the *recA* mutant (11,12). The proper substrate for RecA recognition and binding contains a stretch of 3'single-strand DNA, which is usually produced by a heterotrimeric enzyme called RecBCD in gram negative bacteria (9,13) or by a heterodimeric enzyme AddAB with similar function in gram positive bacteria (14,15).

The whole genome sequence of *D. radiodurans* released in 1999 seems to be unremarkable, as many of the DNA-repair proteins encoded by this organism are common to other bacteria (3,16). This suggests that *D. radiodurans* uses many of the same DNA repair pathways previously characterized in other bacteria. However, the genes for the enzyme complex RecBCD or AddAB are not detected in *D. radiodurans* genome, except for a homolog of the RecD subunit of RecBCD. The *D. radiodurans* RecD protein was proven to be a DNA-repair related helicase but it is not sufficient to replace RecBCD or AddAB functionally in the recombination repair pathway (17). The enzymes, especially helicases and nucleases, involved in end-processing of RecA substrate remain unclear. The main goals for this study are to characterize two DNA-repair related enzymes (helicase IV and RecJ) and to identify working partners of RecD in *D. radiodurans*.

1.1 Sources of Cellular DNA DSBs

Although different repair mechanisms have evolved according to the organisms, DSBs are a potentially lethal form of DNA damage which can result in significant loss of genetic information and block DNA replication if left unrepaired (2). Cellular DSBs can be generated directly or indirectly, by a wide variety of endogenous and exogenous agents.

1.1.1 Artificially Induced DSBs

Cellular DSBs can be introduced artificially by various agents including ionizing radiation (IR), UV light (UVC), oxygen radicals and other DNA damaging agents (e.g., alkylating agents), either in direct or indirect pathways (18).

IR, which is radiation with sufficient energy to ionize molecules, can be divided into two groups: electromagnetic (X- and γ- radiation) and particulate (α- and β- particles). α- and β- particles produce ionization by collision and deposit their energy within a short range after entering matter. X- and γ- rays, generating ions by several types of energy-absorption events, are highly penetrating and can cause damage to all cellular components including a variety of DNA lesions (e.g., DSBs). Gamma rays can be produced by the decay of radioactive ^{60}Co and is widely used to artificially induce DSBs in cells (2,10,19).

As a consequence of IR treatment, DSBs can be induced directly by attacking the sugar and phosphate backbone which will subsequently lead to a single-strand break (19). The single-strand breaks caused by direct interaction with IR are randomly distributed throughout the genome and any two single-strand breaks located closely on

opposite strands may give rise to a DSB (2) (figure 1.1 A). Alternatively, DSBs are introduced indirectly by the radiolysis products of water (e.g., reactive oxygen species). Among the IR-induced reactive oxygen species (ROS), hydroxyl radical ($HO^{\bullet}$) is most reactive and can react indiscriminately with organic and biological molecules, oxidizing DNA, RNA, lipids and proteins (10). When hydroxyl radicals react with DNA sugars in the backbone, single-strand breaks may happen. About 20% of the hydroxyl radicals that react with DNA attack the sugars (20). If clusters of hydroxyl radical induced single-strand breaks are located on opposite strands in close proximity, DSBs can also be generated. Because of the predominance of water in biological systems, water radiolysis based ROS are the major sources in IR treatment to induce DSBs (20).

In addition to attacks of DNA backbone, a wide variety of base damage can be introduced by IR, directly or indirectly. When cells attempt to enzymatically remove the damaged bases via, for example, the base excision repair pathway, single-strand breaks can be produced if the resulting nicks are not sealed (2). Closely spaced single-strand breaks on opposite strands may lead to DSBs during the biological base repair process. UVC or DNA alkylating agents may indirectly cause cellular DSBs in the similar way, by introducing base modifications in close proximity on opposite strands followed by enzymatic base or nucleotide excision (21).

1.1.2 DSBs Occurring in DNA Replication

DSBs may be formed by DNA replication due to imperfect DNA templates. As shown in figure 1.1 B, if there is a nick or gap in front of the replication fork, a DSB can be produced. When the replisome encounters the nick on the template, the continuity of

replication progression is disrupted and the replication fork collapses, producing one intact parental DNA and one partially-replicated daughter DNA with broken ends (22,23). Alternatively, unrepaired DNA damage or some physical blocks (e.g., DNA binding proteins) may stop the progression of the replisome (24,25), if they are located in front of the replication fork (figure 1.1 C). The stalled fork can undergo fork reversal to form a four-way Holliday like junction (also called chicken foot Holliday junction) (19), either by the supercoiling-promoted (25) or the RecG-catalyzed regression (26,27). The resulting Holliday junction DNA can be cleaved by RuvABC enzymes to generate a DSB (18). The replication fork can be reconstructed between the parent template and the partially-replicated daughter DNA via recombination-dependent replication, to complete the replication cycle (9).

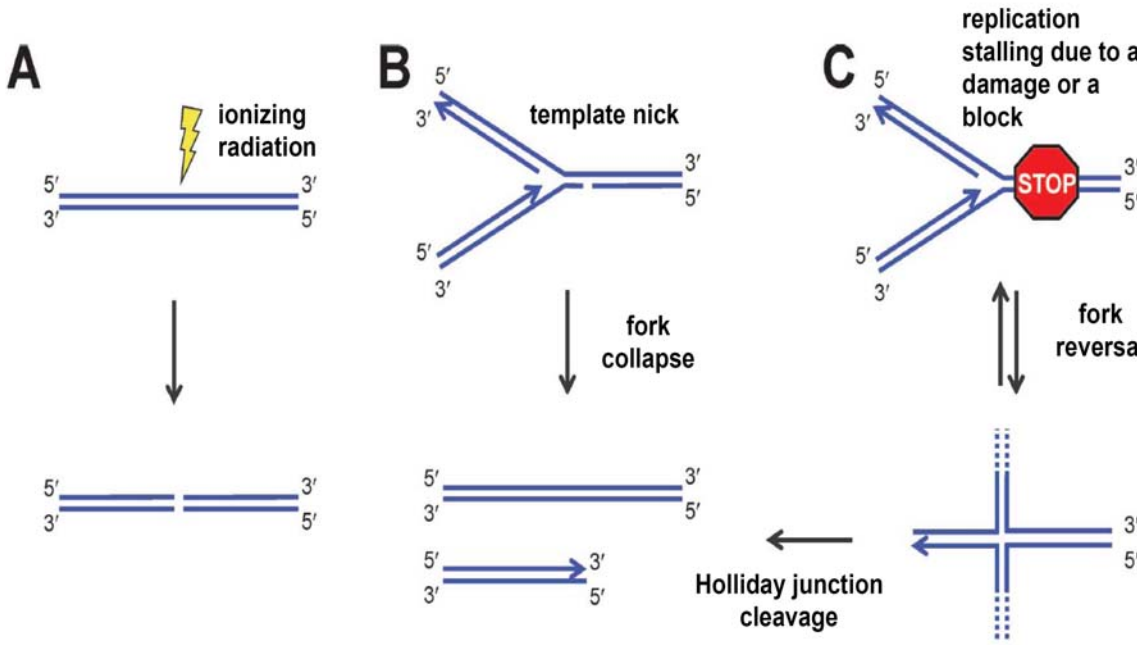

Figure 1.1 Direct and indirect sources of DSBs. (A) A DSB can be formed directly by, for example, ionizing radiation. This results in the production of two free DNA ends. (B) If a replication fork encounters a nick in the template strand, an arm will detach to generate a single DSB. This is commonly referred to as replication fork collapse. (C) Following replication fork arrest due to a DNA damage or a block in the template strands, the chicken foot structure is formed and resolved, which can lead to a DSB. Figure is adapted from Dillingham and Kowalczykowski, 2008 (18).

1.1.3 Spontaneous Cellular DSBs

DSBs can also be introduced by endogenous base damage via the same pathways discussed in the previous section. For example, ROS are constantly generated as by-products of aerobic metabolism and the subsequent various base damage may be caused by endogenous ROS (19), leading to spontaneous DSBs.

Spontaneous cellular DSBs are also present as transient intermediates in many biological processes found in both prokaryotes and eukaryotes. For example, during the process of conjugative recombination, in *E. coli* host cells, a single-stranded donor DNA is replicated and becomes a linear duplex DNA with two free dsDNA ends which then can be recognized and processed by RecBCD (18,28).

In eukaryotic cells, for example, DSBs may arise by topoisomerase (Topo) induced DNA strand breaks during the cell cycle. Topoisomerases are the essential enzymes cells used to change the superhelical state of DNA in replication, recombination, and transcription. Topo II generates a reversible DSB, which is a necessary step in both mitosis and meiosis for sister chromatid separation (29). Another example of eukaryotic spontaneous cellular DSB comes from the V(D)J recombination process. The V(D)J recombination is a genetic mechanism applied in vertebrates to generate a diverse repertoire of T cell receptors and immunoglobulins. The process involves random selection and reassembly of V, D and J genes through a programmed DNA rearrangement. This V(D)J recombination is initiated by a DSB that is introduced by a nuclease complex Rag1/Rag2 and re-ligated by non homologous end joining repair pathway (30).

1.2 Possible DSB Repair Pathways in *D. radiodurans*

D. radiodurans can survive gamma irradiation doses that introduce hundreds of DSBs in the genomic DNA and the reassembly of intact chromosomes from shattered fragments only takes a few hours (4,12). Several mechanisms have been proposed for the efficient DSB repair and genome reconstruction. The mechanisms as well as potential participating proteins in *D. radiodurans* will be discussed below.

1.2.1 Homologous Recombination DSB Repair in *E. coli*

Homologous recombination (HR) is the major DSB repair pathway in bacteria (31) and in yeast *Saccharomyces cerevisiae* (32). It involves genetic exchanges between two DNA molecules that share an extended region of homologous sequence (19). The sequence of DNA with DSB or other damage is corrected and restored from the intact homologous template DNA.

In *E. coli*, the RecBCD catalyzed HR repair pathway is responsible for over 90% of DSB repair in wild type cells (33). The heterotrimeric RecBCD enzyme (exonuclease V) has multiple enzymatic activities, including ssDNA exonuclease, ssDNA and dsDNA endonuclease, DNA-dependent ATPase and DNA helicase activities (33). To initiate the HR repair pathway, RecBCD binds to the blunt end of DNA and unwinds it using its helicase activity. At the same time, RecBCD uses its 3'-5' exonuclease activity to preferentially degrade the strand which is 3' terminal at the entry point (9). When the trimeric complex encounters the recombination hotspot χ, a significant change of its biochemical activities occurs. The 3'-5' nuclease activity is attenuated and a weaker 5'-3' nuclease is activated, while its helicase activity remains unchanged. The consequence of

these biochemical changes is the generation of 3' single-stranded DNA tail with a χ site at its 3' terminus (figure 1.2), which is an optimal substrate for binding by RecA (34-36). The octameric χ sequence 5'-GCTGGTGG-3' is only recognized within dsDNA by the translocating RecBCD (37).

Following interaction with the χ site, RecBCD directs the loading of RecA to the resulting processed 3' ssDNA tail, to exclude the binding of potential competitive single strand binding protein (SSB) to the same substrate (38).The formation of a functional RecA-ssDNA filament is also called presynapsis (19). The presynaptic RecA-ssDNA filament can search for and invade homologous dsDNA, which is termed synapsis (9). Once the Holliday junction is established, in the postsynapsis step, branch migration can occur, with the help of a specialized RuvAB motor protein complex (figure 1.2). The RuvAB complex functions as a DNA helicase that extends the region of DNA heteroduplex (39,40). The Holliday junction is resolved by a specific endonuclease RuvC protein, generating either spliced or patched products (40).

In *E. coli* cells where RecBCD is inactivated, an alternative RecF repair pathway can efficiently deal with DSB repair via recombination at nearly wild type levels if the SbcB (exonuclease I) and SbcC (or SbcD) nuclease are rendered non-functional at the same time (13,41,42). The RecF pathway in general predominantly functions in single-stranded gap repair in wild type *E. coli* cells (9,41). In DSB repair, at least five proteins from RecF pathways are involved in 3' terminus processing and subsequent RecA loading, including RecQ, RecJ, RecF, RecO and RecR. The helicase RecQ combining with the 5'-3' exonuclease RecJ work on free dsDNA ends to produce a 3' terminal ssDNA tail which is

a suitable substrate for RecA binding (figure 1.2) (9). In contrast to the direct loading of RecA on ssDNA in the RecBCD pathway, in the RecF pathway SSB assembles on the ssDNA tail first and RecFOR-facilitated displacement by RecA occurs (43). Recently, a part of RecF pathway that recapitulates the early steps in DSB repair has been reconstituted *in vitro* (44). This reconstituted system, containing all the five RecF pathways proteins, RecA and SSB, showed that RecO and RecR are responsible for displacing SSB and they act with RecF to load RecA and form the RecA nucleoprotein filament (44). The subsequent steps of RecA mediated strand invasion, Holliday junction formation and resolution in RecF pathway are the same as in the RecBCD pathway (9) (figure 1.2).

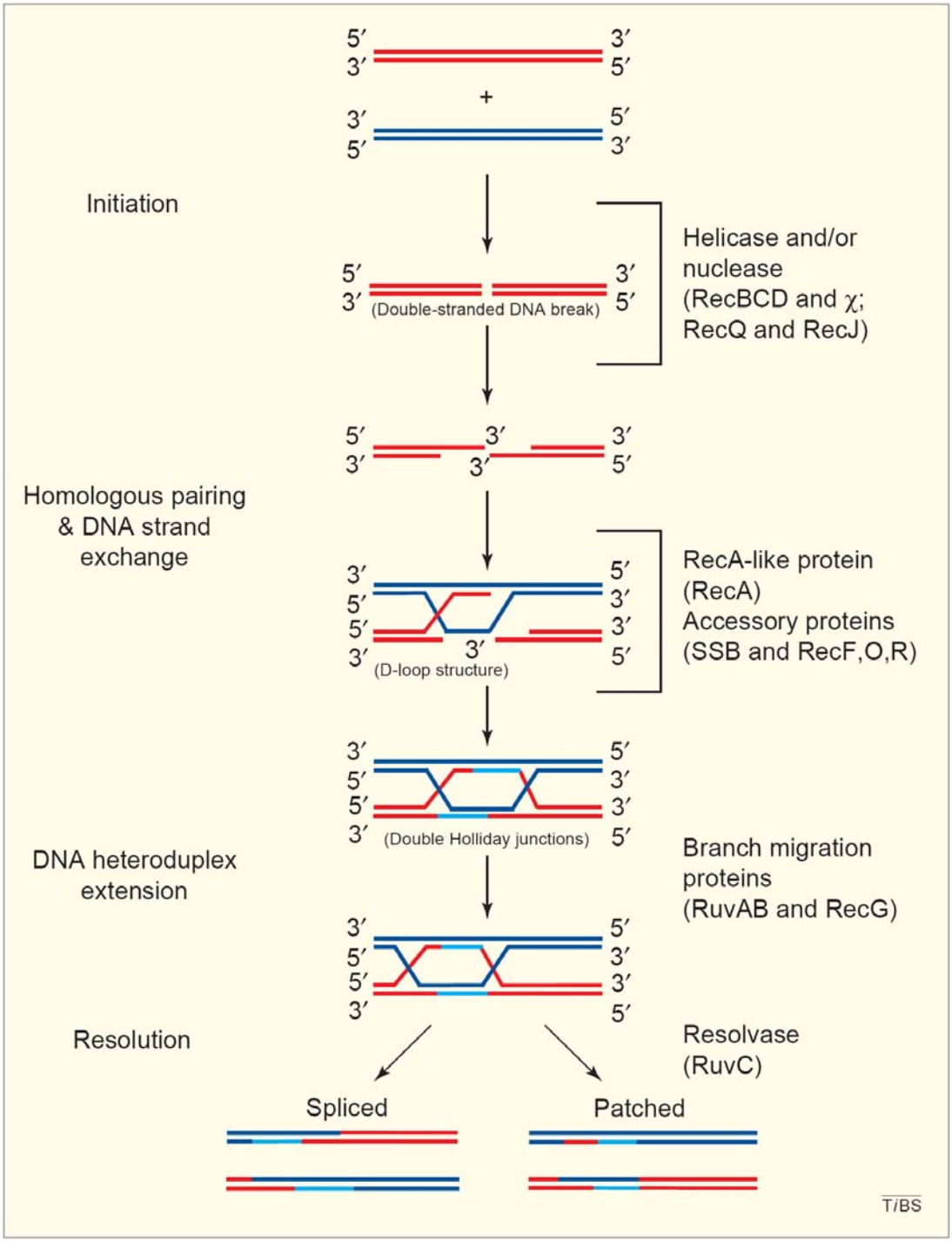

Figure 1.2 General model for DSB repair via RecBCD or RecF mediated pathways of homologous recombination. Figure is adapted from Kowalczykowski, 2000 (9).

1.2.2 Potential Homologous Recombination Pathways in *D. radiodurans*

D. radiodurans only encodes a RecD (DR1902) subunit homolog and has no genes that code for RecB or RecC homologs (3). RecD protein present in cells without RecBC is not only found in *D. radiodurans*, but also in mollicutes, firmicutes and *Streptomyces* (45). The *D. radiodurans* RecD is expressed as an active helicase with a 5'-3' polarity and relatively low processivity *in vitro* (17). A *recD* deletion mutant is more sensitive to gamma irradiation, UV irradiation and hydrogen peroxide compared to the wild type strain. It is as resistant as wild type to methyl methanesulfonate (MMS) and mitomycin C (MMC) (46). The exact biological function of RecD is still not clear and further work is required to assign RecD to a specific DNA repair pathway.

RecA protein encoded by *D. radiodurans* is 57% identical to the *E. coli* RecA (2) in amino acid sequence. Purified *D. radiodurans* RecA displayed all the predicted recombinogenic activities *in vitro*: it forms filaments on DNA, hydrolyzes ATP in a DNA-dependent manner and promotes DNA strand exchange (47). The RecA filament formation is different from the conventional RecA binding order: *D. radiodurans* RecA binds to the duplex DNA first and the homologous ssDNA substrate second, which is believed to promote an inverse DNA strand exchange pathway (48). A similar inverse strand exchange reaction is also found in *E. coli*, in which it is suggested to promote RNA-DNA hybrid generation (also called R-loop) (49). The *D. radiodurans recA* mutant has significant lower radioresistance compared to wild type, indicating an important role for RecA in homologous recombination based DSB repair (50,51).

Although *D. radiodurans* lacks RecBCD enzyme complex, it encodes all of the RecF pathway components including RecQ (DR1289), RecJ (DR1126), RecF (DR1089), RecO (DR0819) and RecR (DR1098) (3). Thus, the RecF pathway presumably could be the DSB repair means via recombination in *D. radiodurans*. The RecF pathway in *E. coli* is inhibited by SbcB (a 3'-5' exonuclease encoded by *sbcB* gene) (13). SbcB is naturally absent in *D. radiodurans* (3), and the expression of *E. coli* SbcB in *D. radiodurans* renders the cells much more sensitive to IR than wild type (52).

D. radiodurans RecQ helicase is expressed in an active form *in vitro* with a dsDNA uwinding polarity of 3'-5'. It contains three Helicase and RNase D C-terminal (HRDC) domains which have been proven to be involved in regulation of its affinity and specificity to substrates (53). *In vivo* survival assays showed that the helicase including all the three regulatory HRDC domains were necessary for its functions, as any of their deletion mutants was hypersensitive to gamma irradiation, UV, hydrogen peroxide and MMC (54). These *in vivo* results indicated that the RecQ could be a key player in the RecF pathway for DSB repair.

RecO, together with RecF and RecR form a complex and facilitate the displacement of SSB by RecA on ssDNA tails. *In vitro* assays with *D. radiodurans* RecO protein showed that it supported DNA annealing and RecA-mediated recombination reactions (55). Mutant cells devoid of *recO* exhibited a growth defect and extreme sensitivity to gamma or UV irradiation (56). The crystal structures of RecR and RecF showed that RecR forms a ring-shaped tetramer (57) and RecF forms a dimer which functions as a clamp-loader for the terameric RecR ring-structure (58).

The homologous proteins involved in postsynaptic branch migration and Holliday junction cleavage are present in *D. radiodurans*, including RuvA (DR1274), RuvB (DR0576) and RuvC (0440) (3). A *ruvB* mutant exhibited moderate sensitivity to gamma irradiation, UV and interstrand crosslink reagents (59).

In addition, the unique inverse strand exchange property of *D. radiodurans* RecA can be well accommodated in the RecF pathway. In *E. coli*, SSB binds to the 3' ssDNA tail first and is then replaced by RecA with the help of RecFOR. Similarly, in *D. radiodurans*, SSB recognizes the ssDNA tail whereas RecA binds to the homologous dsDNA region initially. With the help of RecFOR, RecA can dissociate from dsDNA and replace SSB on ssDNA tail to form the RecA filament.

1.2.3 Extended Synthesis-Dependent Strand Annealing Repair Pathway

In addition to homologous recombination, another DSB repair mechanism called single strand annealing (SSA) has been proposed by Daly and Minton (51). They suggest that the early stage of DNA repair (within the first 1.5 hour) after ionizing irradiation is RecA-independent, as both wild type and *recA* cells showed similar increases in the average sizes of chromosome fragments. During this time, the SSA pathway is responsible for annealing the homologous ssDNA overhangs of partially overlapping dsDNA fragments, to enlarge the dsDNA fragment size (figure 1.3). So the SSA pathway is considered to be a preparatory step for further DSB repair in *D. radiodurans* (51).

Recently, a modified version of the SSA pathway, called extended synthesis-dependent strand annealing (ESDSA) (12,60), has been proven to work on the hundreds of DNA DSBs after IR in *D. radiodurans*. The ESDSA mechanism is a

two-stage DSB repair pathway and is highly dependent on two groups of proteins: RecA and its homolog RadA; DNA polymerases I and III (encoded by *polA* and *dnaE* genes) (60). The *radA* deletion in *D. radiodurans* confers moderate sensitivity to IR (61). In *E. coli*, Pol I primarily functions to fill DNA gaps that arise during replication, excision repair and recombination, whereas Pol III holoenzyme is the essential complex that replicates chromosomal DNA (19).

The ESDSA model requires at least two chromosomal copies that are broken at different positions by IR. As shown in figure 1.3, after gamma irradiation (7 kGy), the first stage repair involves extensive DNA synthesis triggered by DNA fragmentation. An IR-generated short DNA fragment is end-recessed and its ssDNA tail invades the homologous duplex region of another partially overlapping fragment. In this step, the strand invasion is mediated by RecA and RadA (60). The invading ssDNA tail subsequently primes a single-round of PCR-like DNA synthesis. Pol III is essential for the initiation of the DNA synthesis. The elongation requires Pol III with Pol I filling gaps arising from excision repair of damaged bases or Pol I alone (60). Inactivation of both polymerases leads to degradation of DNA fragments and rapid cell death (60).

Genearally, the larger number of DSB fragments, the higher precision required for avoiding their assembly and the longer homology required. It is estimated that the newly synthesized overhangs are about 20 to 30 kb long, which is a comparable size to the DNA fragments generated immediately after IR. The new tail is much longer than the longest *D. radiodurans* repetitive sequences (about 1 kb), which can greatly contribute to ssDNA annealing specificity and the sequence accuracy during the repair process (12). It is also

proposed some repeat-binding protein may also prevent sequence repeats from becoming single-stranded or from annealing (12). The hundreds of DNA fragments with their 20-30 kb synthesized tail then undergo a single strand annealing step, based on the extraordinarily long complementary region, to form even longer double strand intermediates (figure 1.3).

In the second stage, the long linear intermediates can reassemble into a circular chromosome, via the RecA-dependent recombination (figure 1.3). Although it accomplished substantial DNA synthesis, a *recA* mutant did not reconstruct complete chromosomes after 24 hours, as shown by pulse field gel electrophoresis (PFGE). It only took 4.5 hours to completely reassemble chromosomes for wild type cells after the same dose of irradiation. This result indicates the key role of RecA protein in the late stage process of chromosome circularization (12).

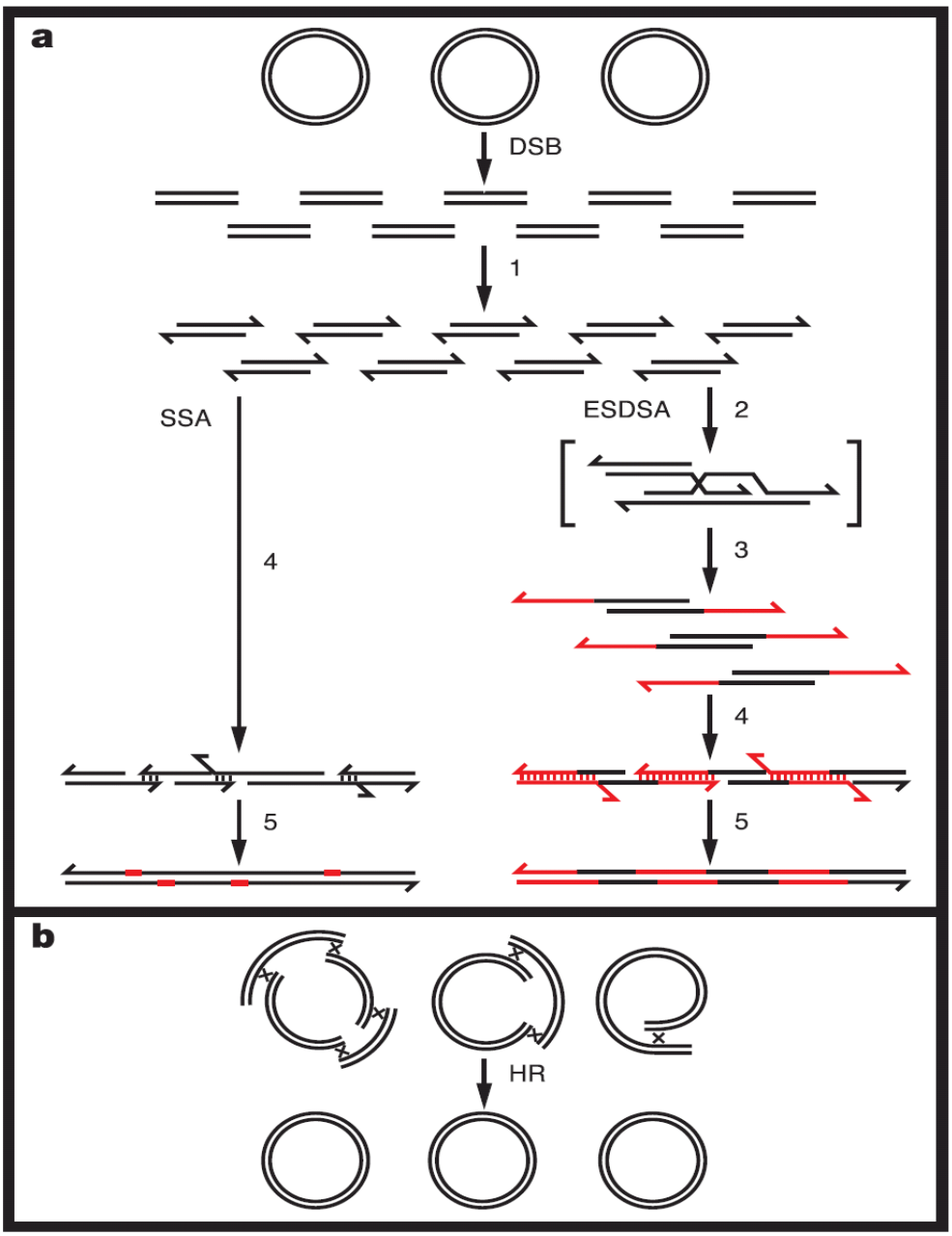

Figure 1.3 Schematic SSA and ESDSA DSB repair models in *D. radiodurans*. a: stage one. Random IR-induced DSBs produce numerous fragments. After 5'-3' end recession (step1), DNA fragments can rejoin directly via single-stranded annealing (SSA pathway) through complementary overlapping overhangs. The gaps are repaired by synthesis and strand excess is digested by nucleases (step 5). In the ESDSA pathway, the end-recessed fragments (step1) prime synthesis using the homologous regions of partially overlapping fragments as a template (step 2). The strand extension can run to the end of the template, producing fragments with long, newly synthesized (red) single-stranded overhangs (step 3).Step 4 and step 5 are the same in SSA and ESDSA. b: stage two. Crossovers (X) happen by means of RecA-dependent homologous recombination (HR). Figure is adapted from Zahradka et al., 2006 (12).

However, some aspects of ESDSA repair model still remain unclear. For example, in the first RecA-independent stage, the ssDNA tail needs to be properly processed to generate 3' ssDNA tail for subsequent strand invasion and DNA synthesis priming. This must be done by a combination of helicase and nuclease activities that are not identified yet, although the RecF pathway components RecQ and RecJ (5'-3' exonuclease) are possible candidates.

1.2.4 Non Homologous End Joining Repair Pathway

Another DSB repair pathway proposed in *D. radiodurans* is a non homologous end joining (NHEJ) pathway, which does not require a second copy of chromosome and relies on minimal base-pairing at the ligation junction (62,63). In eukaryotic cells, NHEJ is the major DSB repair pathway and is critical for genome stability. Until recently, it was widely accepted that the NHEJ mechanism was absent in prokaryotes and archaea (64). However, a functionally homologous NHEJ repair system has now been identified and characterized in mycobacteria, such as *Mycobacterium tuberculosis*, and other genera (65,66).

In eukaryotic NHEJ, the DNA broken ends are first recognized by the Ku 70/80 heterodimer. The functions of the Ku dimer include binding DNA ends, aligning the ends, recruiting and stimulating the ligase IV/XRCC4 complex. The enzymes involved in end-processing (by nuclease, e.g. human Artemis and yeast Mre11) and gap filling (by polymerase, e.g. human Pol μ, λ and yeast Pol4) are also recruited to the repair machinery at the damage site. The nuclease is used to produce short stretches of homologous sequence (also called micro-homologies), in order to facilitate alignment of broken

termini. The stimulated ligase IV/XRCC4 complex can join the two broken ends in the last step to complete the repair process (63,64). By contrast, the NHEJ repair pathway in bacteria is dependent on two key proteins: the multifunctional DNA ligase LigD and the DNA-end binding protein Ku (66) (figure 1.4). Bacterial Ku is usually encoded by a single gene and is further confirmed to form a homodimer in biochemical studies (65). The bacterial ligase LigD possesses three functional domains: the core ligase, the polymerase and the nuclease domains (67,68). The LigD polymerase domain belongs to the Pol X family which includes enzymes (e.g., human Pol μ, λ and yeast Pol4) implicated in the gap-filling reaction of the eukaryotic NHEJ pathway (69).

Although a homologous Ku protein is absent in *D. radiodurans*, the PprA protein is proposed to act as DNA end binding protein in the potential NHEJ pathway (62). The *pprA* gene is one of the five most highly induced genes in response to IR and desiccation (70). The *pprA* mutant is much more sensitive to IR compared to wild type cells (62). *In vitro* biochemical assays showed that the purified PprA protein preferentially bound to dsDNA carrying strand breaks. It also stimulated the DNA end-joining reactions catalyzed by ATP-dependent (T4 ligase) and NAD-dependent ligases (*E. coli* ligase) *in vitro* (62).

In the bacterial NHEJ pathway, the ATP-dependent ligase, rather than the standard NAD^+-dependent ligase, plays the role of joining the broken ends (4). *D. radiodurans* encodes a standard NAD^+-dependent liagase with Mn^{2+} as a preferred cofactor (71). A small predicted ATP-dependent ligase has been identified in *D. radiodurans*, but no ligation activity could be detected in *in vitro* reactions (71).

A family X polymerase Pol X_{Dr} has been identified recently and it contains a Pol X domain and a PHP (polymerase and histidinol phophatase) domain (72). *In vitro* assays showed Pol X_{Dr} has a Mn^{2+}-dependent polymerase activity (73) and a 3'-5' exonuclease activity (72). The presence of Pol X domain is rather uncommon in bacteria and is often implicated in NHEJ repair. Cells that are devoid of Pol X_{Dr} displayed significantly higher sensitivity to IR at elevated doses (73).

In summary, although some proteins consistent with the NHEJ repair pathway have been identified, the NHEJ mechanism as a whole has never been experimentally established in *D. radiodurans* (4). It requires further *in vivo* and *in vitro* work to prove the existence of this pathway in *D. radiodurans*.

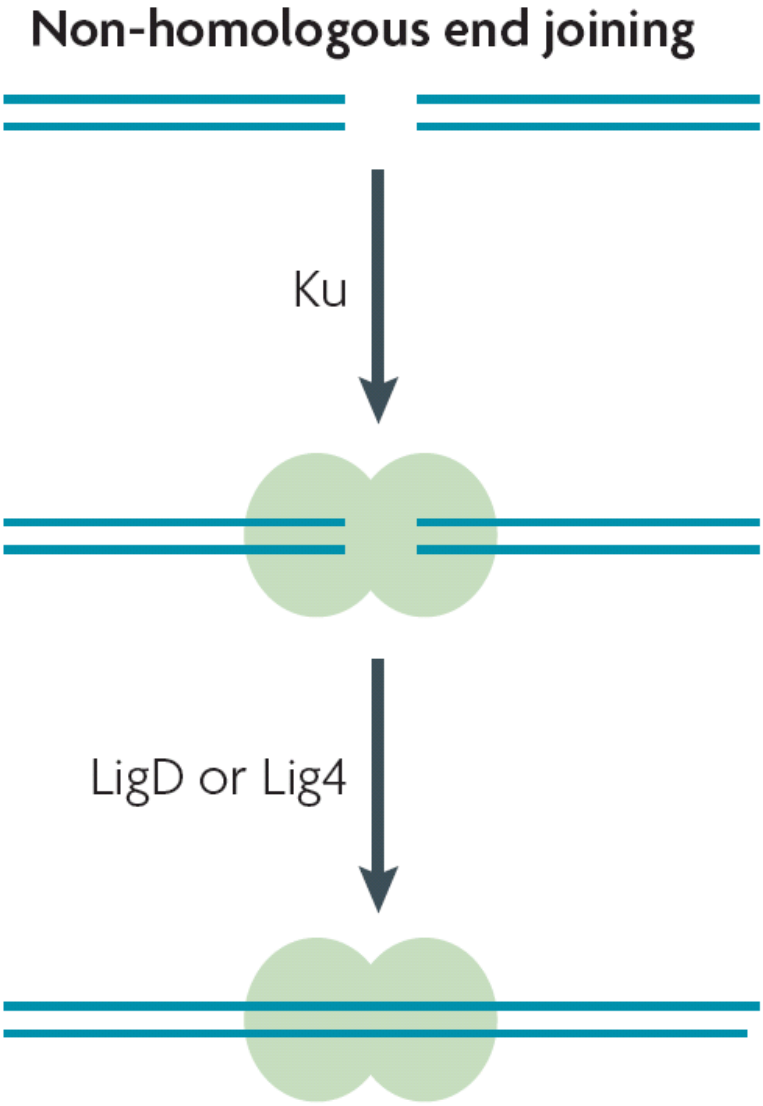

Figure 1.4 Schematic model for NHEJ repair pathway in bacteria.
In NHEJ, there is no requirement for a homologous sister chromatid. Rather, the DSBs are approximated by the end-binding protein Ku (depicted as a pair of green spheres) and then sealed by a specialized DNA ligase LigD that is unique to NHEJ. Figure is adapted from Shuman and Glickman, 2007 (66).

1.3 Other Aspects Contributing to *D. radiodurans* Radioresistance

In addition to the proposed DSB repair pathways in *D. radiodurans*, there are some physiological and morphological features of the organism that can provide passive contributions to its extraordinarily high radioresistence. Some of the features will be presented below.

1.3.1 Genome Copy Number

Enhanced IR resistance has been observed in different cells with increased genome copy numbers (74,75). The number of genome copies in *D. radiodurans* has never been reported to be less than four in all of its growth stages (76). This multi-genome physiology is believed to contribute passively to its radioresistance (2). *D. radiodurans* can presumably be protected by extra genetic material in two ways. First, the larger the genome copy number, the smaller the probability that a given dose of IR can inactivate all the copies of a specific gene. The estimate of the probability of inactivating all the copies of a specific gene can be given as P^N, where P is the probability of inactivation of one specific gene and N is the genome copy number (2). If there is a 10% probability of inactivating a gene in a single-copy genome cell, the probability to inactivate both copies of the same gene is 1% in a two-copy genome cell. Second, the two potential DSB repair pathways (either HR or ESDSA) in *D. radiodurans* require at least two copies of each chromosomes, to use one copy as a homologous template to restore the other chromosome copy. However, *D. radiodurans* cells with four copies of genome showed no difference in their resistance to gamma irradiation and UV light, compared to the cells

with eight copies of genome (76).This indicates that the contributions of genome redundancy in *D. radiodurans* was still not clear.

1.3.2 Nucleoid Organization

The hypothesis that in *D. radiodurans* a novel chromosome alignment structure can keep homologous regions as well as broken ends of DNA in close proximity was proposed by Minsky and colleagues (77). The idea is based on the observation that the nucleoid of stationary *D. radiodurans* cells is arranged as a tightly structured ring that remains unaltered by high dose of IR (2,77). This contribution of the nucleoid structure to radioresistance has been controversial (10,78). In tests with some of the other radioresistant *Deinococcus* species, the ring-shaped nucleoid structure is not always observed in all the species examined by epifluorescence microscopy, suggesting there is no obvious relationship between nucleoid shape and radioresistance (79). Cryoelectron microscopy showed directly that in *D. radiodurans* the DNA fragments were mobile, rather than in form of a condensed structure (80). Thus, the nucleoid structure of in *D. radiodurans* may not play a key role in its radioresistance.

1.3.3 *D. radiodurans* Cellular Mn (II) Concentration

Recently, Daly proposed that the accumulation of Mn^{2+} in *D. radiodurans* decreases the cellular concentration of ROS formed during irradiation. This in turn prevents IR-induced protein oxidation and enables functional DNA repair machinery to work efficiently on DSBs in the genome (10,81).

Water is the most abundant chemical in living cells and its radiolysis during IR produces the primary source of ROS (19). After radiolysis, H_2O is converted to $HO^{\bullet}$

(hydroxyl radical), H^+ and e^-_{aq} (10). Two $HO^\bullet$ react with each other to generate H_2O_2 (hydrogen peroxide) which can diffuse throughout the cell (10). Dissolved O_2 (oxygen), either derived from atmosphere or generated endogenously, reacts with e^-_{aq} to form $O_2^{\bullet-}$ (superoxide radical) (10). Therefore, IR-induced major ROS include $HO^\bullet$, H_2O_2 and $O_2^{\bullet-}$ (figure 1.5). The $HO^\bullet$ is the most reactive and can react with any organic or biological molecules it encounters. Although its half-life is very short (10^{-9} second *in vivo*), $HO^\bullet$ is still the major source of IR -induced DNA DSBs (19).

In contrast, H_2O_2 and $O_2^{\bullet-}$ are relatively inert. H_2O_2 can undergo catalytic decomposition by ferrous ions (Fe^{2+}) in Fenton chemistry (figure 1.5) (19). The newly formed $HO^\bullet$ from H_2O_2 becomes the secondary source of cellular $HO^\bullet$ in irradiation. Although $O_2^{\bullet-}$ does not react with DNA or most proteins, it has relatively high reactivity with the Fe-S clusters attached to some enzymes and triggers the release of ferrous ions (Fe^{2+}) (10). When the librated Fe^{2+} ions are made accessible to H_2O_2, more Fenton reactions will be catalyzed, leading to the production of $HO^\bullet$ in cells. Mn^{2+} ions accumulated in IR-resistant bacteria, however, can specifically react with $O_2^{\bullet-}$ and reduce it to H_2O_2, which can be decomposed into H_2O and O_2 by catalase (figure 1.5) (10). Thus, Mn^{2+} and Mn^{3+} redox cycling during IR favors $O_2^{\bullet-}$ scavenging, minimizes the global damaging effects of Fenton chemistry and allows DNA repair enzymes to survive and maintain their function (10).

Accumulation of a high level of Mn^{2+} (millimolar concentration) (81) and a low level of Fe^{2+} is found in several radioresistant bacteria including *D. radiodurans*, but not in radiosensitive organisms (81-84). For example, *D. radiodurans* (manganese:iron = 0.24)

accumulates 157 times more manganese and 3.3 times less iron than the IR-sensitive *S. oneidensis* (85). When *D. radiodurans* grows in medium that provides limited manganese (to bring the manganese to iron ratio down to 0.04 from 0.24), the cells become highly IR-sensitive (85). In assays to assess total IR-induced protein oxidation damage, bacteria with high manganese to iron ratios are extremely resistant to protein oxidation. In contrast, bacteria with low manganese to iron ratios are hypersensitive to protein oxidation (81,85). Interestingly, the accumulation of manganese does not affect the DSB level induced by IR (85).

To conclude, the accumulation of manganese in *D. radiodurans* clearly shields protein from massive IR-induced protein oxidation and is necessary for cells to survive high doses of irradiation.

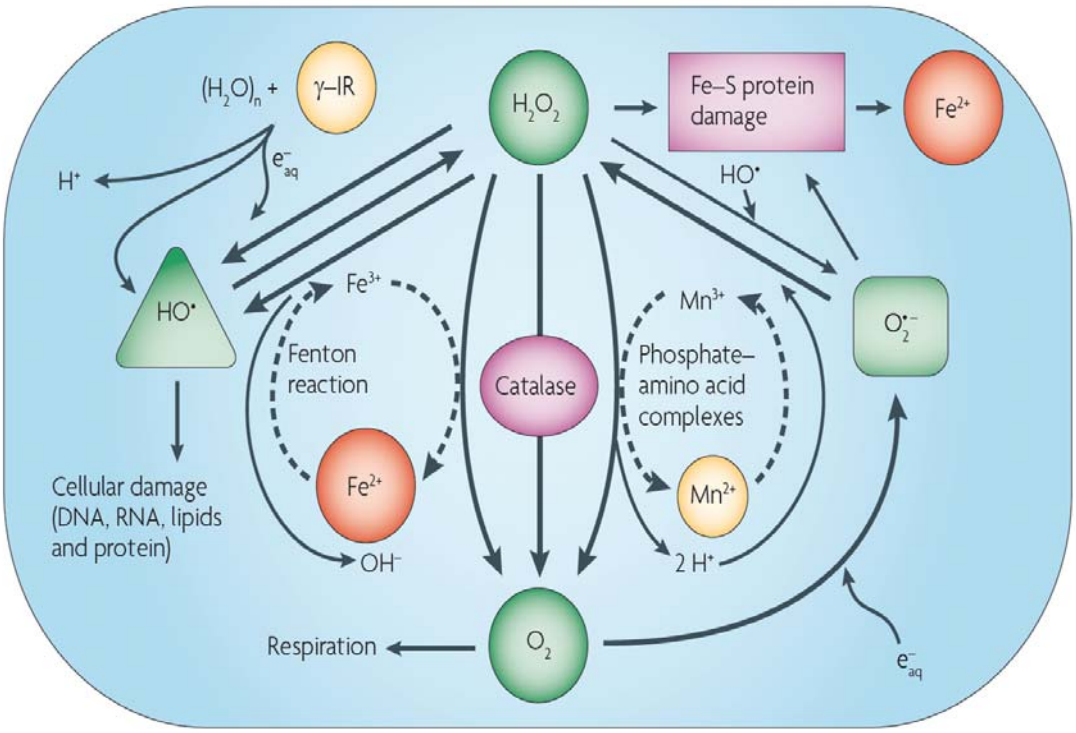

Figure 1.5 Model of ionizing radiation-driven manganese and iron redox cycling. Under ionizing radiation (IR), Fe^{2+} and Fe^{3+} redox cycling is predicted to generate $HO^{\bullet}$, whereas Mn^{2+} and Mn^{3+} redox cycling is predicted to favor $O_2^{\bullet-}$ scavenging without $HO^{\bullet}$ production. Catalase is a common enzyme that catalyses the decomposition of H_2O_2 to O_2 and H_2O. The $O_2^{\bullet-}$ would damage and inactivate enzymes with exposed Fe–S clusters, triggering the release of Fe^{2+} which in turn promotes IR-driven Fe^{2+} and Fe^{3+} redox cycling (86). Fe–S clusters participate in a range of biochemical processes, such as electron transfer, redox catalysis, regulation of gene expression etc. (87). Thus, Mn^{2+} and Mn^{3+} redox cycling is predicted to prevent the proliferation of iron-dependent ROS and protect diverse cellular functions (81).
Radiolysis of water by IR , $H_2O + \gamma\text{-IR} \rightarrow HO^{\bullet} + H^+ + e^-_{aq}$;
primary radiolytic reaction yielding H_2O_2, $2\ HO^{\bullet} \rightarrow H_2O_2$;
IR-induced superoxide, $O_2 + e^-_{aq} \rightarrow O_2^{\bullet-}$;
Fenton reaction, $H_2O_2 + Fe^{2+} \rightarrow HO^{\bullet} + OH^- + Fe^{3+}$;
iron reduction, $Fe^{3+} + HO_2^{\bullet} \rightarrow Fe^{2+} + O_2 + H^+$ and
$2\ Fe^{3+} + H_2O_2 \rightarrow 2\ Fe^{2+} + O_2 + 2\ H^+$;
manganese oxidation (81), $Mn^{2+} + O_2^{\bullet-} + 2\ H^+ \rightarrow H_2O_2 + Mn^{3+}$;
manganese reduction (81), $2\ Mn^{3+} + H_2O_2 \rightarrow 2\ Mn^{2+} + O_2 + 2\ H^+$.
Figure is adapted from Daly, 2009 (10).

1.4 Importance of Studying DNA Repair Helicases and Nucleases in *D. radiodurans*

The bacterium *D. radiodurans* is known to withstand high doses of ionizing radiation which can cause hundreds of DSBs and even more single-strand breaks (10). DSB is considered as the most lethal DNA damage as a single unrepaired DSB can kill a host cell. The multi-genome-copied *D. radiodurans* is capable of reconstructing the intact circular chromosomes from about 150 shattered fragments in 4.5 hours after irradiation (12). Although the accumulation of high manganese concentration in *D. radiodurans* can sufficiently protect proteins from oxidation (10), a robust DSB repair system is still required to fix the massive DSBs and other damage in several hours after IR treatment.

Several pathways for DSBs have been proposed based on mutational and biochemical results. The recent repair model ESDSA involving polymerase dependent synthesis and RecA dependent crossover is likely to be a major pathway for DSB repair in *D. radiodurans*. However, enzymes responsible for some steps shared by both HR and ESDSA still remain unclear and need to be identified. For example, the initiation step in both repair models involves the resection of DNA ends to produce recombinogenic 3' single-stranded DNA tails, which requires helicase to unwind dsDNA and nuclease to recess the ssDNA from 5' to 3'. Surprisingly, *D. radiodurans* lacks RecBCD complex and its functional homolog AddAB complex, the important enzymes working in the HR initiation step in most bacteria. Thus, the identification of the initiation step helicase and nuclease can lead to a better understanding of *D. radiodurans* DSB repair in the overall picture.

1.5 Specific Aims

The identification of the unknown helicase and nuclease involved in DSB repair (especially in the initiation step) is the goal of this project. They could be either the homologues of known enzymes involved in other DNA repair pathways or novel proteins. Three specific aims are included in the project.

1.5.1 Specific Aim 1: Characterization of a Novel Helicase HelIV

D. radiodurans locus DR1572 (*helD* gene) encodes a helicase superfamily I protein (HelIV) with unknown function. This protein has sequence similarity to several DNA repair helicases found in other bacteria, including UvrD and HelIV. The specific aim is to study the biological function *in vivo* with *helD* mutant and the enzyme activities *in vitro* with purified HelIV protein.

1.5.2 Specific Aim 2: Characterization of *D. radiodurans* RecJ Nuclease.

The RecJ homolog in *D. radiodurans* is encoded by locus DR1126. In *E. coli*, RecJ is one of the essential components found in the RecF pathway that is the alternative DSB repair model when RecBCD is rendered non-functional. The RecF pathway has been suggested to be an important DSB repair pathway in *D. radiodurans* based on the study of other RecF pathway players (4). The RecJ protein is the only component that has not been characterized. Thus, the specific aim is to study biologically and biochemically the RecJ protein, to contribute to a better understanding of the RecF pathway in *D. radiodurans*.

1.5.3 Specific Aim 3: Investigation of *D. radiodurans* RecD Binding Partner

Because of the lack of RecBC homologue proteins in *D. radiodurans*, its RecD homolog seems to be an isolated helicase. The specific aim is to test that whether the

RecD acts in the cell as part of a larger multiprotein complex or makes transient interactions with other proteins, using *in vitro* protein-protein interaction techniques.

CHAPTER 2 CHARACTERIZATION *IN VIVO* AND *IN VITRO* OF HELIV FROM *DEINOCOCCUS RADIODURANS*

2.1 Introduction

A recent model called ESDSA has been suggested for the rapid repair of extensive IR-induced DNA DSBs in the extremely-radioresistant bacterium *Deinococcus radiodurans*. This DSB repair mechanism involves two stages: DNA polymerase I and III dependent ssDNA tail synthesis in stage one; RecA-dependent homologous recombination in stage two (12,60). However, some necessary enzymes, such as helicases, involved in ESDSA are not known yet (4). Double-stranded DNA unwinding reactions performed by helicases are required at least in two steps in the ESDSA repair model (stage one) (figure 1.3): 3' ssDNA tail recession in the initiation step (involving both helicase and nuclease activity); branch migration after strand exchange in postsynaptic steps.

The commonly-used RecBCD helicase/nuclease complex responsible for the initial 3' tail processing in most bacterial DSB repair is not found in *D. radiodurans* (3), which makes the helicase(s) functioning in ESDSA initiation step more mysterious. Thus far, three DNA repair helicases have been studied in *D. radiodurans*, including RecQ, UvrD and RecD. RecQ exhibited efficient DNA unwinding activity in a 3'-5' direction *in vitro* (53) and the *recQ* mutant is sensitive to gamma rays, UV irradiation and mitomycin C (54). Similar to its function in *E. coli*, RecQ from *D. radiodurans* is suggested to be involved in RecF pathway catalyzed DSB repair (54). Additionally, RecQ should have other functionally overlapping helicase(s) in *D. radiodurans* as the deletion of *recQ* is not

lethal to the cell. UvrD has only been studied *in vivo*, and cells devoid of *uvrD* gene are deficient in mismatch repair, which is one of the DNA repair pathways where *E. coli* UvrD is involved (19,88). The *D. radiodurans recD* mutant is sensitive to gamma rays, UV and hydrogen peroxide (46). Because of the lack of RecBC in *D. radiodurans*, it is not quite clear what DNA repair pathways RecD is involved in. All in all, none of the previously studied DNA repair helicases is specifically attributed to the initiation step of DSB repair in *D. radiodurans*.

As part of the effort to identify and characterize new helicases in DSB repair, we have studied the properties of a novel protein encoded by *D. radiodurans* locus DR1572 (*helD* gene). The gene was predicted to encode a helicase superfamily I enzyme that shared some sequence similarity with several known DNA repair helicases, including UvrD, PcrA and HelIV (helicase IV) (89). However, there was an apparent frameshift found inside the coding region of DR1572 in the GenBank annotated sequence. The *helD* gene was amplified and sequenced. The later sequencing results indicated that the predicted frameshift did not exist because an extra G residue was found in the *helD* gene (see Results in this chapter).

The *in vivo* biological function of the *helD* gene was tested by replacing the *helD* gene with a chloramphenicol resistance cassette via homologous recombination. The growth rate and sensitivity of the resulting *helD* mutant to different types of DNA damaging agents were compared with those of wild type *D. radiodurans* strain.
For *in vitro* studies, the 83 kDa full length helicase IV (HelIV) protein (encoded by the 2.3 kb *helD* gene) was expressed in *E. coli* and purified. The 59 kDa truncated version of

HelIV protein (encoded by the 1.6 kb *helD* gene fragment), in which the extended N-terminal region was missing, was also expressed and purified. ATPase, helicase and DNA-binding assays were performed with both of the HelIV proteins under various reaction conditions.

2.2 Materials and Methods

2.2.1 Bacterial Strains and Plasmids

Wild type *D. radiodurans* R1 strain was purchased from the American Type Culture Collection (ATCC), Manassas, Va. The other wild type *D. radiodurans* wild type strain BAA-816 used in this study was a gift from Dr. Michael Daly at the Uniformed Services University of the Health Sciences, Bethesda, MD. The plasmid pTNK101 was a gift from Dr. John Battista at Louisiana State University.

D. radiodurans was grown at 30°C in TGY medium (0.5% tryptone, 0.3% yeast extract, 0.1% glucose) or on TGY agar (1.5%) plates. *E. coli* was grown in Luria-Bertani (LB) medium (1.0% tryptone, 0.5% yeast extract, 1.0% NaCl) or LB agar (1.5%) plate at 37°C. Antibiotics used for *D. radiodurans* were chloramphenicol (3 μg/ml), kanamycin (8 μg/ml) and streptomycin (5 μg/ml). Antibiotics used for *E. coli* were ampicillin (100 μg/ml), kanamycin (50 μg/ml) and chloramphenicol (15 μg/ml).

2.2.2 Genomic DNA Extraction

D. radiodurans genomic DNA was isolated as described (90). A 5 ml overnight culture of *D. radiodurans* was started from isolated colonies and grown at 30°C in TGY medium. The culture was spun down at 10,000 ×G for 30 seconds and the supernatant

was removed. The cell pellet was resuspended and incubated with 500 µl 95% ethanol at room temperature (23°C) for 10 minutes to break down the outer membrane. The remaining cell pellet was collected by centrifugation at 5,000 ×G for 1 minute and the supernatant was discarded. The cells were then treated with 400 µl TE buffer (10 mM Tris-HCl, 0.1 mM EDTA, pH 8.0) with 0.25 mg/ml lysozyme (Sigma Aldrich) added, and incubated in a 37°C water bath for 30 minutes. The cell lysate was then supplemented with 9 µl of 10% SDS and 1 µl of protease K (20 mg/ml, Fermentas) and incubated in a 57°C water bath for 3 hours. To remove proteins, the cell lysate was extracted three times with 250 µl of phenol:chloroform:isoamyl alcohol 25:24:1 (Sigma Aldrich). At the end of third extraction, the upper aqueous layer containing genomic DNA was carefully transferred into a sterile microcentrifuge tube. To precipitate genomic DNA, three volumes of 95% ethanol and one tenth volume of 3.0 M sodium acetate pH 7.0 were added. The resulting solution was incubated at -20°C overnight. The next day the precipitated genomic DNA was spun down by centrifugation at 10,000 ×G for 3 minutes, then washed with 1 ml 70% ethanol three times to remove remaining salt. After the final wash, the genomic DNA pellet was air-dried at room temperature and dissolved in 300 µl of TE buffer at 37°C overnight. The concentration of extracted genomic DNA was determined from the absorbance at 260 nm using a UV spectrophotometer (Varian).

2.2.3 Transformation of *D. radiodurans*

DNA transformation into *D. radiodurans* was conducted as described (46). A 10 ml culture was started by inoculating 1 ml overnight *D. radiodurans* culture into 9 ml fresh TGY medium and grown at 30°C until its OD_{600} reached ~0.5. The cell pellet from 3 ml

culture was spun down at 5,000 ×G for 1 minute and resuspended with 25 µl of sterile 0.1 M $CaCl_2$ and 75 µl of TGY medium. The cell resuspension was then supplemented with transforming DNA and placed on ice for 10 minutes. After the incubation step, the transformation mixture was shaken at 30°C at 250 rpm for 1hour. The mixture then was diluted with 1 ml fresh TGY medium and shaken at 30°C overnight. The next day about 100 µl transformation culture was plated onto TGY agar plate with appropriate antibiotic added. After three days incubation at 30°C, plates were checked for transformants.

2.2.4 Other Molecular Biology Techniques

PCR reactions were performed in 50 µl mixtures including 200 ng genomic DNA or 1 ng plasmid DNA as templates, 0.6 µM of each primers, 200 µM of each deoxynucleoside triphosphates (dNTP), 5% (v/v) dimethyl sulfoxide (DMSO) and *Pfu* (Stratagene) or *Taq* (Fermentas) DNA polymerase which was used in supplied reaction buffer according to the manufacturer's instructions. PCR reactions were carried out using an Ericomp Powerblock 2 thermocycler.

DNA fragments were analyzed and purified on 0.7%-1.0% agarose (Invitrogen) gels supplemented with 1 µg/ml ethidium bromide (BioRad). Agarose gels were visualized on a UV transilluminator (UVP Inc.) and photographed with a Polaroid camera. Target fragments were excised with a fresh razor blade and purified using the Qiaquick® Gel Extraction Kit (Qiagen). Circular plasmids were extracted from 5 ml overnight *E. coli* host cultures grown at 37°C using the GeneJET® Plasmid Miniprep Kit (Fermentas) and dissolved with 36 µl elution buffer. DNA digestions were performed with restriction enzymes from New England Biolabs or Fermentas according to the manufacturer's

instructions. In DNA ligation reactions, vector and insert were mixed in a ratio of 3 : 1 and incubated with T4 DNA ligase (Fermentas) in a 16°C water bath overnight. Plasmid or ligation mixture transformation was performed using chemically-competent *E. coli* strains (Novagen) using heat-shock procedure as follows. Plasmid DNA or ligation mixture was added to 100 µl pre-thawed competent *E. coli* strain and incubated on ice for 30 minutes. The cell-DNA mixture was heat-shocked at 42°C for 30 seconds and then diluted with 1 ml fresh LB medium and shaken at 37°C for 1 hour before plating.

Protein detection with western blotting was carried out as follows. Briefly, the protein sample (or mixture) was separated by running 10% SDS-PAGE and then transferred to a piece of PVDF membrane (Millipore) at 30 mA for 20 hours using a Bio-Rad blot transfer system. The next day, the PVDF membrane with transferred proteins was blocked with 4% milk to occupy any remaining sticky places on the membrane. The primary antibody which could recognize its specific protein was then applied and incubated with the blot. After washing off free or loosely bound primary antibody with 1 × t-TBS (0.1% Tween 20, 10 mM Tri-HCl, pH 7.6, 150 mM NaCl), the secondary antibody was applied to recognize the primary antibody. The secondary antibody is conjugated with alkaline phosphatase which can produce fluorescent products (detected by Storm PhosphorImager, GE Healthcare) after incubation with its phophatase substrates.

2.2.5 *helD* Gene Cloning and Sequencing

PCR reactions described in previous section using *pfu* (stratagene) DNA polymerase were set up to amplify the *helD* gene. Two versions of *helD* gene were cloned. A 2236 bp (2.2 kb) fragment encompassing the entire putative *helD* open reading frame (bp # 1,592,040 to 1,594,276 of *D. radiodurans* chromosome 1) was amplified from *D. radiodurans* wild type strain R1 using primers UvrD up and UvrD down; a 1625 bp (1.6 kb) fragment encoding a truncated version of the protein (bp # 1,592,534 to 1,594,158) was amplified from wild type strain BAA-816 using primers UvrD1 and UvrD2. PCR cycling conditions were as follows. Cycle 1 had one step, 94°C for 10 minutes initial denaturation. Cycle 2 repeated 30 times had three steps: step 1 denaturation (94°C for 1 minute); step 2 annealing (56°C for 1 minute); step 3 extension (72°C for 4 minutes). Cycle 3 had one step, 72°C for 10 minutes.

The amplified products were ligated to PCRblunt vector (Invitrogen) and transformed into *E. coli* Top 10 strain (Invitrogen). The complete sequences for both 1.6 kb and 2.2 kb *helD* gene inserts were determined at the DNA sequencing facility in the Center for Biosystems Research, University of Maryland. Three sequencing primes were M13Rev, M13 (-21) and UvrD mid (M13Rev and M13(-21) are the two universal primers provided by the DNA sequencing facility). Primers used for *helD* gene cloning and sequencing are listed in Table 1.

Table 1 Primers used for *helD* gene cloning and sequencing

UvrD1	↓NdeI 5'-CAT**ATG**CGCGACGTGGTGGAGACG-3' —— start
UvrD2	↓BamHI 5'-GGATCC**TCA**GCGCACCAGCGGGTGCAG-3' —— stop
UvrD up	5'-CTGATTTCGAGGCCGAATCTAGTCATC-3'
UvrD down	↓BamHI 5'-GGATCCGAGGATAGCGGGAAGGAGCTG-3'
UvrD mid	5'-CAGAGCTTGCAGGAAAACATCG-3'
UvrD top	↓NdeI 5'-CAT**ATG**CAGGCCACTCCAGATAAAAGGCG-3' —— start

2.2.6 Construction of *D. radiodurans* Δ*helD::cam*

The *helD* gene was knocked out from the *D. radiodurans* genome and replaced by a chloramphenicol resistance gene (*cat* gene), using overlap PCR and subsequent homologous recombination. Three overlapping PCR fragments were generated separately by PCR reactions: a 968 bp fragment located upstream of 1.6 kb *helD* gene (C-terminal coding region) in the genome (using primers Fw2 and Rev2), a 948 bp product located downstream (using primers Fw3 and Rev3) of *helD* gene and a 829 bp product (using primers Fw1 and Rev1) including *cat* gene fused to the *kat* promoter. The two PCR products of *helD* flanking region were amplified from *D. radiodurance* genomic DNA. The *cat* gene and the *kat* promoter were amplified from pTNK 101 plasmid (70). The 5' end of the *cat* gene overlapped the 3' end of the *helD* upstream fragment and the 3'end of

the *cat* gene overlapped the 5' end of the *helD* downstream fragment. The three PCR fragments were mixed in a 1:1:1 ratio in a PCR reaction with primers Fw2 and Rev3 to amplify the entire DNA fragment (91). The resulting 2705 bp product was used to transform *D. radiodurans* wild-type strain BAA-816 to resistance to chloramphenicol. Primers used for *helD mutant construction* and verification are listed in Table 2.

Table 2 Primers used for Δ*helD* mutant construction

Fw1	5'-CCTGAAAGAGCAGAGCACCGC↓EcoRI GAATTCGCG AGGGCCTGAGGGCC-3'
Rev1	5'-AGACCTTAGACGGTTCGGCA↓HindIII AGCTTCAGGC GTAGCAACCAGGCG-3'
Fw2	5'-GGACGACACAAAGGGCTTCAGG-3'
Rev2	5'-GCCCTCAGGCCCTCGC↓EcoRI GAATTCGCGGTGCT CTGCTCTTTCAGG-3'
Fw3	5'-CGCCTGGTTGCTACGCCTG↓HindIII AAGCTTGCCGA ACCGTCTAAGGTCTATATGC-3'
Rev3	5'-GCCCTGCTCCTCAAGTGCC-3'

2.2.7 Genotyping of *D. radiodurans* Δ*helD::cam* by PCR and Southern Blotting

Genomic DNA from different isolated *helD* mutants was extracted for the PCR reactions described as follows to verify their genotypes. Two sets of primers were used to do the PCR verification. With the primers Fw2 and Rev3, the PCR product amplified from wild type should be a 3563 bp fragment and the product from *helD* mutant should be

2705 bp fragment, since the *cat* gene was ~ 850 bp smaller than the replaced *helD* gene. With the primers UvrD mid annealing to the internal region of *helD* gene and Rev3, only wild type genome could produce a 2144 bp fragment whereas *helD* mutant genome should not produce any product if the target *helD* gene was completely removed. All above PCR reactions were examined by running the reactions mixtures on 0.8% agarose gels.

As an alternative means to verify *helD* mutant genotype, southern blotting was performed to further confirm the PCR results. In contrast to PCR method, southern blotting could also provide the information about the location of the *cat* gene cassette insertion in the *D. radiodurans* chromosomes. According to the instructions provided in the kit used for southern blotting, even one copy of the wild type *helD* gene per cell could be detected. Southern blots were carried out as decribed (46). Freshly isolated genomic DNA (~5 μg) from wild-type *D. radiodurans* and *helD* mutant were used for southern blotting. The genomic DNA from each strain was first digested separately at 37°C overnight with two different restriction endonucleases and one pair of restriction endonucleases. The enzymes used for single digestion were *EcoR*I and *Apa*I; the enzymes used for double digestion were *BamH*I and *Sca*I. Then the digestion mixtures were applied to a 1.0% agarose gel for electrophoresis.

After denaturation and neutralization steps, the digested DNA in the agarose gel was transferred to a nitrocellulose membrane (Bio-Rad) by capillary interaction and fixed on the membrane by baking at 80°C for 2 hours. Two digoxigenin (DIG)-labeled probes were created by PCR reactions using dNTP mixed with DIG-11-dUTP (a derivative of

dUTP, provided in DIG Probe Synthesis kit, Roche) followed by gel purification. The two southern blots probes were 1.6 kb *helD* gene probe (amplified using primers UvrD1 and UvrD2) and the 890 bp *cat* gene probe (amplified using primers Fw1 and Rev1). Hybridization was done at 42°C with shaking for 16 hours after prehybridization with 100 μg/ml denatured salmon sperm DNA (Sigma-Aldrich). Two stringency washes at 50°C and blocking with 4% milk were required, before detection using anti-DIG-11-dUTP antibody (Roche) and ECF™ substrate (Amersham). The alkaline phosphatase conjugated to the antibody could dephosphorylate ECF substrate to produce a fluorescent product which emits light at 540nm to 560nm, when scanned using a Storm PhosphorImager (GE Healthcare).

2.2.8 Growth Assay

Overnight cultures of wild type and *helD* mutant were diluted 1:100 into a fresh culture flask containing 100 ml TGY medium with or without chloramphenicol. Cells were grown at 30°C and shaken at 250 rpm for 28 hours. Cell density was monitored at OD_{600} using a UV spectrophotometer and a 1-cm-path-length quartz cuvette. Aliquots of the cultures were diluted and plated to ensure optical density reflected viable cell numbers. Verification of the each strain's genotype was performed by PCR as described previously with genomic DNA isolated from the cultures after the last optical density data points were obtained

2.2.9 *In Vivo* Biological Survival Assays with Treatments of Gamma Irradiation, UV Irradiation, Hydrogen Peroxide, Methyl Methanesulfonate and Mitomycin C

Cells for each of the following assays were grown in TGY without antibiotic to mid-log phase (OD_{600} = ~0.5, corresponding to ~1 $\times 10^9$ CFU/ml). Cells were treated as described below and then spread on triplicate TGY plates without antibiotic, followed by incubation at 30°C for 2 days before colonies were counted.

For gamma radiation sensitivity examination, cells in 5.0 ml portions were irradiated with gamma rays from a ^{60}Co source (Neutron Products model 200324) at 2.5 kGy/hour on ice. Irradiated cells were serially diluted in triplicate in TGY medium and spread on TGY plates without antibiotics.

In UV sensitivity experiments, cells were serially diluted in TGY medium and spread on TGY plates. After the culture soaked into the plates, the plates were opened and exposed to UV light from a 15 Watt germicidal lamp (FG15T8; Fisher) at 90 J/(m^2 *min) measured with a UVX Radiometer (UVP, Upland, CA) for different time periods.

Hydrogen peroxide sensitivity test was carried out by adding various concentrations of hydrogen peroxide into cell cultures and incubating them for 1 hour at 30°C without shaking. Then aliquots from culture samples containing different amount of hydrogen peroxide were serially diluted and spread on TGY plates.

Sensitivity to methyl methanesulfonate (MMS) was measured by incubating cells in liquid TGY medium containing 30 mM MMS with shaking at 30°C. At selected time points cells from 0.5 ml of each culture were harvested by centrifugation and then resuspended with 0.5 ml of fresh TGY medium. Resuspended cells were serially diluted with TGY media and spread on TGY plates.

Sensitivity to mitomycin C (MMC) was measured by incubating cells in liquid TGY medium containing 10 μg/ml MMC with shaking at 30°C. At selected time points aliquots from each culture were serially diluted with TGY medium and spread on TGY plates.

2.2.10 Construction of Full Length and Truncated HelIV Expression Plasmid

A 2267 bp (2.3 kb) PCR fragment of *helD* gene (bp # 1,591,893 to 1,594,158) was amplified from *D. radiodurans* wild-type strain BAA-816 using primers UvrD top and UvrD2 (see Table 1) which added *Nde*I and *BamH*I sites respectively at the edges of PCR product.The PCR product was ligated into the PCRblunt vector (Invitrogen). Complete sequences of the 2.3 kb inserts were verified by sequencing using primers M13Rev, M13 (-21) and UvrD mid. The 2.3 kb and the 1.6 kb *helD* inserts were excised from PCRblunt-2.3kHelIV and PCRblunt-1.6kHelIV with *Nde*I and *BamH*I and they were ligated into pET15b (Novagen) vector digested with the same enzymes. The resulting plasmids pET15b-2.3kHelIV and pET15b-1.6kHelIV were confirmed by double digestions with *Nde*I and *BamH*I. The 2.3 kb insert encoded the entire HelIV protein while the 1.6 kb insert only encoded a truncated HelIV whose N-terminal preceding region was missing. The 1.6 kb fragment still retained C-terminal region including all the helicase motifs.

2.2.11 Expression and Purification of Full Length and Truncated HelIV

A single colony of *E. coli* strain Rosetta2(DE3) (Novagen) containing pET15b-2.3kHelIV (expressing 83 kDa HelIV, 755 amino acids) or pET15b-1.6kHelIV (expressing 59 kDa HelIV, 541 amino acids) was used to inoculate 10 ml of LB medium containing 100 μg/ml ampicillin and grown at 37°C overnight. The overnight culture was

diluted by 1:100 into 1 liter ZYP-5052 medium (1.0% tryptone, 0.5% yeast extract, 50 mM Na_2HPO_4, 50 mM KH_2PO_4, 25 mM $(NH_4)_2SO_4$, 1 mM $MgSO_4$, 0.5% glycerol, 0.05% glucose, 0.2% lactose) containing 100 μg/ml ampicillin as described (92). The culture was grown at 23°C (room temperature) with vigorous shaking for 20 hours for auto-induction of HelIV protein. The cells were harvested by centrifugation at 5,000 ×G and stored at -80°C.

The frozen cell pellets (~8 to10 grams) from each culture were thawed on ice and suspended with 50 ml of native binding buffer (20 mM sodium phosphate, 500 mM NaCl, pH 7.8) containing 20 mM imidazole. 1 mM PMSF and 50 μl /g cells protease inhibitor cocktail for polyhistidine-tagged proteins (Sigma-Aldrich) were also added into the suspension. The cells were sonicated in an ice bath with a microtip using 30 second bursts and 30 second breaks (50% duty cycle, Branson Sonifer 450) for a total time of 15 minutes. The cell debris was removed by centrifugation at 10,000 ×G, at 4°C for 2 hours and the supernatant containing soluble portion of HelIV proteins was saved.

For the purpose of solubility test, small aliquot of sonicated cell lysate (100 μl) was centrifuged at 10,000 ×G, at 4°C for 3 minutes. The 100 μl of supernatant was transferred to a fresh micorcentrifuge tube and the debris was resuspended with 100 μl water. The soluble and insoluble portions were then mixed with SDS-PAGE loading buffer and analyzed by 10% SDS-PAGE.

The above cell extract from 1 liter expression culture of 83 kDa or 59 kDa HelIV was applied to a 3-ml Ni^{2+}-NTA column (ProBond® resin, Invitrogen) that was already equilibrated with 50 ml native binding buffer. The column was washed with 30 ml of

native wash buffer (20 mM sodium phosphate, pH 7.8, 500 mM NaCl) containing 60 mM imidazole, and then eluted in a 60 ml gradient of 60-500 mM imidazole in native wash buffer.

The nickel column fractions containing 83 kDa HelIV protein were analyzed and visualized by running 10% SDS-PAGE followed by coomassie blue staining. Only the fractions containing significant amount of 83 kDa HelIV were pooled and dialyzed against Buffer A (20 mM potassium phosphate, pH 7.5, 1 mM EDTA, 1 mM DTT, 10% (v/v) glycerol) containing 50 mM NaCl at 4°C overnight. Protein that precipitated after dialysis was removed by centrifugation and the supernatant was loaded onto a 5-ml single-strand DNA (ssDNA) cellulose column (Sigma Aldrich) equilibrated in Buffer A containing 50 mM NaCl. The column was washed with 50 ml of Buffer A with 50 mM NaCl, and the protein was eluted with 20 ml of 300 mM NaCl and 20 ml of 600 mM NaCl in Buffer A. After running 10% SDS-PAGE, the fractions containing 83 kDa HelIV were collected, dialyzed against Buffer A containing 50 mM NaCl and concentrated by ultrafiltration (Amicon).

The nickel column fractions containing 59 kDa HelIV protein were collected, dialyzed at 4°C against Buffer A with no added salt and applied to a 5 ml ssDNA column in Buffer A (no salt). The column was washed with 50 ml Buffer A (no salt) and eluted with a 60-ml gradient of 0-300 mM NaCl in Buffer A. The fractions were analyzed by 10% SDS-PAGE.

The protein concentration was determined from the absorbance at 280 nm, using $\varepsilon_{280} = 73465\ M^{-1}\ cm^{-1}$ for His-tagged 83 kDa HelIV and $\varepsilon_{280} = 49390\ M^{-1}\ cm^{-1}$ for

His-tagged 59 kDa HelIV (calculated with the program ProtParam at ca.expasy.org/tools/protparam.html).

2.2.12 N-Terminal His Tag Removal by Thrombin Protease

The N-termianl His-tag polypeptides on both 83 kDa and 59 kDa were removed using a Thrombin Cleavage Capture Kit® (Novagen). The protein (0.1 mg) was treated with thrombin (0.44 units) at 4°C overnight. Removal of the His-tag was verified by analysis on 10% SDS-PAGE and by western blotting using anti-His-tag monoclonal antibody (Novagen).

2.2.13 ATPase Assay

ATPase assay was carried out by Thin Layer Chromatography (TLC) on polyethyleneimine (PEI)-cellulose plates (J. T. Baker). ATP, ADP, and phosphate in solution have different negative charges so that they can be easily separated on TLC plate. Standard ATPase reaction (20 μl total volume) contained: 50 mM Tris-HCl, pH 7.5, 2 mM $MgCl_2$, 10 μM 30-nt ssDNA (or with circular dsDNA, linear dsDNA and no DNA added as control), 1 mM DTT, 5% glycerol, 0.1 mg/ml BSA, 250 μM ATP (mixed with 1% [γ-^{32}P] ATP) and enzyme. Concentrated enzyme stock was serially diluted by the enzyme dilution buffer (25 mM potassium phosphate, pH 7.5, 0.1 mM EDTA, 0.1 mM DTT, 0.1 mg/ml BSA and 10% glycerol) if necessary. The ATPase reactions were started after adding enzyme and incubated at 30°C water bath. A small aliquot (0.6 μl) was taken out and spotted on TLC plate at selected time points. The TLC plates used here were pretreated with 10% NaCl solution and air-dried for use. The TLC plates were then developed in 0.5 M LiCl and 1 M formic acid solution, dried, exposed to the

PhosphorImager screen (Molecular Dynamics) and scanned by the Storm PhosphorImager (GE Healthcare). ImageQuant software was used to quantitate the fraction of ATP hydrolyzed based on the ratios of radioactivity of the [γ-^{32}P] ATP to [^{32}P] phosphate group in the images.

2.2.14 Helicase Assay

Four oligonucleotides (HMC 1-4) listed in Table 3 were annealed in pairs and used to make helicase assay substrates, all of which had 20-base pair double-strand DNA region. The four double-strand helicase substrates were: (a) a 20 bp full duplex with blunt ends (HMC 2 + HMC 3); (b) a 20 bp with a 12 nt single-strand 5'overhang (HMC 3 + HMC 4); (c) a 20 bp with a 12 nt single-strand 3'overhang (HMC 1 + HMC 2); (d) a 20 bp with a forked end of 12 nt single-stranded DNA (HMC 1 + HMC 4). HMC 1 and 3 were labeled at 5' ends with [γ-^{32}P] ATP by T4 polynucleotide kinase (PNK) (Fermentas) so that each of the four structures had one single strand labeled, as shown in figure 2.1. The labeling reaction (20 μl) included: 1 × T4 polynucleotide kinase buffer, 0.5 μM HMC 1 or 3, 15 units of T4 polynucleotide kinase, and 0.2 μM [γ-^{32}P] ATP. The reaction mixture was incubated at 37°C for 60 minutes. The fraction and quality of the labeled oligomers were estimated by running TLC plates developed in 1 M NaH_2PO_4, pH 3.5, followed by exposure and scanning steps as previously described. The labeled oligomers were purified with QIAquick® Nucleotide Removal Kit (Qiagen). Scintillation counting was used to trace the radioactivity and estimate recovery yield by mixing 1 μl of labeling reaction mixture with 3.0 ml of scintillation fluid. The final concentration (D_{final}) of radiolabeled oligomer after purification was calculated with the following equation:

$$D_{final} = 0.5\ \mu M\ *\ \frac{R_{final}}{R_{initial}}\ *\ \frac{T_{final}}{T_{initial}}$$

Here, R_{final} = final radioactivity after purification

$R_{initial}$ = initial radioactivity before purification

T_{final} = percentage radioactivity of the labeled DNA with respect to the total radioactivity in the final purified mixture

$T_{initial}$ = percentage radioactivity of the labeled DNA with respect to the total radioactivity in the initial mixture before purification

The four double strand DNA substrates were prepared by mixing 4 nM ^{32}P-labeled HMC 1 or 3 with 16 nM of its unlabeled type and 20 nM of the unlabeled complementary strand HMC 2 or HMC 4 in annealing buffer that contained 50 mM NaCl, 20 mM Tris-HCl, pH 7.5, 1 mM $MgCl_2$. The mixtures were heated at 95°C for 2 minutes and then cooled down slowly to room temperature, allowing two complementary oligomers to anneal.

Table 3 Oligomers used for helicase assays

HMC 1	5'-GCCGTAGTATGCACATCGACATCCATCGACAT-3'
HMC 2	5'-GTCGATGTGCATACTACGGC-3'
HMC 3	5'-GCCGTAGTATGCACATCGAC-3'
HMC 4	5'-TACAGCTACCTAGTCGATGTGCATACTACGGC-3'

Helicase substrates and structures

HMC 1 + 2	20 bp, 12 nt 3'- tail	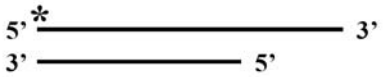
HMC 3 + 2	20 bp, blunt end	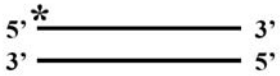
HMC 3 + 4	20 bp, 12 nt 5'- tail	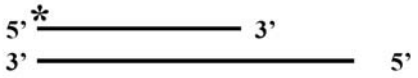
HMC 1 + 4	20 bp, 12 nt forked end	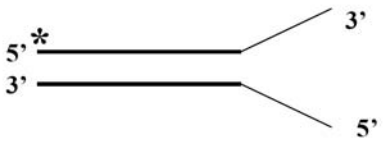

Figure 2.1 The structures of four substrates of 5'-^{32}P-end-labeled 20 bp dsDNA with blunt end, 3'tailed, 5'tailed or 12-nt non-complementary ssDNA fork at one end of the duplex DNA.

The unwinding reaction mixture (20 µl) included: 50 mM Tris-HCl, pH 7.5, 2 mM $MgCl_2$, 1 mM ATP, 1 mM DTT, 0.1 mg/ml BSA and 1 nM of duplex substrate. The re-annealing of single strand products can be ignored based on previous observations (17). After incubation in 30°C water bath for desired amount of time, 10 µl aliquots were

palced on ice and mixed with 3 µl 4 × quench buffer (40% glycerol, 2.4% SDS, 100 mM EDTA, 0.12% bromophenol blue and 15 nM of unlabeled HMC 1 or 3 to prevent re-annealing).

Non-denaturing 15% polyacrylamide gels (37.5 :1, acrylamide : bis-acrylamide) were pre-run under 10 mA for 1 hour. About 10 µl of quenched reaction sample was applied to each lane and gels were run in 1 × TBE buffer (90 mM Tris, 89 mM boric acid, 2 mM EDTA, pH 8.3), at 150 constant volts. The gels were then dried by gel drier (Bio-Rad), exposed and scanned as previously described.

2.2.15 DNA Binding Assay

DNA binding abilities of both 83 kDa and 59 kDa HelIV were assessed with ^{32}P radiolabeled ssDNA (HMC 1 and HMC 3) or dsDNA (5'tailed and forked) using gel mobility assay. The theoretical basis for gel mobility assay was that a small DNA molecule had a much faster migration rate in gel electrophoresis than the same DNA bound to a protein. Each 20 µl binding mixture contained: 50 mM Tris-HCl, pH 7.5, 2 mM $MgCl_2$, 1 mM DTT, 0.1 mg/ml BSA, 5% glycerol, 1 nM of ^{32}P labeled HMC 1 or HMC 3 and various amount of HelIV proteins. After all the ingredients for DNA binding assay were added together, the mixtures were kept at room temperature for 15 minutes before 3 µl of 50% glycerol was added. The samples were then loaded quickly onto 10% polyacrylamide gels and the gels were run at 4°C in 1 × TBE buffer at 150 constant volts. The gels were dried and analyzed with the PhosphorImager.

DNA binding assay was also performed using a nitrocellulose-DEAE double-filtered method to study the interaction between HelIV and DNA (93). There were two layers of

different membranes set up: the nitrocellulose membrane sitting on top and the DEAE membrane on bottom. The nitrocellulose membrane could immobilize HelIV protein or protein-DNA complex and the DEAE secondary membrane could trap all the DNA that does not bind to the nitrocellulose membrane, enabling a direct determination of total amount of free DNA filtered. The standard double-filter DNA binding mixture set up and incubation were the same as in the gel mobility assay, except for that the mixture's total volume was enlarged proportionally to 100 μl from 20 μl. After binding mixtures were applied to the double-filter system, the radioactivity from ^{32}P labeled HMC 1 on nitrocellulose and DEAE membranes were quantified separately.

2.3 Results

2.3.1 *helD* Gene Cloning and Sequencing Results

With two different pairs of primers, a 2236 bp product (using template DNA from wild type R1 strain) and a 1625 bp product (using template DNA from wild type strain BAA-816) were amplified from the *helD* gene locus (DR1572) by PCR reactions, as shown in figure 2.2. Both of the 2.2 kb and 1.6 kb fragments, were purified from PCR reaction mixture and ligated into the vector PCRblunt. The resulting plasmids PCRblunt-2.2kHelIV-A and B (isolated from 2 different colonies) and PCRblunt-1.6kHelIV-A, B, C and D (isolated from 4 different colonies) were sent for sequencing.

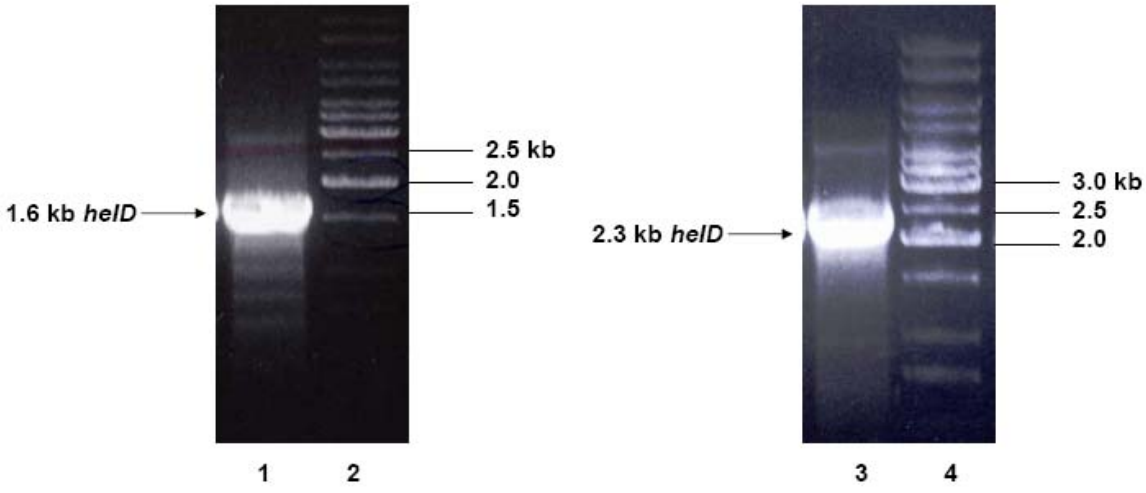

Figure 2.2 PCR products of *helD* genes with two different pairs of primers on 0.8% agarose gel. Lane 2 and 4: Fermentas 1 kb ladder; lane 1: 1.6 kb *helD* fragment with primers UvrD1 and UvrD2; lane3: 2.2 kb helD gene with primers UvrD up and UvrD down.

As discussed in the introduction of this chapter, locus DR1572, which is predicted to encode a helicase, appears to have a frameshift mutation in its sequence. The sequencing results from all six plasmids showed that there was an additional G right after bp # 1,593,382 which is around two thirds of the *helD* gene after the start codon. With the additional G residue that corrected the apparent frameshift, the *helD* gene can encode a protein of 755 amino acids beginning at a predicted TTG start codon (Appendix 1).

A BLASTp search of the GenBank database with the full length HelIV protein sequence as the query found similar protein sequences in several other bacteria including *E. coli* and *B. subtilis*. The highest scoring *E. coli* proteins were UvrD ($E = 2e^{-6}$) and HelIV ($E = 3e^{-5}$). The closest match of *D. radiodurans* HelIV in *B. subtilis* is Yvgs ($E = 2e^{-27}$), which has been proposed to be the orthologue of *E. coli* HelIV. The sequence identity between *E. coli* HelIV and *B. subtilis* Yvgs is low, but they are grouped into the same helicase subfamily (94). Both of them share a similar spacing pattern of the clusters of conserved helicase motifs, including an extended N-terminal region preceding the first conserved helicase motif (94). As shown in Figure 2.3, the protein encoded by locus DR1572 has helicase-motif spacing pattern very similar to *E. coli* HelIV and *B. subtilis* Yvgs. The protein is referred as *D. radiodurans* HelIV and the gene as *helD*.

A

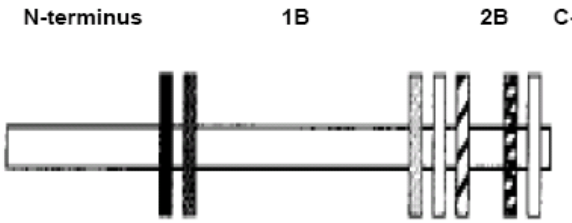

B

	N-terminus	1B	2B	C-terminus
Yvgs	228	262	89	18
*Eco*HelIV	211	170	79	21
*Dr*HelIV	243	290	99	17

Figure 2.3 The spacing pattern of the conserved helicase motifs in the HelIV subfamily belonging to superfamily I helicase. (A) Schematic structure of the HelIV subfamily: seven conserved motifs are separated by four domains: N-terminus, 1B, 2B and C-terminus. (B) The distances (in amino acids) separating the different clusters of motifs are listed in the table from three members of the HelIV subfamily: Yvgs from *B. subtilis*, HelIV from *E. coli* and *D. radiodurans*. Figure is adapted from Carrasco et al., 2001 (94).

2.3.2 Genotyping of *D. radiodurans* Δ*helD::cam* Mutant by PCR

To disrupt the *helD* gene from *D. radiodurans* chromosome 1, a homologous recombination method was used (figure 2.4 A). A 2.7 kb *cat* gene cassette was generated by overlap PCR (figure 2.4 B) in which equal amount of *helD* upstream fragment, downstream fragment and *cat* gene were mixed and used as templates. This 2.7 kb overlap PCR product was extracted from 0.8% agarose gel and then used to transform *D. radiodurans* BAA-816 wild type strain, to disrupt the *helD* gene by replacing its 1.6 kb C-terminal region encoding all helicase motifs with the 0.9 kb *cat* gene. After transformation, *helD* mutants with chloramphenicol (*cam*) resistance provided by the *cat* gene were selected using TGY agar plates containing 5 μg/ml *cam*.

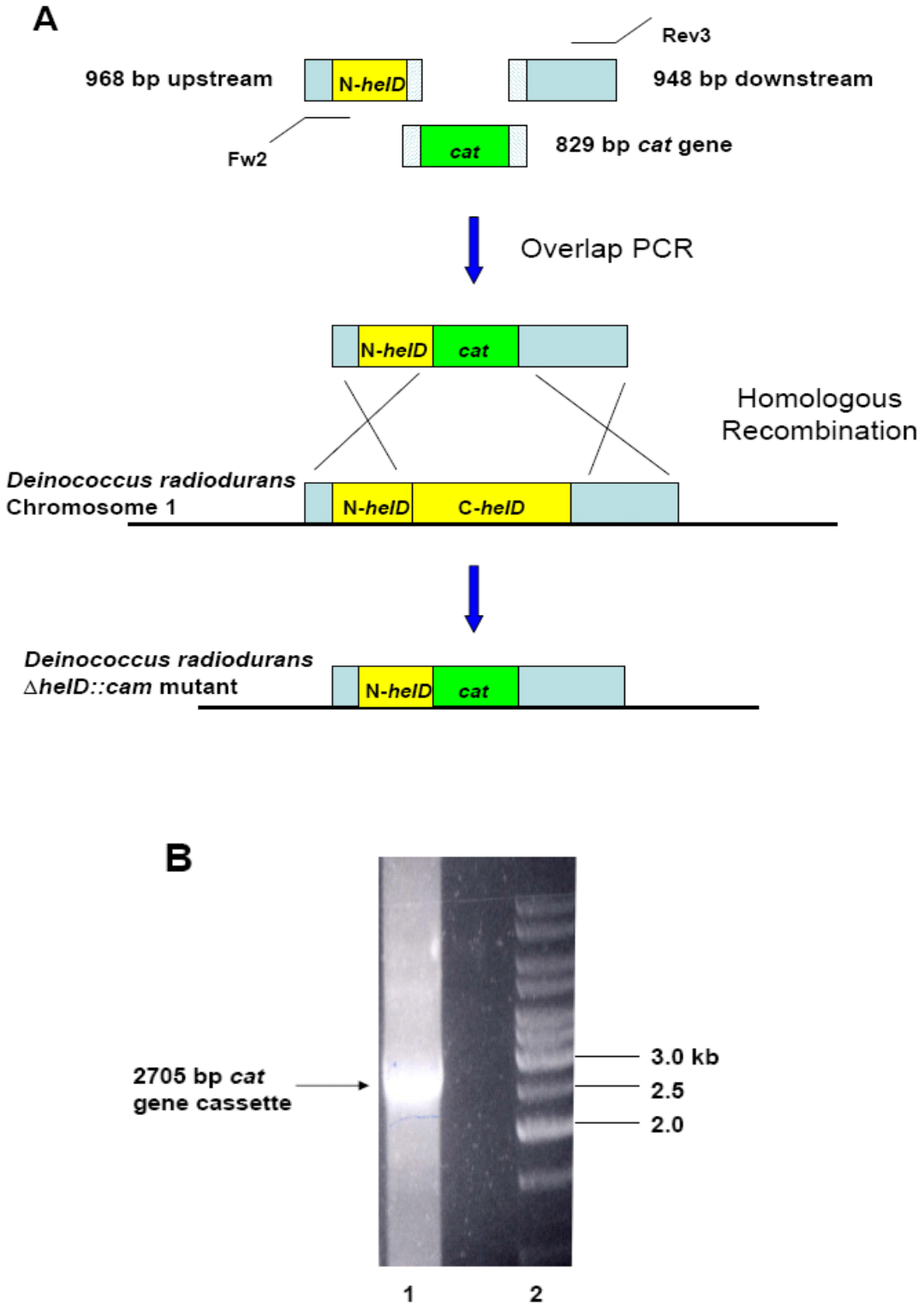

Figure 2.4 Construction of Δ*helD::cam* mutant via homologous recombination. (A) Schematic view of the strategy and major steps involved in Δ*helD::cam* mutant construction. (B) The image of 2705 bp cat gene cassette generated by overlap PCR on 0.8% agarose gel. Lane 1: overlap PCR product; lane 2: Fermentas 1 kb ladder.

The genotype of the resulting Δ*helD::cam* mutant was verified by PCR reactions with two different sets of primers as shown in figure 2.5 A. Primers Fw2 and Rev3 are complementary to the 5' end of the *helD* gene upstream fragment and the 3' end of the downstream fragment, respectively. In PCRs with Fw2 and Rev3, the size of the product amplified from *D. radiodurans* wild type genomic DNA is 3.6 kb while the product from *helD* mutant is 2.7 kb. The other set of primers used for *helD* mutant genotyping were UvrD mid and Rev3. In PCRs with UvrD mid which anneals to the internal region the *helD* gene and Rev3, only the reaction with wild type genomic DNA can produce a 2.1 kb product and no product is expected from *helD* mutant. As shown in figure 2.5 B and C, on the left gel, the expected bands of 3.6 kb from wild type and 2.7 kb from *helD* mutant were observed. On the right gel, there was a single band with expected size of 2.1 kb from wild type PCR mixture and no products at all can be seen from lane 3 (PCR from *helD* mutant). The results suggest that all the *helD* genes from the multiple copies of the *D. radiodurans* chromosomes have been completely replaced by the *cat* gene.

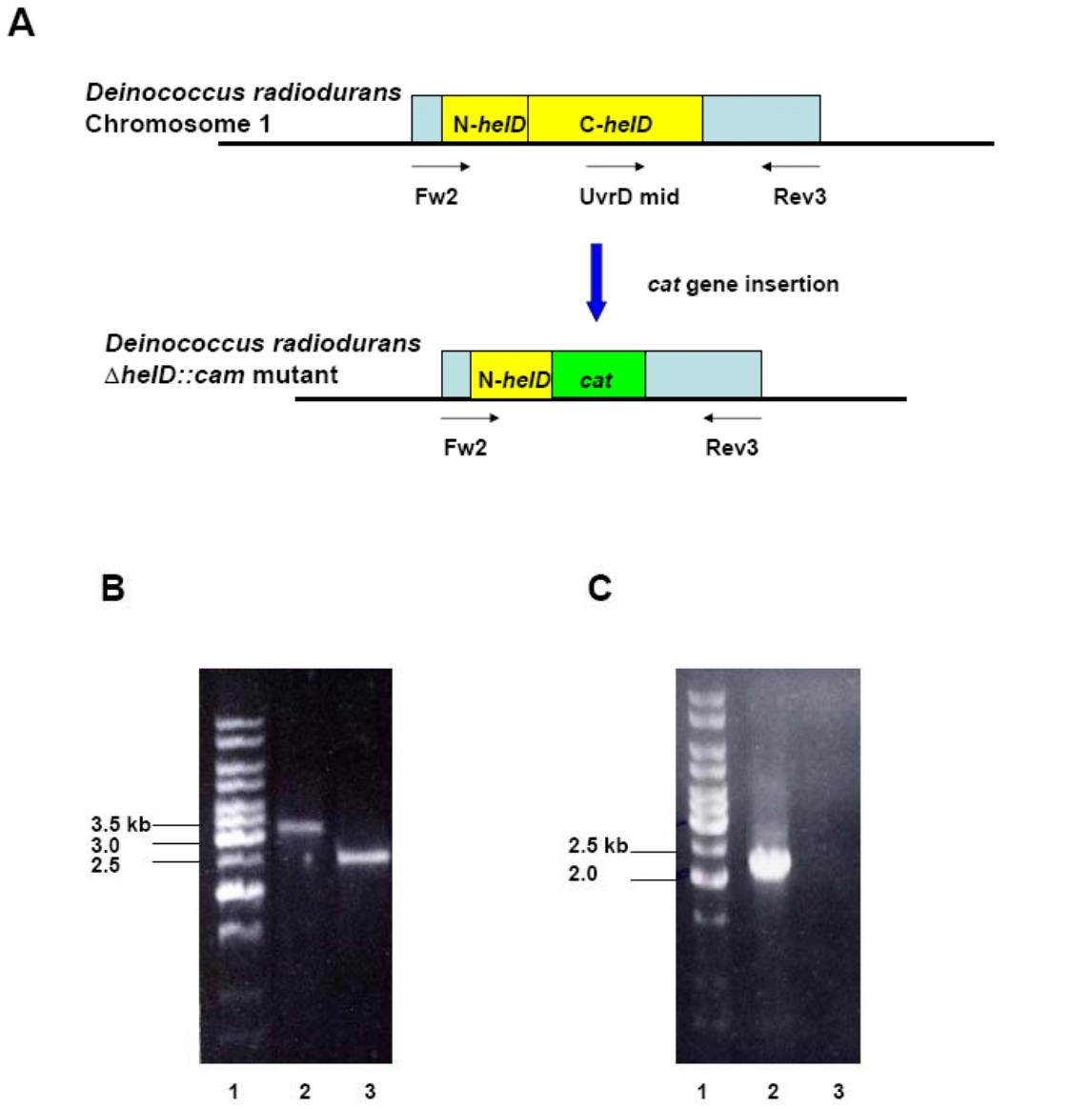

Figure 2.5 PCR genotyping of Δ*helD::cam* mutant. (A) Schematic view of wild type *helD* gene and the Δ*helD::cam* mutation in *D. radiodurans* chromosome 1, including primers used for PCR genotyping. (B) Images of PCR genotyping products using primers Fw2 and Rev3 on 0.8% agarose gel. Lane 1: 1 kb ladder; lane 2: template DNA from wild type strain; lane 3: template DNA from *helD* mutant. (C) Images of PCR genotyping products using primers UvrD mid and Rev3 on 0.8% agarose gel. Lane 1: 1 kb adder; lane 2: template DNA from wild type strain; lane 3: template DNA from *helD* mutant.

2.3.3 Genotyping of *D. radiodurans* Δ*helD::cam* Mutant by Southern Blots

Due to the polyploid nature of the bacterium, southern blotting, which can tell more information about the mutants genotypes than PCR, was employed to detect any remaining wild type *helD* gene in *D. radiodurans* chromosomes. The genomic DNA isolated from the wild type BAA-816 strain and *helD* mutant strain were digested separately with two different restriction endonucleases and one pair of restriction endonucleases. The enzymes used for single digestion were *EcoR*I and *Apa*I; the enzymes used for double digestion were *BamH*I and *Sca*I (figure 2.6 A and B). The two DIG-labeled probes generated by PCR were the 1.6 kb *helD* fragment (*helD* probe) and the 0.9 kb *cat* gene fragment (*cat* probe). Genomic DNA digested with selected restriction enzymes and hybridized with a proper probe could produce very different probing bands as shown in figure 2.6 A.

In the southern blot of wild type genomic DNA hybridized with a *helD* probe (figure 2.6 C), the probed bands with expected sizes were found on the blot. The digestions with *BamH*I and *Sca*I result in a 20 kb band and with *Apa*I result in a 8.2 kb band. The *EcoR*I digestion should produce 3.5 kb and 8.4 kb probed fragments. From the actual blot image, 8.4 kb band was much weaker than 3.5 kb band. It could be caused by the fact that the *helD* probe has much longer complementary region to the 3.5 kb band than to the 8.4 kb fragment. On the same southern blot, the *helD* probe did not hybridize to any digestion product from the *helD* mutant genomic DNA, indicating that no residual wild type *helD* gene existed in *helD* mutant.

In the southern blot hybridized with a *cat* probe (figure 2.6 D), different bands with expected sizes were found in the lanes from digestions of *helD* mutant genomic DNA with selected enzymes. A 9.1 kb band in lane 1 from *EcoR*I digestion and a 4.8 kb band in lane 2 from *Apa*I digestion are observed on the blot. The 2.6 kb band from *BamH*I and *Sca*I digestion in lane 4 could be also be identified although the image is a little fuzzy. The *cat* probe should not be able to hybridize to any digestion products of wild type genomic DNA in which there was no complementary region to this foreign gene. As a result, the two bands (one was well above 10 kb and the other was around 5 kb) found in wild type genomic DNA digestion lanes should result from some non-specific interaction with the *cat* probe.

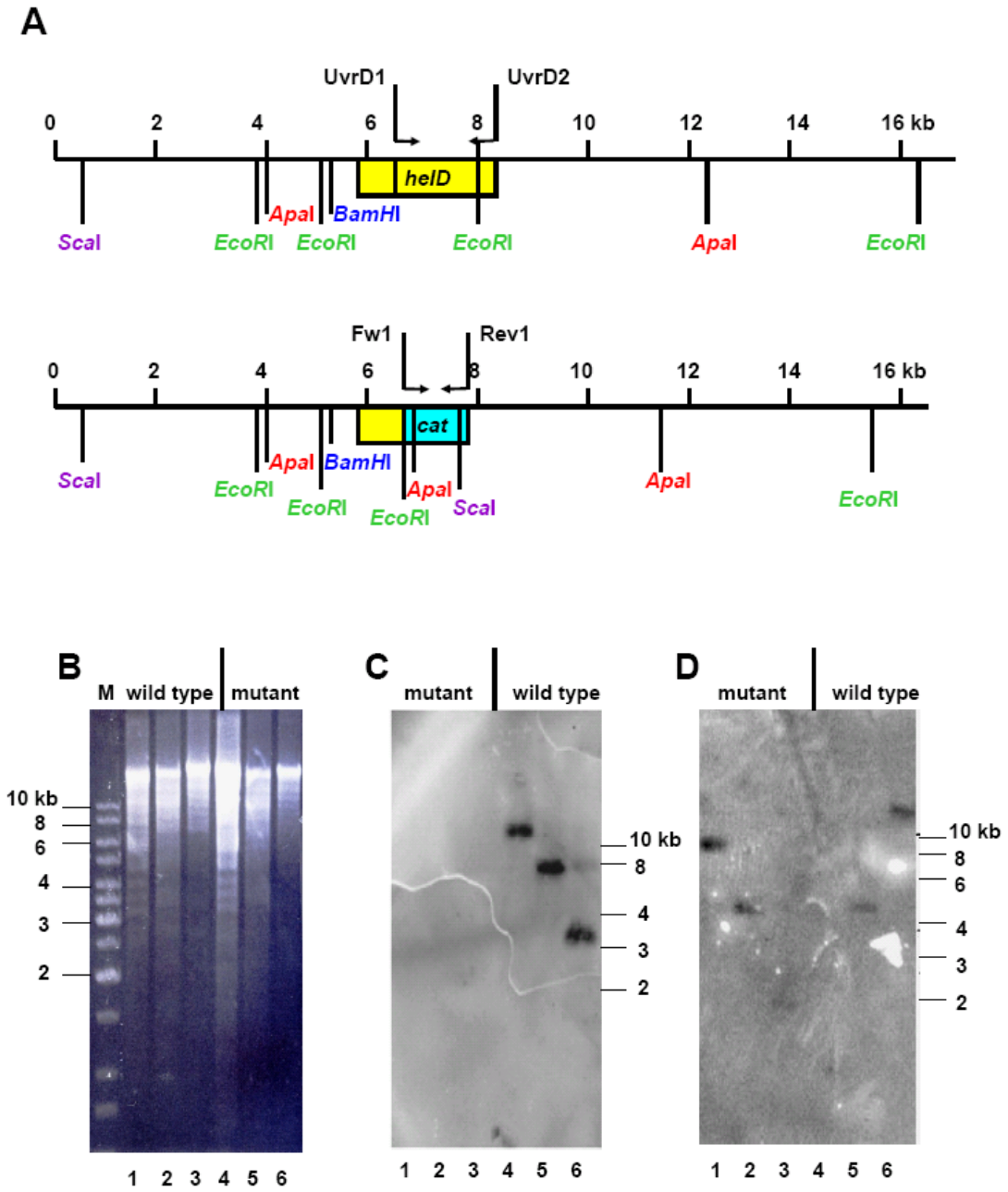

Figure 2.6 Southern blots of wild type D. radiodurans and Δ*helD::cam* mutant. (A) Schematic of wild type *D. radiodurans* and the Δ*helD::cam* mutant at *helD* locus, including primers used for DIG-labeled probe synthesis. (B) Image of 5 µg digested genomic DNA from wild type strain (lane 1-3) and Δ*helD::cam* mutant (lane 4-6) on 1.0% agarose gel. Lane M: 1 kb Fermentas ladder; lane1,4: digestion with *BamH*I and *Sca*I; lane 2,5: digestion with *Apa*I; lane 3,6: digestion with *EcoR*I. (C) Southern blot of genomic DNA from Δ*helD::cam* mutant (lane 1-3) and wild type strain (lane 4-6) probed with DIG-labeled 1.6 kb *helD* fragment. Lane 1,4: digestion with *BamH*I and *Sca*I; lane 2,5: digestion with *Apa*I; lane 3,6: digestion with *EcoR*I. (D) Southern blot of genomic DNA from Δ*helD::cam* mutant (lane 1-3) and wild type strain (lane 4-6) probed with DIG-labeled 890 bp *cat* gene. Lane 1,4: digestion with *EcoR*I; lane 2,5: digestion with *Apa*I; lane 3,6: digestion with *BamH*I and *Sca*I.

2.3.4 Growth Assay

The growth of *helD* mutant in liquid TGY medium with or without 5 μg/ml chloramphenicol was compared to wild type strain. The *helD* mutant culture with or without antibiotic grew at about the same rate as the *D. radiodurans* wild type BAA-816 strain (figure 2.7), and they reached almost the same cell density (measured by OD_{600}) at the end of the growth curves. The *helD* mutant growth with chloramphenicol had little effect compared with the *helD* mutant growth curve without antibiotic. Plating results showed similar colony numbers for both wild type and *helD* mutant strains at matched cell densities. Genotypes for both the wild type and mutant maintained unchanged compared to their genotypes before the growth assay based on PCR (data not shown).

2.3.5 *In Vivo* Biological Survival Assays with Treatments of Gamma Irradiation, UV Irradiation, Hydrogen Peroxide, Methyl Methanesulfonate and Mitomycin C.

The *helD* mutant and wild type D. radiodurans strains were compared under the treatments of various DNA damaging agents.

In three biological survival tests using gamma irradiation (figure 2.8), UV irradiation (figure 2.9) and MMC (figure 2.10), the *helD* mutant is as resistant as the wild type to these agents and they both exhibited a shoulder of resistance. Gamma irradiation can directly and indirectly cause various types of damage to DNA, including base damage, single strand and double strand breaks (19). DNA lesions introduced by UV and MMC can also lead to double strand breaks (DSBs) when DNA replication forks encounter these lesions (18). In bacteria like *E. coli*, one of the most important DSB repair pathways is homologous recombination repair. The fact that *helD* mutant is not sensitive to the

DNA damaging agents (especially gamma irradiation) indicated that the *helD* gene and its protein do not play an essential role in DSB repair.

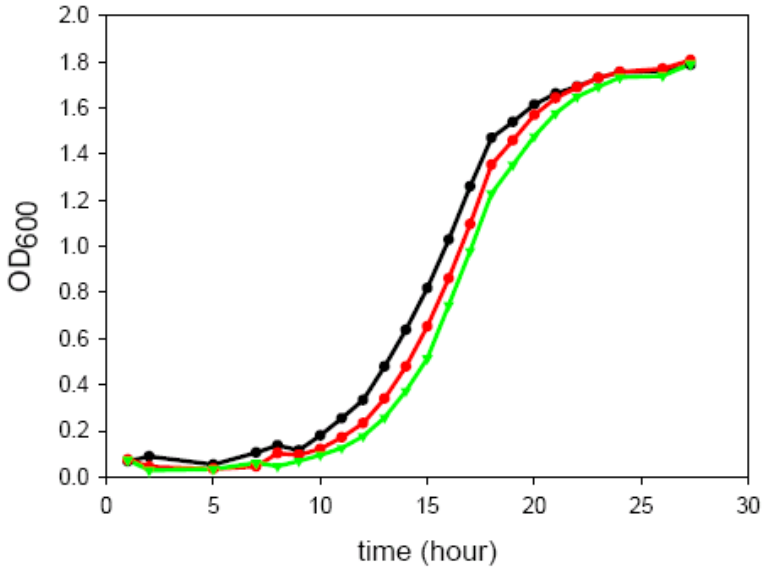

Figure 2.7 Growth curves of wild type and Δ*helD::cam* mutant *D. radiodurans* strains. Cells were grown at 30°C in TGY medium, with or without 5 μg/ml chloramphenicol for the mutant. Samples were removed at the indicated times, and the OD_{600} was measured. Black dots, wild type strain BAA-816; red dots, *helD* mutant grown without chloramphenicol; green triangles, *helD* mutant grown with chloramphenicol. Results are from one experiment with single OD_{600} determination.

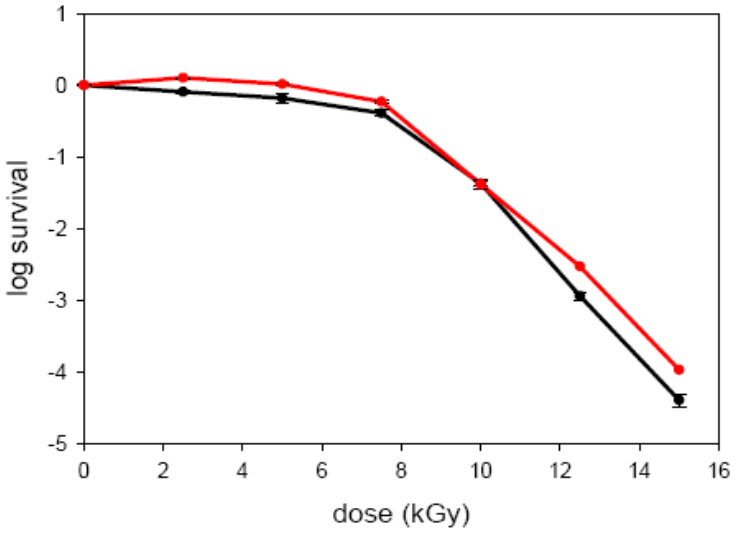

Figure 2.8 Sensitivity of wild-type and Δ*helD::cam* mutant *D. radiodurans* strains to gamma irradiation. Gamma irradiation was performed on ice, from a ^{60}Co source at 2.5 kGy/hour, for indicated doses. Black dots, wild type strain BAA-816; red dots, *helD* mutant. Results are from one experiment, with error bars generated from three independent determinations (triplicate plating results). The whole experiment was performed twice with comparable results.

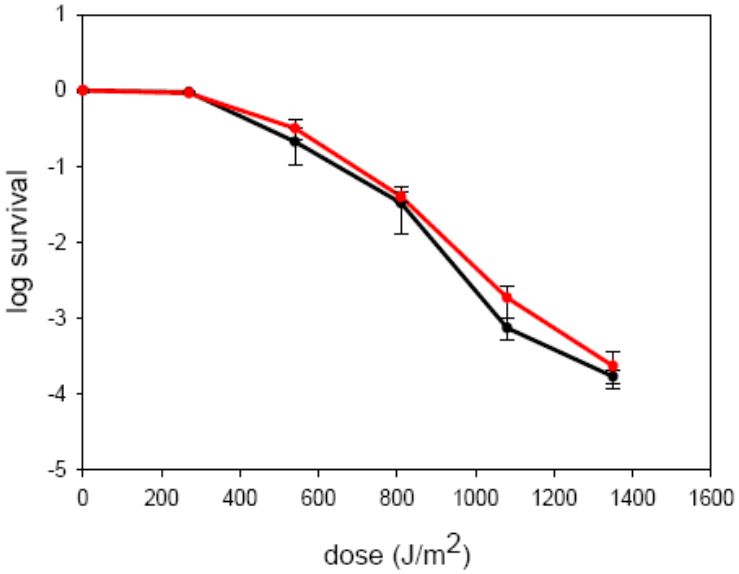

Figure 2.9 Sensitivity of wild-type and Δ*helD::cam* mutant *D. radiodurans* strains to UV irradiation. Cells grown to exponential phase were spread onto TGY plates and irradiated with UV light from a germicidal lamp at 90 J/m^2/min. Black dots, wild type strain BAA-816; red dots, *helD* mutant. Results are from one experiment, with error bars generated from three independent determinations (triplicate plating results). The whole experiment was performed three times with comparable results.

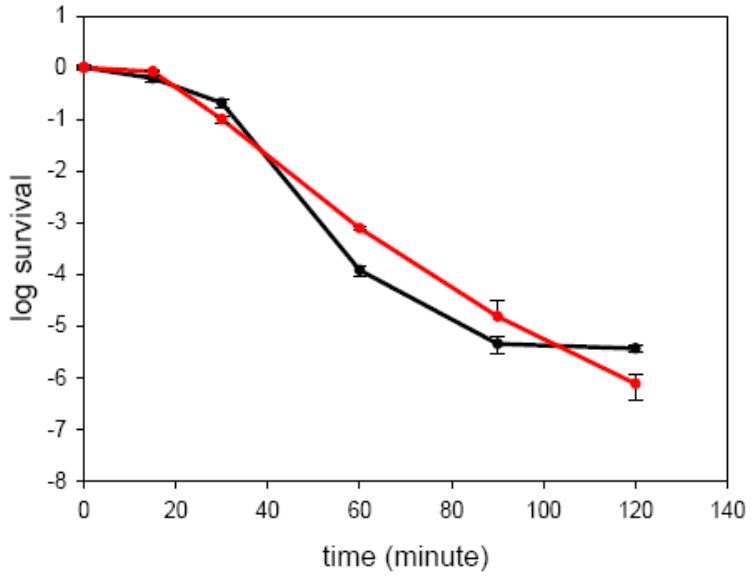

Figure 2.10 Sensitivity of wild-type and Δ*helD::cam* mutant *D. radiodurans* strains to MMC. Cells were treated with 10 μg/ml MMC for indicated times, serially diluted and plated on TGY agar plates. Black dots, wild-type strain BAA-816; red dots, *helD* mutant. Results are from one experiment, with error bars generated from three independent determinations (triplicate plating results). The whole experiment was performed twice with comparable results.

In the survival assays with hydrogen peroxide (figure 2.11) and MMS (figure 2.12), the *helD* mutant exhibited somewhat higher sensitivity compared to the wild type BAA-816 strain. Hydrogen peroxide is an oxidant and can function as a precursor of hydroxyl radical, which is capable of causing DNA base damage and single and double strand breaks. MMS methylates DNA bases at several positions and produces lesions that can also lead to double strand breaks by blocking replication fork progression (95). The sensitivity of *helD* mutant to MMS indicates that the protein encoded by *helD* may act in processing stalled replication forks.

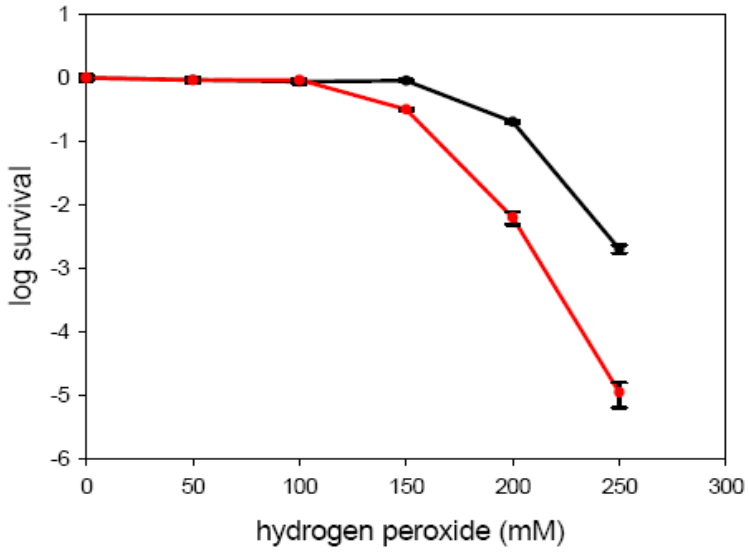

Figure 2.11 Sensitivity of wild-type and Δ*helD::cam* mutant *D. radiodurans* strains to hydrogen peroxide at 30°C. Cells were treated with hydrogen peroxide for one hour without shaking at 30°C, serially diluted and plated on TGY agar plates. Black dots, wild-type strain BAA-816; red dots, *helD* mutant. Results are from one experiment, with error bars generated from three independent determinations (triplicate plating results). The whole experiment was performed five times with comparable results.

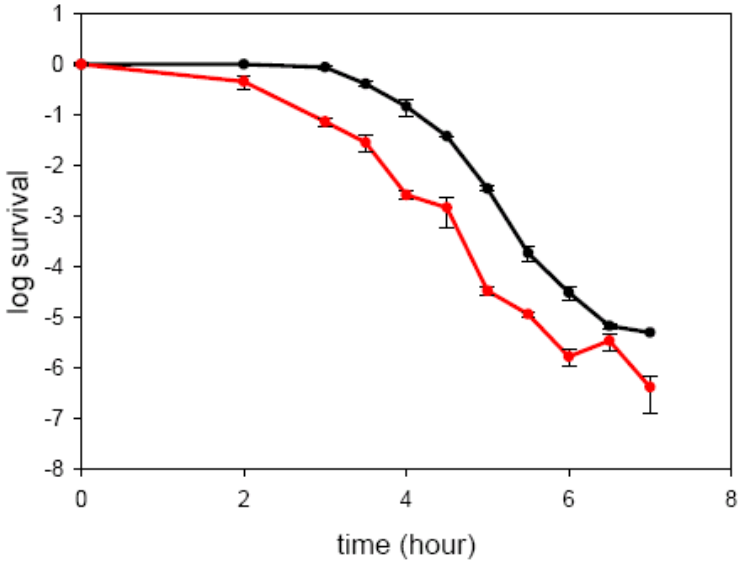

Figure 2.12 Sensitivity of wild-type and Δ*helD::cam* mutant *D. radiodurans* strains to MMS. Cells were treated with 30 mM MMS for indicated times, serially diluted and plated on TGY agar plates. Black dots, wild-type strain BAA-816; red dots, *helD* mutant. Results are from one experiment, with error bars generated from three independent determinations (triplicate plating results). The whole experiment was performed three times with comparable results.

2.3.6 Construction of Full Length and Truncated HelIV Expression Plasmids

The HelIV expression plasmids were constructed with two inserts: the 2.3 kb *helD* gene (the start TTG codon was modified to ATG by primer UvrD top in PCR) encompassing the entire HelIV coding sequence and the 1.6 kb *helD* gene fragments corresponding to the C-terminal region of the HelIV. Both of the 2.3 kb and 1.6 kb *helD* gene inserts were cloned (from the wild type BAA-816 strain) into PCRblunt vector (Invitrogen) followed by sequencing with three primers as described in Materials and Methods. The cloning plasmids PCRblunt-2.3kHelIV and PCRblunt-1.6kHelIV were digested with *Nde*I and *BamH*I and the two inserts were ligated into the 5.7 kb expression vector pET15b (Novagen) linearized by the same enzymes. The resulting expression plasmids pET15b-2.3kHelIV (encoding 83 kDa full HelIV) and pET15b-1.6kHelIV (encoding 59 kDa truncated HelIV) were confirmed by double digestion of *Nde*I and *BamH*I as shown in figure 2.13.

2.3.7 Expression and Purification of Two Forms of HelIV

Initial expression levels of the 83 kDa and 59 kDa HelIV tested in *E. coli* strain BL21(DE3) induced by IPTG were relatively low (data not shown). The expression yields were significantly improved by expressing the HelIV proteins in *E. coli* strain Rosetta2(DE3) and in auto-induction medium ZYP-5052 (figure 2.14 A). The *E. coli* strain Rosetta2(DE3) supplies tRNAs for some rare codons on a compatible chloramphenicol resistant plasmid. With the auto-induction ZYP-5052 medium, cultures need only be inoculated and grown to saturation, and yields of target protein are typically

several-fold higher than obtained by conventional IPTG induction based on the other proteins that have been tested (92).

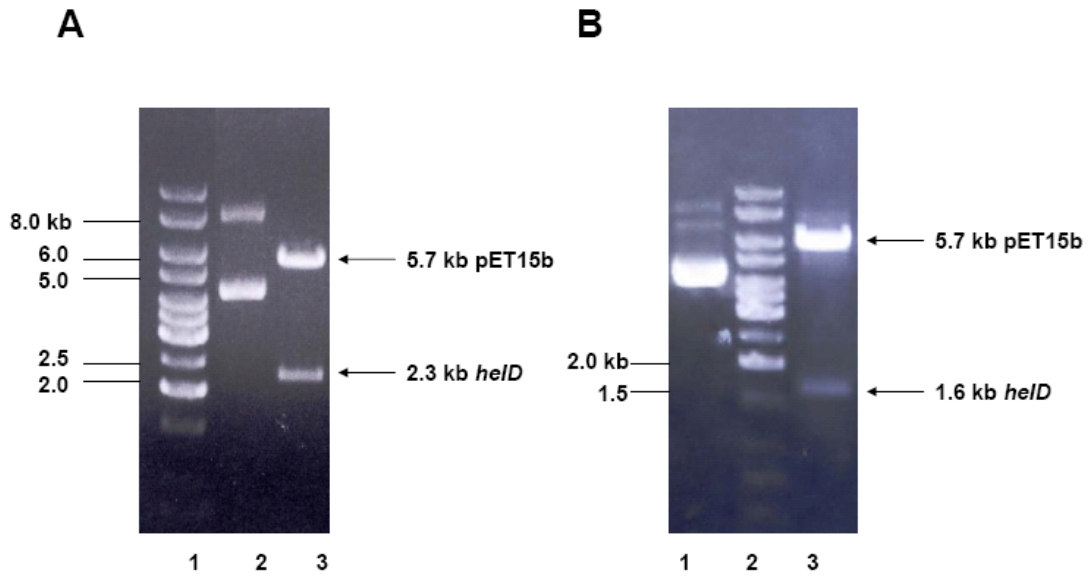

Figure 2.13 HelIV expression plasmids and their digestion products with *Nde*I and *BamH*I on 0.8% agarose gels. (A) Lane 1: 1 kb Fermentas ladder; lane 2: undigested plasmid pET15b-2.3kHelIV; lane 3: pET15b-2.3kHelIV digestion products wth *Nde*I and *BamH*I. (B) Lane 1: undigested plasmid pET15b-1.6kHelIV; lane 2: 1 kb Fermentas ladder; lane 3: pET15b-1.6kHelIV digestion products wth *Nde*I and *BamH*I.

The majority of expressed target proteins were soluble (figure 2.14 A), which was convenient for later multi-step purification procedures. The first purification step of the N-terminal His-tagged 83 kDa HelIVwas a nickel column. The protein bound relatively tightly, so it was not eluted off the column until the imidazole concentration reached or was greater than 200 mM, as shown in figure 2.14 B. Most of the host proteins from *E.*

coli cells were washed off the column during the wash step with 20 column volumes of 60 mM imidazole in native loading buffer. The eluted 83 kDa HelIV protein was collected and dialyzed against the native loading Buffer A used for the second column step. After overnight dialysis, a large fraction of the total 83 kDa HelIV protein was precipitated. After removal of the precipitate, the remaining soluble HelIV protein was further purified via a single-strand DNA cellulose column. As shown in figure 2.15, the majority of 83 kDa HelIV protein was eluted with 300 mM NaCl in Buffer A. Compared to another *D. radiodurans* helicase, RecD (which requires at least 0.6M NaCl to be washed off the same type of column), the full length HelIV protein does not bind to the ssDNA on the column very tightly. After elution from the ssDNA column, the 83 kDa HelIV protein from fraction tubes containing relatively low NaCl (300 mM) were pooled and concentrated for later biochemical assays.

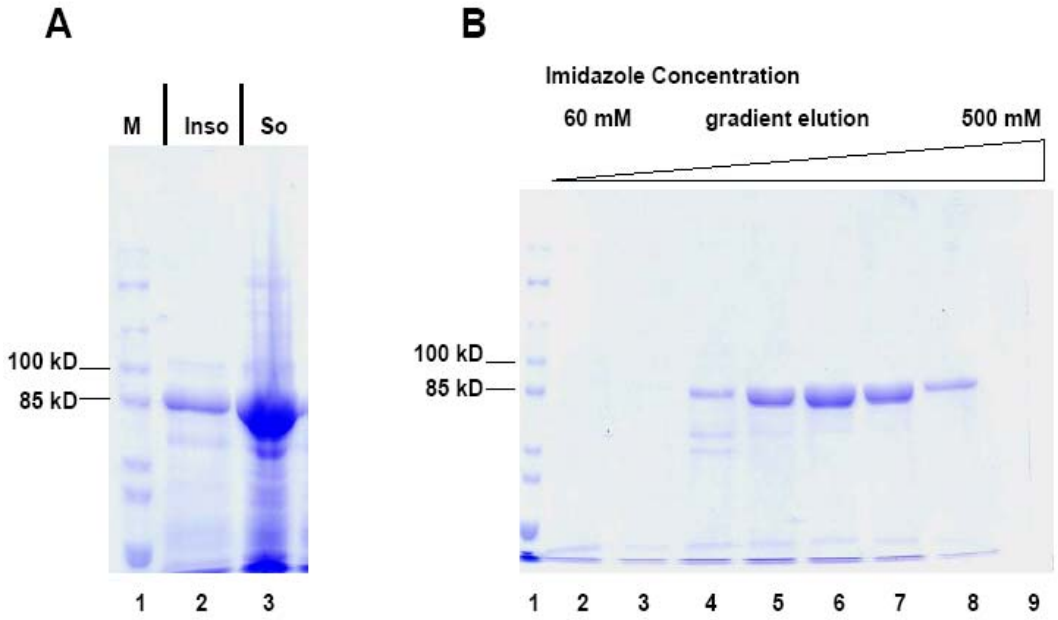

Figure 2.14 10% SDS-PAGE gels for the solubility test of N-terminal His-tagged 83 kDa HelIV and its elution fractions from a nickel column. (A) SDS-PAGE of HelIV solubility test (the samples were prepared as described in Materials and Methods). Lane 1: Fermentas Pageruler unstained protein maker; lane 2: insoluble portion after sonication; lane 3: soluble portion after sonication. (B) N-terminal His-tagged 83 kDa HelIV nickel column elution fractions analyzed on a 10% SDS-PAGE. Lane 1: Fermentas unstained protein marker; lane 2-9: elution fractions 1-8 (corresponding to imidazole gradient from 60 mM to 500 mM).

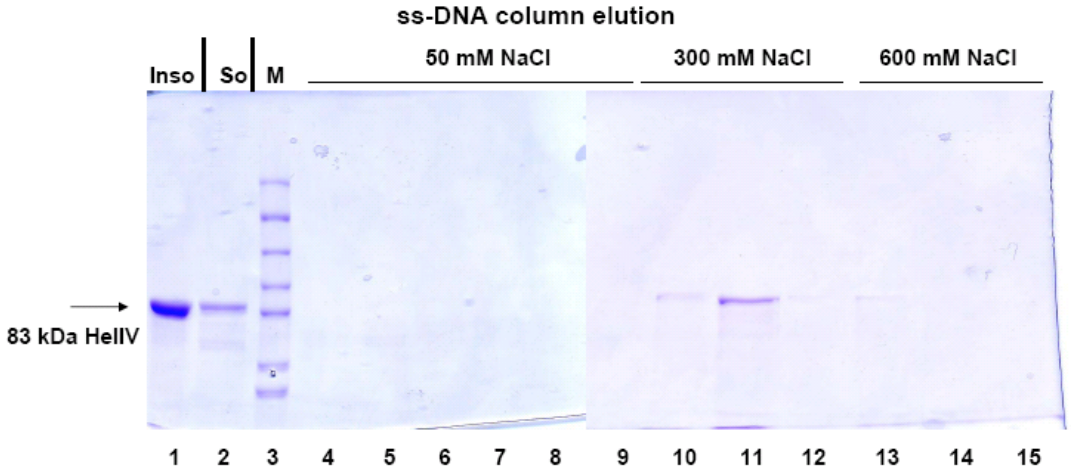

Figure 2.15 10% SDS-PAGE gels for the N-terminal His-tagged 83 kDa HelIV from a ssDNA column. The fractions containing 83 kDa HelIV protein from nickel column were collected and dialyzed against Buffer A containing 50 mM NaCl. The precipitated proteins were removed by centrifugation after overnight dialysis and the soluble portion was applied to a 5-ml ss-DNA column. The ss-DNA column was washed and eluted as described in Materials and Methods. Lane 1: the insoluble portion after overnight dialysis; lane 2: the soluble HelIV applied to ss-DNA after dialysis; lane 3: Fermentas unstained protein marker; lane 4-9: wash with 50 mM NaCl; lane 10-12: wash with 300 mM NaCl; lane 13-15: wash with 600 mM NaCl.

For the purification of the 59 kDa truncated HelIV, a similar two-step purification strategy was employed. After the first step nickel column, the fractions containing 59 kDa HelIV protein were pooled and dialyzed against Buffer A with no NaCl added. In this dialysis step, NaCl needs to be excluded from the dialysis buffer for two reasons: first, 59 kDa HelIV binds to the following ssDNA column so weakly that even in 50 mM NaCl the protein sample could cause significant decrease of column binding affinity (data not shown); second, the 59 kDa HelIV is much more stable in Buffer A with no salt (no detectable precipitation formed after dialysis) than the full length protein. As shown in figure 2.16, even when the protein sample was prepared in Buffer A without salt, quite

large amount of 59 kDa HelIV were still found in the loading flow through or in the no-salt wash fractions because of the protein's low affinity for the ssDNA column. The remaining 59 kDa HelIV protein bound to the ssDNA column was eluted with a NaCl concentration between 50 to 100 mM. Given its high purity and concentration, 59 kDa HelIV fractions from the ssDNA column were used directly for biochemical assays without any further concentration step.

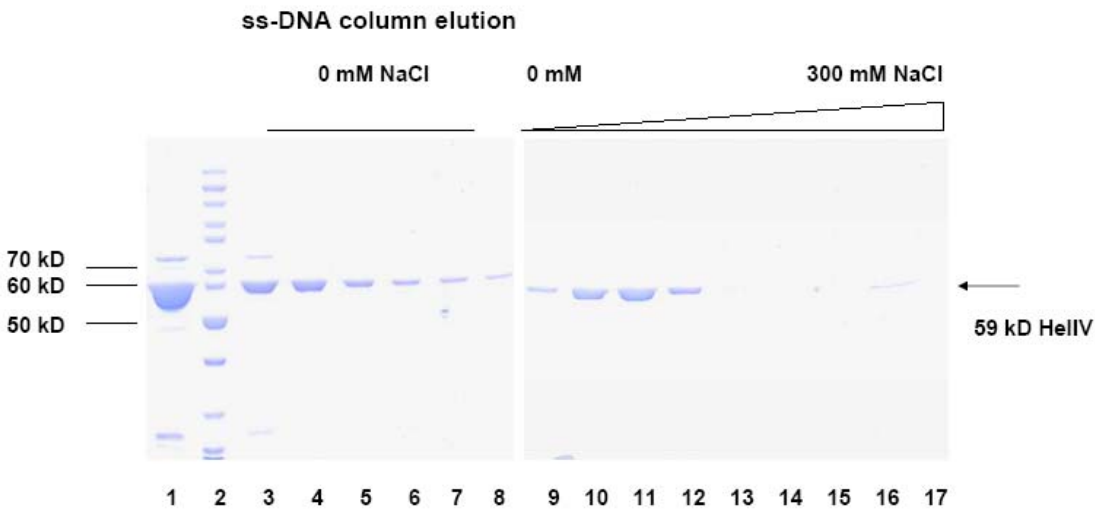

Figure 2.16 10% SDS-PAGE gels for N-terminal His-tagged 59 kDa HelIV from a ssDNA column. The fractions containing 59 kDa HelIV protein from nickel column were collected and dialyzed against Buffer A (no salt added). Since no precipitation occurred after overnight dialysis, the dialyzed 59 kDa HelIV was directly applied to a 5-ml ssDNA column followed by washing with Buffer A (no salt) and elution with a gradient of NaCl in Buffer A as described in Materials and Methods. Lane 1: 59 kDa HelIV used for ssDNA column; lane 2: Fermentas unstained protein marker; lane 3: loading flowthrough; lane 4-9: wash with Buffer A (no salt); lane 9-17: elution with a 0 mM – 300 mM NaCl gradient in Buffer A.

2.3.8 N-Terminal His Tag Removal by Thrombin Cleavage.

On both of the 83 kDa and 59 kDa HelIV proteins expressed in pET15b vector, there is a 20 amino acid leader peptide preceding the N terminal start codon: Met-Gly-Ser-Ser-His-His-His-His-His-His-Ser-Ser-Gly-Leu-Val-Pro-Arg-Gly-Ser-His. The His-tags were moved from both proteins by thrombin digestion as described in Materials and Methods, which left a Gly-Ser-His tripeptide at the N-terminus of each protein. Cleavage of the His-tags was verified by analysis on 10% SDS-PAGE and by western blotting using anti-His-tag monoclonal antibody. As shown in figure 2.17, after cleavage, the un-tagged 83 kDa HelIV protein was not detected on the western blot (data not show for 59 kDa His-tag removal).

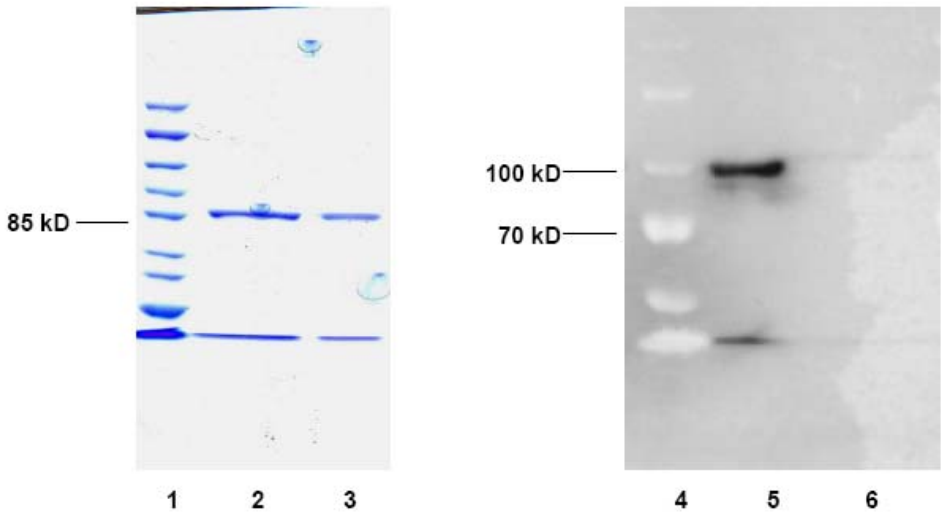

Figure 2.17 83 kDa HelIV His-tag removal by thrombin protease on 10% SDS-PAGE (lane 1-3) and western blots (lane 4-6) using anti-His-tag antibody. Lane 1: Fermentas unstained protein make; lane 4: Fermentas pre-stained protein maker; lane 2, 5: N-terminal His-tagged 83 kDa HelIV protein; lane 3, 6: un-tagged 83 kDa HelIV (His-tag removed by thrombin).

2.3.9 ATPase Assay

In all the *in vitro* biochemical assays of *D. radiodurans* HelIV including ATPase assays discussed in this section and the helicase assays in the next section, the 83 kDa HelIV protein refers to N-terminal His-tagged 83 kDa HelIV and the 59 kDa HelIV refers to un-tagged 59 kDa HelIV, unless otherwise stated.

Both of the 83 kDa and 59 kDa HelIV were tested for their ATPase activities as described in Materials and Methods. As shown in figure 2.18, both proteins exhibited ATP hydrolysis activity in the presence of 10 μM 30-nt ssDNA.

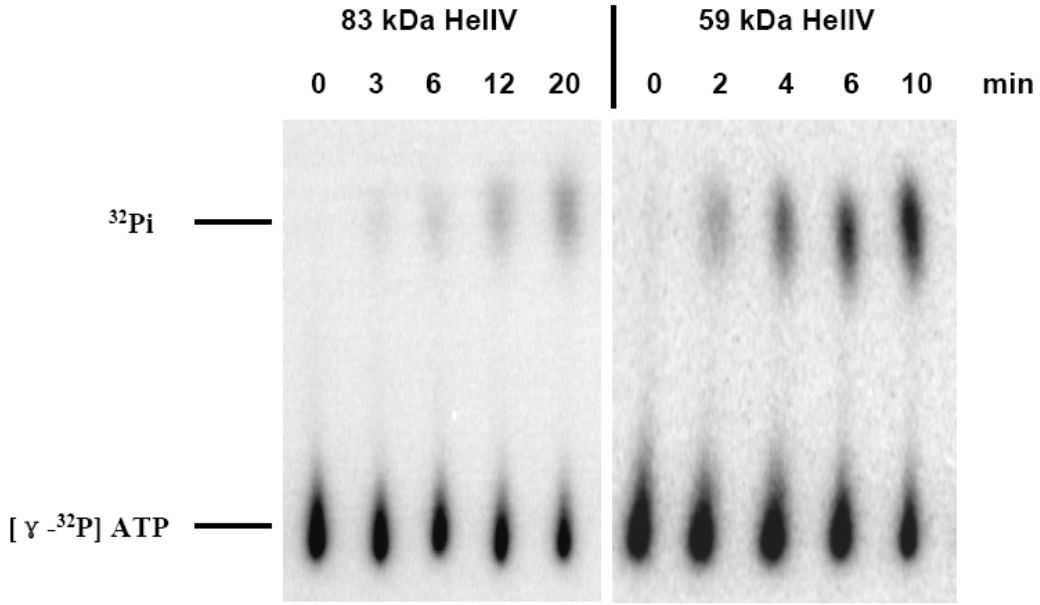

Figure 2.18 ATP hydrolysis at 30°C by 83 kDa HelIV and 59 kDa HelIV on TLC plates. Reaction mixtures contained 50 mM Tris-HCl, pH 7.5, 2 mM $MgCl_2$, 10 μM 30-nt ssDNA, 1 mM DTT, 5% glycerol, 0.1 mg/ml BSA, 250 μM ATP (mixed with 1% [γ-^{32}P] ATP), 0.12 μM 83 kDa HelIV or 0.09 μM 59 kDa HelIV.

Under standard reaction conditions, the ATP substrate (250 μM) was in large excess over HelIV (0.12 μM for 83 kDa HelIV and 0.09 μM for 59 kDa HelIV). We plotted the fraction of ATP hydrolyzed during time course (figure 2.19). It is found that during the reaction time (30 minutes for 83 kDa HelIV and 10 minutes for 59 kDa HelIV), nearly linear curves were observed for each time course reaction, indicating the reaction rate was unchanged. The slope of the plotted data in each time course was determined by linear regression to calculate the reaction rate (figure 2.19 and Table 4). From the plotted time course and the calculated reaction rate table, we can tell that with the presence of ssDNA, the ATPase activity of the 83 kDa HelIV protein was only moderately stimulated (around 20% increase). The ATPase activity of 59 kDa HelIV proteins was not affected by the presence of ssDNA. Under standard conditions, the reaction rate of the truncated HelIV was about 8-10 fold higher than that of the full length HelIV.

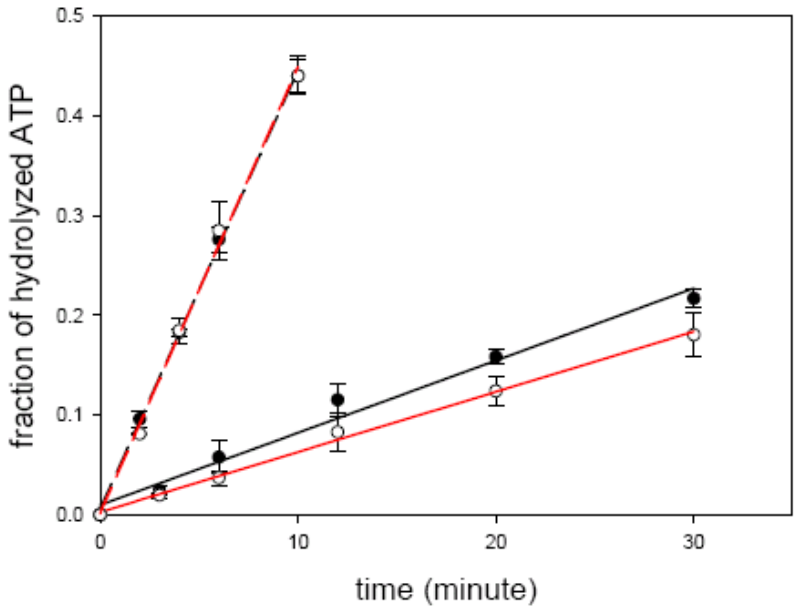

Figure 2.19 ATP hydrolysis by the two forms of HelIV proteins and calculation of reaction rates. Reactions contained 0.12 μM 83 kDa HelIV or 0.09 μM 59 kDa HelIV. ATP hydrolysis was carried out in time course, with or without 10 μM ssDNA. The slopes for each time course reaction were determined using linear regression (SigmaPlot software). Black dots and solid line, 83 kDa HelIV ATP hydrolysis with ss-DNA; red dots and solid line, 83 kDa HelIV ATP hydrolysis without ssDNA; black dots and dashed line, 59 kDa HelIV ATP hydrolysis with ssDNA; red dots and dashed line, 59 kDa HelIV ATP hydrolysis without ssDNA. Results are from one experiment with error bars generated from three independent determinations (triplicate-reaction results). The whole experiment was performed three times with comparable results.

Table 4 Calculation of ATP hydrolysis rate for HelIV

	Enzyme concentration (μM)	Slope by linear regression (min^{-1})	Reaction rate [a] mol Phosphate /(mol enzyme*min)
83 kDa HelIV with ssDNA	0.12	0.0076 ± 0.0004	16 ± 0.8 [b]
83 kDa HelIV without ssDNA	0.12	0.0069 ± 0.0020	14 ± 4 [b]
59 kDa HelIV with ssDNA	0.09	0.0439 ± 0.0021	122 ± 5 [c]
59 kDa HelIV without ssDNA	0.09	0.0448 ± 0.0022	124 ± 6 [c]

[a] Reaction rate is calculated in the following equation:
Reaction rate = 250*slope/enzyme concentration.
[b] Standard deviation of three separate experiments, each of which includes triplicate reactions.
[c] Standard deviation from triplicate reactions in one experiment.

With the 83 kDa full length HelIV proteins, a number of variations in the reaction conditions were tested (Table 5) and the maximal activity was observed in the standard conditions in the presence of ssDNA. A 40% lower activity was seen with the un-tagged 83 kDa HelIV, which is the major reason why the N-terminal Hi-tagged 83 kDa HelIV was used for most of the biochemical assasys. No ATPase activity difference was found between His-tagged and un-tagged 59 kDa HelIV (data not shown).

Table 5 ATP hydrolysis activity in various conditions

Reaction conditions	Relative activity
Standard[a]	1.0[b]
Standard with un-tagged HelIV[c]	0.6
No DNA	0.6
ds circular DNA	0.8
ds linear DNA	0.4
23℃	0.5
37℃	1.1
+ 200 mM NaCl	0.4
+ 50 mM KCl	0.7
+ 1mM $MnCl_2$	0.9
pH 6.5	0.7
pH 8.5	1.1

[a] Standard reaction conditions were 50 mM Tris-HCl, pH 7.5, 2 mM $MgCl_2$, 10 μM 30-nt single-strand DNA, 1 mM DTT, 5% glycerol, 0.1 mg/ml BSA, 250 μM ATP, 0.53 μM 83 kDa HelIV, incubated at 30°C for 30 min.

[b] Activity was 8.5 mol phosphate/(mol 83 kDa HelIV * min).

2.3.10 Helicase Assay

Helicase reactions were carried out with 20 bp dsDNA molecules with either blunt ends, a 3' or 5' 12-nt single strand tail, or with a 12-nt non-complementary ssDNA fork at one end of the duplex. As shown in figure 2.1, each substrate was 5'-^{32}P-labeled at a blunt double strand end. Under the standard conditions as described in Materials and Methods, DNA unwinding was tested with both forms of HelIV proteins on all four substrates. As indicated in figure 2.20, the 83 kDa HelIV was capable of unwinding dsDNA with a 5'-ssDNA extension and a forked end. Under the same reaction conditions, there was no detectable unwinding activity in reactions with 3' tailed and blunt end substrates. As expected, the unwinding reactions with 83 kDa HelIV were ATP-dependent. In control reactions without adding ATP, no helicase activity was observed (figure 2.21). For standard reactions with 5'tailed and forked substrates in figure 2.21, the initial reaction rates were determined from the slopes of the linear part of the time curves: 5.7×10^{-5} bp/HelIV/sec (5'tailed substrate) and 2.2×10^{-4} bp/HelIV/sec (forked substrate).

In the unwinding reactions with 59 kDa HelIV, however, no detectable helicase activity was observed on any of the four dsDNA substrates (figure 2.22), indicating the N-terminal region of the 83 kDa HelIV is clearly necessary for its helicase activity.

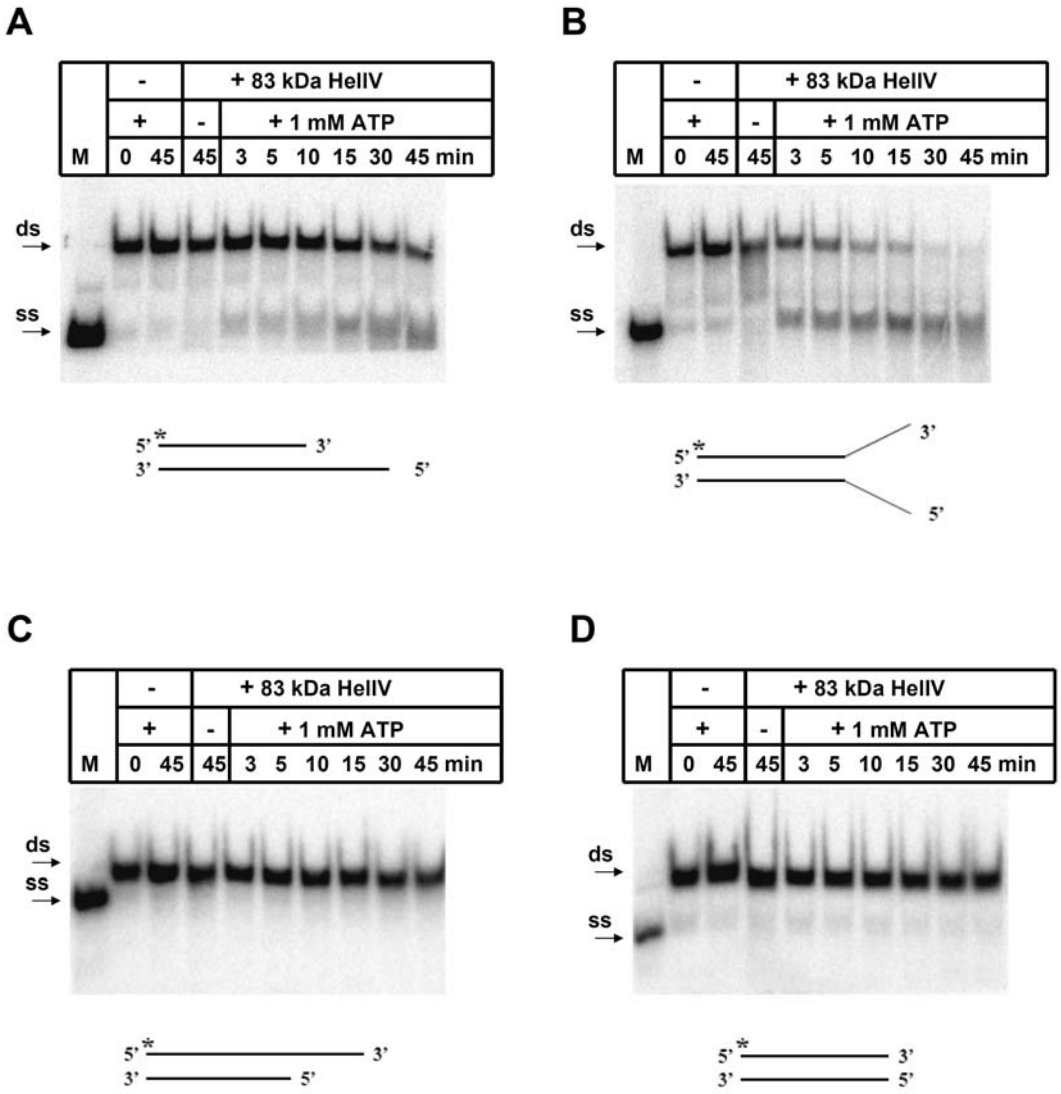

Figure 2.20 DNA unwinding by the 83 kDa full length HelIV protein. Reactions mixtures contained 50 mM Tric-HCl, pH 7.5, 2 mM $MgCl_2$, 1 mM ATP, 1 mM DTT, 0.1 mg/ml BSA, 0.12 μM HelIV protein and 1 nM of ^{32}P labeled dsDNA including 5'tailed (A), forked (B), 3'tailed (C) and blunt (D) substrates. Reactions were incubated at 30°C for the indicated time and then analyzed on native 15% polyacrylamide gels as described in Materials and Methods. Samples in the first lane of each gel were from the ^{32}P-labeled ssDNA used for annealing to each dsDNA substrates, to provide a ssDNA marker.

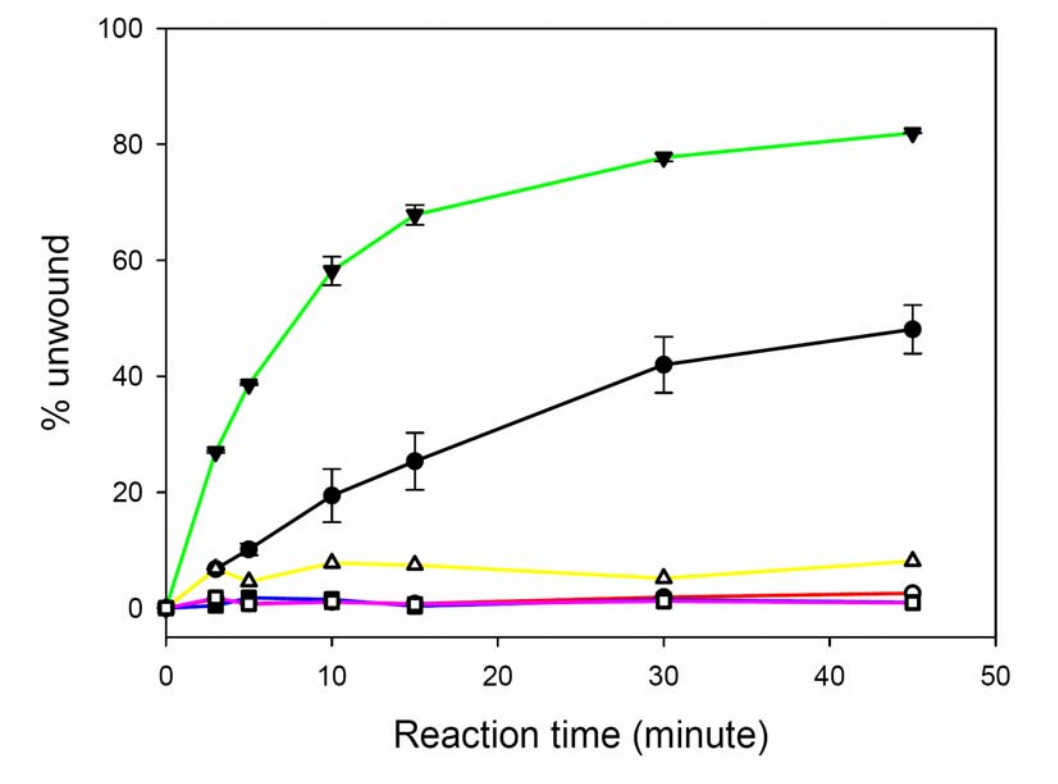

Figure 2.21 DNA unwinding reaction time courses with 83 kDa full length HelIV protein and four types of dsDNA containing different tails. Reactions containing 0.12 μM HelIV were performed under the standard conditions as described in Materials and Methods at 30°C for the indicated times, with or without 1 mM ATP. Filled circles (black line), reaction with 5'tailed dsDNA and 1 mM ATP; open circles (red line), reaction with 5'tailed dsDNA but no ATP added; filled triangle (green line), reaction with forked dsDNA and 1 mM ATP; open triangle (yellow line), reaction with forked dsDNA but no ATP added; filled square (blue line), reaction with 3'tailed dsDNA and 1 mM ATP; open square (pink line), reaction with blunt-ended dsDNA and 1 mM ATP. The results with error bars are the ranges derived from two independent experiments including one reaction in each experiment. The results without error bars are from one experiment including one reaction.

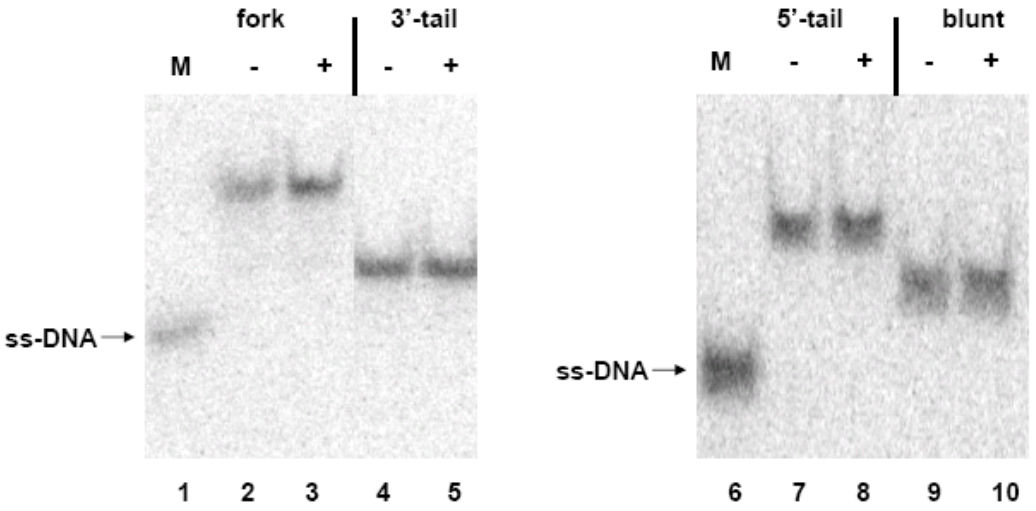

Figure 2.22 DNA unwinding by 59 kDa truncated HelIV proteins with four types of double-strand substrates containing different tails. Reactions were performed under the conditions as described in Materials and Methods at 30°C for 30 minutes. The lanes marked "+" contained 1 mM ATP and 0.8 μM truncated HelIV and the lanes marked with "-" had no HelIV added. Lane 1: ^{32}P labeled ssDNA HMC 1 (32-nt); lane 2, 3: reactions with forked dsDNA; lane 4, 5: reactions with 3'tailed dsDNA; lane 6: ^{32}P labeled ssDNA HMC 3 (20-nt); lane 7, 8: reactions with 5'tailed dsDNA; lane 9, 10: reactions with blunt-ended dsDNA.

2.3.11 DNA Binding Assay

DNA binding was tested with both of the purified HeIIV proteins as described in Materials and Methods. In the DNA binding mixtures, with or without 1 mM ATP, 1 nM 5' labeled 32-nt ssDNA (HMC 1) was mixed with various amounts of the 83 kDa HelIV (from 120 nM to 0.12 nM) and incubated at room temperature for 15 minutes. Then the DNA-protein interaction was analyzed by 15% native PAGE gels. As shown in figure 2.23 A, no DNA binding was detected for 83 kDa HelIV in any of the binding mixtures. Similar gel mobility assays were done with three other ^{32}P labeled DNA substrates (data

not shown) including a 20-nt ssDNA (HMC 3), a 5'tailed double strand (ds) DNA and a forked dsDNA (the same double-stranded substrates used in helicase assays). No DNA binding was detected with above three alternative DNA substrates. There was no detectable DNA binding in reactions with the 59 kDa HelIV either on any of the DNA substrates tested for 83 kDa protein (data not shown).

The nitrocellulose-DEAE double-filter method was also employed to detect the DNA binding of 83 kDa HelIV. In the binding mixture, 1 nM ^{32}P labeled HMC 1 and 120 nM of 83 kDa HelIV were mixed and incubated at room temperature (23°C) for 15 minutes. Then the binding mixture was applied to the vacuum based double-filtered system. DNA-protein complex can bind to the nitrocellulose membrane and free DNA will be trapped by DEAE paper. Then the radioactivity on nitrocellulose membrane and DEAE paper were quantified separately. The fraction of DNA that sticks to nitrocellulose membrane over the total DNA added could reflect the relative DNA-protein binding ability. As shown in figure 2.23 B, the fraction of DNA on nitrocellulose membrane from standard DNA binding reaction was even a little lower than that of background binding, indicating that there was no detectable DNA-HelIV binding.

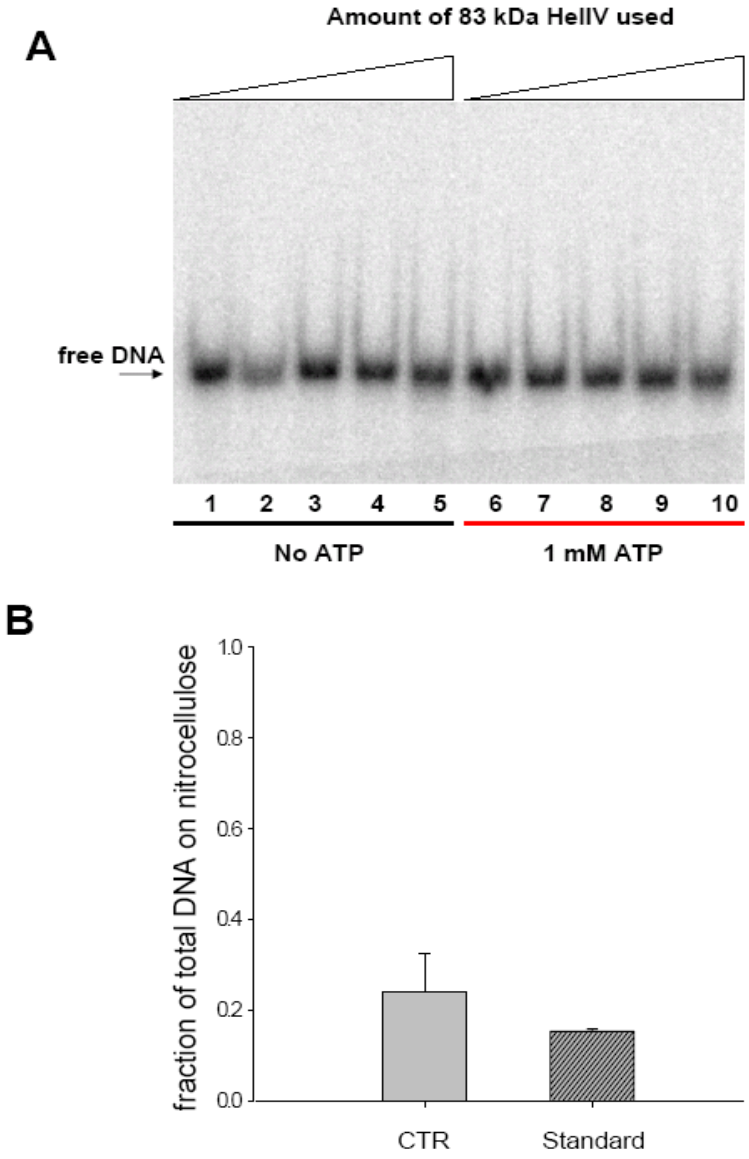

Figure 2.23 The binding of 83 kDa HelIV to ssDNA HMC 1 (32-nt). (A) DNA binding of 83 kDa HelIV was analyzed by gel mobility assay. With (lane 6-10) or without (lane 1-5) 1 mM ATP added, binding mixtures containing 1 nM ^{32}P-HMC 1 ssDNA and various amount of HelIV protein were set up as described in Materials and Methods. Mixtures were incubated at 23°C (room temperature) for 15 minutes and then analyzed on native 10% polyacrylamide gels. Lane 1, 6: no HelIV added; lane 2,7: 0.12 nM HelIV added; lane 3, 8: 1.2 nM HelIV added; lane 4, 9: 12 nM HelIV added; lane 5, 10: 120 nM HelIV added. (B) DNA binding of 83 kDa HelIV was tested by nitrocellulose-DEAE double-filtered method as described in Materials and Methods. In standard binding mixtures, 1 nM ^{32}P-HMC 1 ssDNA and 120 nM HelIV were added and incubated at room temperature for 15 minutes. (no HelIV was added in CTR control reactions.) Results are from one experiment with error bars representing the ranges derived from two independent determinations (duplicate-reaction results).

2.4 Discussion

2.4.1 HelIV Protein Sequence Analysis

D. radiodurans locus DR1572 appeared to have a frameshift mutation inside of the coding sequence. The sequencing results from all six *helD* gene clones, two amplified from strain R1 and four amplified from strain BAA-816, showed that an additional G residue found in the same position of the gene corrected the frameshift. This is not the first time that an apparent frameshift mutation in *D. radiodurans* GenBank-annotated genes turned out not to exist after independent sequencing. For example, the genes of *D. radiodurans* DNA single strand binding protein (SSB) (96), mismatch repair protein MutS1 (88) and Snf2 intein (97) all had apparent frameshifts which were not found in the subsequently-sequenced clones.

The complete *helD* gene encodes a 755-amino acid protein belonging to helicase superfamily I (SF 1) as it contains all the seven SF 1 conserved motifs. Of the BLASTp searches, UvrD and HelIV scored highest in *E. coli*, whereas in *B. subtilis*, the *E. coli* HelIV orthologue Yvgs was the closest match. We named DR1572 locus as *helD* gene and its protein as HelIV, based on its close match to the spacing pattern of the clusters of the helicase motifs to that of *E. coli* HelIV and *B. subtilis* Yvgs (94). All three helicases have a long N-terminal region preceding the first conserved helicase motif and a relatively short spacing between motifs IV and V (figure 2.3 and 2.24), which is distinct from UvrD and other helicases (94).

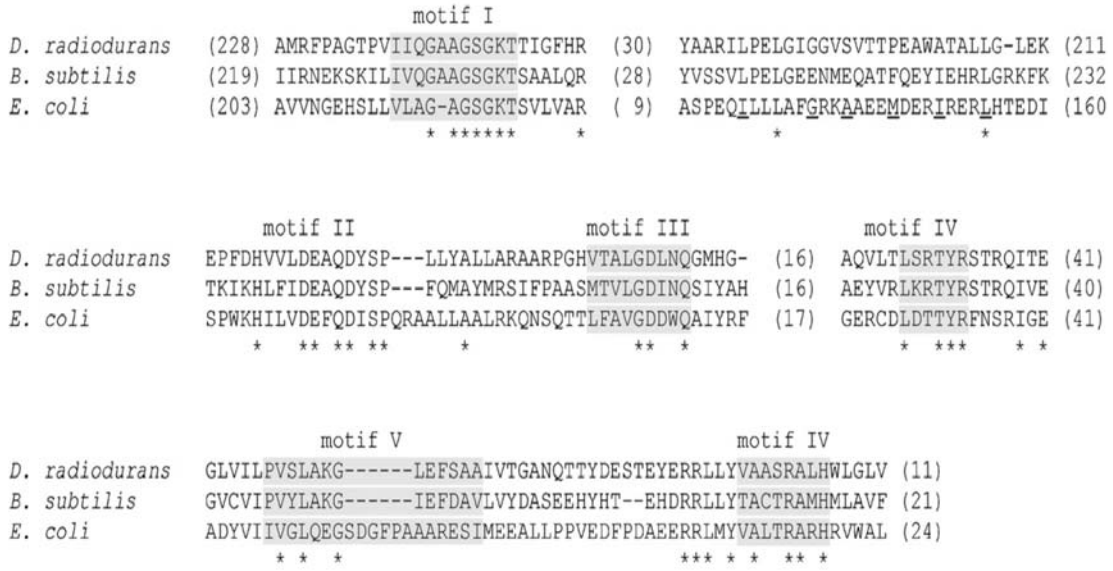

Figure 2.24 Amino acid sequence alignment of *D. radiodurans* HelIV, *B. subtilis* YvgS and *E. coli* helicase IV. The complete amino acid sequences of *D.radiodurans* HelIV (755 residues in corrected sequence), *B.subtilis* YvgS (774 residues) and *E. coli* helicase IV (684 residues) were aligned using CLUSTALW2. The six conserved motifs in Superfamily I helicases are highlighted with gray color. Residues in *E.coli* helicase IV considered to be motif Ia are underlined. The number of residues that are not shown from the complete sequences is indicated in parentheses. Figure is adapted from Cao and Julin, 2009 (89).

2.4.2 The Role of HelIV in DNA Repair

To probe the possible functions of HelIV, the growth rate and sensitivity to DNA damaging agents of a *D. radiodurans helD* mutant were compared to those of wild type cells. Different repair pathways should be required to fix the variety of types of DNA damage induced by the DNA damaging agents. A defect of the *helD* mutant in repairing a certain type of DNA damage indicates a role of HelIV in the specific DNA repair pathway(s) responsible for fixing that type of DNA damage.

During regular cell growth, different types of spontaneous DNA damage including DSB can occur (19). The growth curves of *helD* mutant (with or without antibiotic) exhibited essentially no difference compared to that of wild type strain, indicating that the HelIV did not play an important role in cell growth or spontaneous DNA damage repair. In the assays where cells were treated with gamma rays, UV light and MMC, the *helD* mutant was as resistant as wild type cells. The doses of gamma rays applied in the assays can directly cause extensive DNA damage including massive DSBs and single-strand breaks (19). Large amounts of ROS generated as the products of water radiolysis is the major source for indirect DNA damage caused by IR (10).

UV irradiation primarily causes cyclobutyl pyrimidine dimers and pyrimidine (6-4) pyrimidone photoproducts (19). Nucleotide excision repair (NER) is the major pathway to deal with pyrimidine dimers as *D. radiodurans* lacks photolyases for light-stimulated direct reversal of dimers (4,19). MMC is an alkylating reagent which causes bulky lesions and interstrand crosslinks removed by NER (98). The repair of both UV and MMC induced DNA damage via NER can lead to DSBs, if two damage sites are closely located on opposite strands. The equal resistance of the *helD* mutant to wild type cells in assays with the three agents implied that HelIV does not play an essential role in DSB repair pathway. The NER pathway itself also requires a helicase (UvrD) to unwind the duplex region and release the excised fragment containing DNA damage (19). But there is a real UvrD homologue in *D. radiodurans* which has been shown to be functional in the NER pathway (88). Thus, HelIV apparently is not involved in NER repair in *D. radiodurans*.

The *D. radiodurans helD* mutant was moderately more sensitive to treatments with hydrogen peroxide or the methylating agent MMS than wild type cells. Both hydrogen peroxide and MMS lead to severe base modifications, which requires base excision repair (BER) pathway to fix the base damage (4). However, the fact that the known BER pathway in prokaryotes does not require helicase activity makes it unlikely that HelIV contributes to BER. Although hydrogen peroxide can also cause DSB indirectly (via $HO^{\bullet}$ generated in Fenton chemistry (10)), HelIV cannot be a key player in DSB repair as the *helD* mutant is resistant to gamma rays. It is reported that methylated bases caused by MMS can also lead to DSB by blocking replication fork progression (95). Thus, the sensitivity of *helD* mutant to MMS could indicate that HelIV acts in some aspect of processing stalled replication forks.

A similar moderate phenotype was observed in the *E. coli helD* mutant and *B. subtilis yvgs* mutant respectively. The *in vivo* study results in *B. subtilis* showed that the *yvgs* mutant was only slightly sensitive to MMS (94). Interestingly, a *yvgs recF* double mutant was less sensitive to MMS than *recF* single mutant. It is proposed that Yvgs can extend the number of single strand gaps created by DNA damage. The gaps in turn are intermediates for the RecF pathway and need further processing to complete repair. In the *yvgs recF* background, fewer gaps are generated and the MMS-induced damage can be repaired by other pathways in *B. subtilis* (94). In *E. coli*, the *helD* mutant had no effect on homologous recombination and was as resistant to UV and MMS as wild type cells. However, a reduced level of recombination was observed in *helD uvrD* double mutant

and *helD uvrD recQ* triple mutant, in the genetic background of *recB sbcB sbcC* in which the RecF pathway is active (99,100).

In *D. radiodurans*, as discussed in chapter 1, several lines of evidence show that RecF pathway is operative and can have important roles in the initiation step of recombination repair (4). To understand the potential role of *D. radiodurans* HelIV in RecF pathway, further *in vivo* work has to be done.

2.4.3 *In Vitro* Properties of HelIV

The full length (83 kDa, pI 6.6) and truncated (59 kDa, pI 6.4) HelIV proteins were expressed, purified and compared for their enzymatic activities. Both of the proteins were well expressed in the *E. coli* system used (figure 2.14). During purification, however, the truncated protein exhibited much better solubility than the full length protein (figure 2.15) especially during the overnight dialysis step after nickel column. To avoid precipitation, the 83 kDa HelIV had to be maintained in buffers containing 0.1 M or higher concentration of NaCl. In contrast, the 59 kDa HelIV could remain soluble for a long period in no salt buffers. In addition, the 83 kDa protein bound to ssDNA column more tightly than 59 kDa protein in the second step purification. The behavior of full length HelIV in purification indicates that the N-terminal region (214 amino acids) may have some effect on protein solubility and ssDNA recognition. It could be that at the protein concentration during purification, the 83 kDa protein tends to aggregate in low NaCl-concentrated buffer via N-terminal region interactions. Or the 83 kDa protein may be partially misfolded with the long N-terminal extension, which can lead to decreased solubility.

From the ATPase data in figure 2.19 and Table 4, the ATPase activity of both full length and truncated HelIV were independent of ssDNA, double-stranded linear and circular DNA. The HelIV, like two other characterized *D. radiodurans* helicases RecD and RecQ, did not require Mn^{2+} (Table 5) to hydrolyze ATP. Mn^{2+} is an important antioxidant (10) and used as the specific cofactor in some enzymes from *D. radiodurans* (71,72,101). Interestingly, the reaction rate of truncated HelIV was roughly 10 fold faster than that of full length HelIV, indicating a negative regulatory function of the missing N-terminal extension. The lower ATPase activity may also result from incorrect folding of the full length protein.

In helicase assays, it is clear that the truncated HelIV had no detectable DNA unwinding activity, suggesting the importance and necessity of the N-terminal region to the helicase activity. The missing N-terminal region may have function in coupling ATP hydrolysis with DNA unwinding. Similar behavior has been observed in other DNA helicases which require additional domain(s) that can facilitate the motor domain containing helicase and ATPase activities to unwind or target particular substrate structures (53,102). For example, the *E. coli* hexameric replicative helicase DnaB is composed of two distinct domains: the N-terminal domain and the C-terminal helicase domain separated by a linker region (103). The truncated DnaB devoid of N-terminal region has completely lost the helicase activity, although it still retained ATPase activity and the ability to form a hexamer. It is suggested that the N-terminal domain plays a pivotal role in transducing the ATP hydrolysis energy to DNA unwinding (102).

The full length HelIV exhibited a relatively weak ATP-dependent unwinding activity (5'-3' polarity) in our set of reaction conditions. We had to apply excessive amount of enzyme over the substrates (120-fold more enzyme in reactions) to be able to observe unwinding of products on the gels. The reaction rates calculated from the linear region of the time course curves (figure 2.21) were much lower (roughly 10^4 fold lower) than that of RecD from *D. radiodurans* (17). There has been no biochemical study so far with *B. subtilis* Yvgs. The *E. coli* HelIV, unlike our HelIV from *D. radiodurans*, possesses an ATPase activity that is strongly dependent on ssDNA. In addition, the *E. coli* HelIV unwinds DNA in the 3'-5' direction in an ATP-dependent manner (104).

In gel-shift and nitrocellulose filter DNA-binding assays, neither full length HellV nor the truncated protein bound to any tested form of ^{32}P labeled DNA substrates including ssDNA, 5'tailed dsDNA and forked dsDNA. These results were consistent with their relatively low ssDNA cellulose binding affinity, compared to the behavior of *D. radiodurans* RecD on the same column.

In conclusion, the *D. radiodurans* HelIV is a DNA repair related helicase with some unique biochemical properties. More work has to be done to address its exact role in DNA repair pathways.

CHAPTER 3 *IN VIVO* STUDY OF *DEINOCOCCUS RADIODURANS RECJ* MUTANT AND CHARACTERIZATION OF REFOLDED RECJ PROTEIN

3.1 Introduction

In the well-known radioresistant *D. radiodurans* bacterium, the DNA repair pathway ESDSA has been proposed to deal with hundreds of DSBs after irradiation and to completely reconstruct the chromosome. This experimentally well-validated repair model, however, still has some enzymes unidentified including the nuclease participating in the initial end-processing.

Although lacking the RecBCD enzyme complex that processes DSB ends in *E. coli* and many other bacteria, *D. radiodurans* encodes all the five proteins in the RecF pathway (4). The RecF pathway is an alternative pathway to initiate DSB repair in *E. coli* with the genetic background of *recBC sbcB sbcC* (or *sbcD*) (9). Among the five *D. radiodurans* encoded RecF pathways proteins (RecQ, RecJ, RecF, RecO and RecR), RecJ is the only one that has not been characterized (4). The *in vivo* or/and *in vitro* studies of the other four RecF pathway components implied that the presumed RecF pathway could be an important mechanism to fix IR-induced DSBs (53-56).

In *E. coli*, RecJ protein is a 5'-3' exonuclease specific for single-stranded DNA (105) and works with helicase RecQ to produce 3' tailed ssDNA for RecA binding in RecFOR catalyzed DSB repair (9). In addition, RecJ also functions in recombination-dependent replication, base excision repair and methyl-directed mismatch repair in *E. coli* (106-109).

The RecJ homolog in *D. radiodurans* is encoded by locus DR1126. Similar to the HelIV study in chapater 2, the characterization of the RecJ protein also included *in vivo* and *in vitro* studies.

In the construction of *recJ*-deletion mutant, we were not able to replace all the *recJ* gene copies with the transformed linear streptomycin resistant gene cassettes, based on the results of the regular and quantitative PCR (see Results for details). The growth rate and sensitivity to various DNA damaging agents of the heterozygous *recJ* mutant was compared to those of wild type *D. radiodurans* strain. The RecJ protein was expressed in the form of inclusion body and purified via the denaturation-refolding method. The nuclease assays with refolded RecJ protein were carried out on ^{32}P labeled ssDNA under various reaction conditions.

3.2 Materials and Methods

3.2.1 Materials

Two wild type *D. radiodurans* strains were used in this study: the R1 strain purchased from the ATCC and the strain BAA-816 from Dr. Michael Daly as in the previous chapter. The plasmid pTNK103 was a gift from Dr. John Battista at Louisiana State University. The Smt3-tag expression vector pSmt3 was a gift from Dr. Barbara Gerratana at the University of Maryland, College Park. The purified *D. radiodurans* single strand DNA binding protein (SSB) was a gift from Dr. Michael Cox at the University of Wisconsin.

D. radiodurans was grown at 30°C in TGY medium and *E. coli* was grown in LB medium at 37°C with proper antibiotics as described in previous chapter.

All the primers used in this study are listed in Table 6.

3.2.2 *recJ* Gene Cloning and Sequencing

Genomic DNA used for *recJ* cloning was isolated from *D. radiodurans* wild type strains R1 and BAA-816 separately as described in chapter 2. The *recJ* gene coding region (bp # 1,134,718 to 1,136,772 of *D. radiodurans* chromosome 1) was amplified by PCR using *Deep Vent* DNA polymerase (New England Biolabs), with the primers DRJ1 and DRJ2. PCR reaction mixtures (50 μl) contained 200 ng genomic DNA, 0.6 μM primers, 200 μM of each dNTP, 2 units of *Deep Vent* DNA polymerase and 5% (v/v) DMSO. PCR cycling (repeated 30 times) conditions were: denaturation at 94°C for 1 minute; annealing at 60°C for 1 minute and extension at 72°C for 4.5 minutes.

The 2064 bp (2.1 kb) PCR fragment with a start codon of ATG (modified by DRJ1 primer from the original start codon GTG) was ligated into cloning vector PCRblunt, followed by transformation of *E. coli* Top 10 strain. The resulting plasmids (PCRblunt-recJ) with inserts amplified from two *D. radiodurans* wild type strains (R1 and BAA-816) were sent for sequencing by the DNA sequencing facility at University of Maryland, with the primers M13Rev, M13 (-21) and DRJ mid.

3.2.3 Construction of *D. radiodurans* Δ*recJ::str*

The *recJ* gene was deleted from the *D. radiodurans* and replaced by a streptomycin resistant gene (*aadA* gene), using a homologous recombination strategy (similar to *helD* gene deletion method in chapter 2). Three DNA fragments were generated separately by

PCR reactions: a 967 bp fragment located upstream of *recJ* gene (bp # 1,133,750 to 1,134,717 of the genome, using primers MJ1and MJ2), a 1029 bp product located downstream of *recJ* gene (bp # 1,136,630 to 1,137,659 of the genome, using primers MJ3 and MJ4) and a 1131 bp *aadA* gene fused to the *kat* promoter (with primers MJ5 and MJ6 amp). The two *recJ* flanking region fragments were amplified from *D. radiodurance* genomic DNA and the *aadA* gene including *kat* promoter was amplified from pTNK 103 plasmid (70). The 5' end of the *aadA* gene overlapped the 3' end of the *recJ* upstream fragment and the 3'end of the *aadA* gene overlapped the 5' end of the *recJ* downstream fragment (figure 3.1). An overlap PCR reaction was set up with above three DNA fragments mixed in a 1:1:1 ratio using primers MJ1 and MJ4. The resulting 3181 bp product was transformed into wild-type *D. radiodurans* strain R1, and colonies resistant to streptomycin (5 μg/ml) were selected.

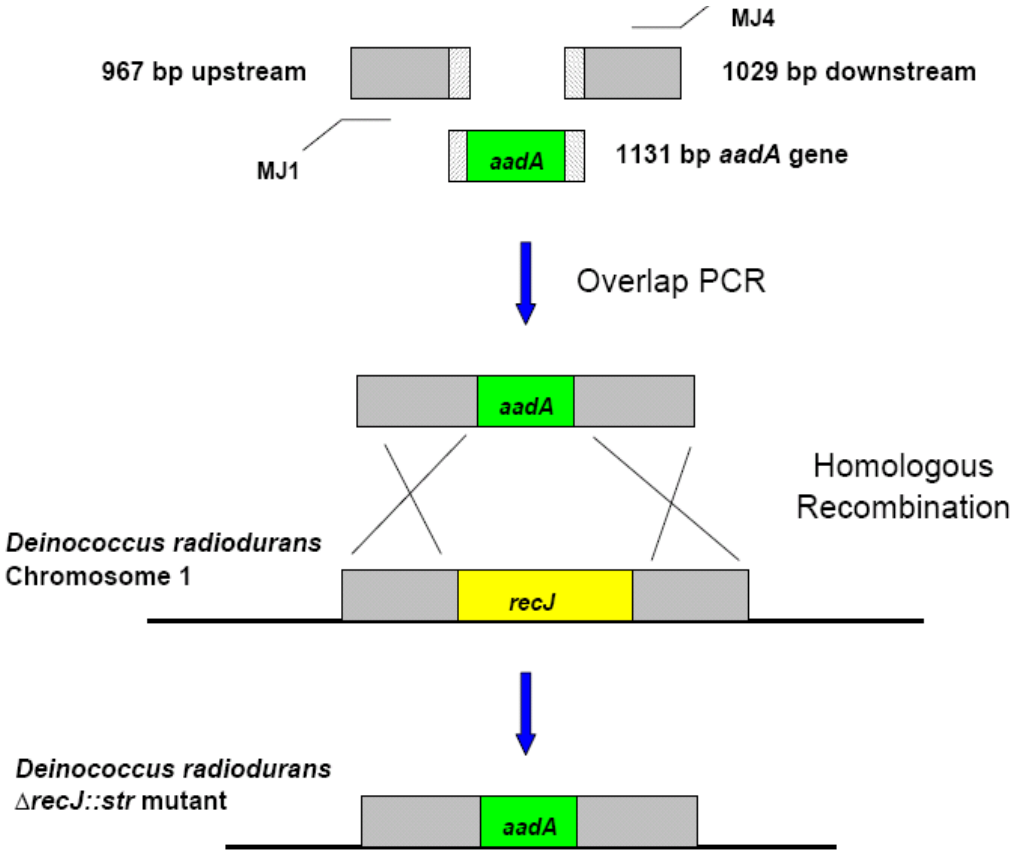

Figure 3.1 Schematic view of the strategy and major steps involved in Δ*recJ::str* mutant construction.

3.2.4 Genotyping of *D. radiodurans* Δ*recJ::str* by Non-Quantitative PCR

Genomic DNA was isolated from different streptomycin resistant colonies and the *recJ* gene structure was analyzed by regular (non-quantitative) PCR reactions. Two sets of primers were used in the PCR analysis: MJ1 and MJ4, with which wild type genome containing *recJ* genes can generate a 3912 bp (3.9 kb) product and mutant genome should produce a 3181 bp (3.2 kb) fragment; DRJ mid and MJ4, with which wild type genome should produce a 2232 bp (2.3 kb) fragment and a *recJ* mutant should not have any product if *recJ* genes were completely deleted.

To visualize the PCR products in *recJ* mutant genotyping, they were analyzed on 0.8 % agarose gels stained with ethidium bromide. The bands with expected sizes were extracted from gels and digested separately with different restriction enzymes, to further confirm that they were the products amplified from the genome regions of interest. The 3912 bp PCR product digested with *Sac*I should produce a 1235 bp and a 2677 bp fragments; the 3181 bp product digested with *BamH*I should produce a 982 bp and a 2199 bp fragments; the 2232 bp product digested *Xho*I with should produce a 883 and a 1349 fragments.

3.2.5 Genotyping of *D. radiodurans* Δ*recJ::str* by Quantitative Real-Time PCR

The initial genotyping results with regular (non-quantitative) PCR indicated that in the analyzed mutants some wild type *recJ* genes still existed, and thus the mutants are heterozygous (see Results in this chapter). Quantitative Real-Time PCR (RT-PCR) was performed to determine the relative number of *recJ* genes remaining in the mutants. Genomic DNA (gDNA) was purified from both wild type and streptomycin-resistant

mutant cells (*recJ* mutant # 31) using a standard phenol:chloroform extraction method (90). The concentration of extracted gDNA was determined from the absorbance at 260 nm using a UV spectrophotometer. All RT-PCR reactions were carried out in triplicate using a MyiQ Real-Time PCR Detection System (BioRad) with iQ SYBR Green Supermix (BioRad) and 150 ng of gDNA. The *D. radiodurans recD* gene (locus DR1902, a DNA-repair related helicase gene) was selected to use in internal control reactions, in order to quantify the actual amount of gDNA applied to *recJ* quantitative PCR. The primers used to amplify the regions of *recJ* gene (77 bp, with FrtRecJ and RrtRecJ primers) and *recD* gene (76 bp, with FrtRecD and RrtRecD) are listed in Table 6.

Real-time quantification of PCR products was done by detection of fluorescence emitted by SYBR green-dsDNA complex, using the MyiQ detection system. After binding to dsDNA (not to single-stranded DNA), SYBR green dye can generate very bright fluorescence. The quality of quantitative PCR products was monitored by the melting curve analysis program built into MyiQ system. At the end of amplification reactions, the melting temperatures of all the PCR products were determined and analyzed to confirm the specificity of the primers used.

Quantitative PCR data were analyzed by the following method as described in (110). The reference gene *recD* was assumed to be present in equal amounts in the wild type and *recJ* mutant gDNA samples. The PCR cycle number (*Ct*) was determined by the internal MyiQ software and a manually-set threshold value where the fluorescence signal reached exponential phase. The efficiency of amplification of each gene target was determined from the *Ct* values of amplification reactions containing serial 10-fold dilutions of gDNA.

The efficiency (E) is given by the equation $E = 10^{(-1/slope)}$ where *slope* is the slope of a plot of log (dilution factor) *vs. Ct*. The relative *recJ* gene copy number in the mutant cells compared to the wild type cells is given by the following equation:

$$relative\ recJ\ copy\ number\ = \frac{(E_{(recJ)})^{\Delta Ct_{(recJ)}}}{(E_{(recD)})^{\Delta Ct_{(recD)}}}$$

where $\Delta Ct_{(recJ)}$ is $Ct_{(recJ)}$(wt) - $Ct_{(recJ)}$(mutant) for PCR reactions using *recJ*-specific primers, and the is $\Delta Ct_{(recD)}$ the same quantity for the *recD*-specific primers; E is the amplification efficiency.

The RT-PCR primer designing, reaction set up and data analysis were completed with the assistance offered by a graduate student Charles Mueller from Dr. Julin's lab. The MyiQ Real-Time PCR Detection System and some of the reaction reagents were kindly provided by Dr. Hatfield's lab from the National Institute of Health in Bethesda, Maryland.

Table 6 Primers used in *D. radiodurans recJ* study

Primers for *recJ* gene cloning and sequencing	
DRJ1	5’-CA↓NdeI**ATG**GCAGCGGTGCGCGAGGGAAAG-3’ (start)
DRJ2	5’-G↓BamHIGATCC**TCA**GTGAAACCATTCGCGTGCTCGATAAGG-3’ (stop)
DRJ mid	5’-CATATGGCCGCCTACCTGGAAATTCGCAAC-3’
Primers for *D. radiodurans* Δ*recJ::str* mutant construction	
MJ1	5’-GCAGCGCGACCGATCCCTACG-3’
MJ2	5’-GAACCGGATCCGGCTGAATTCGCGGATGTGC TGGCGGCCTCACGC-3’
MJ3	5’-CCAGGAAGCTTGGGCGAATTCGCCCGCTGCGG GTTAAAGCCTCAGTTCG-3’
MJ4	5’-CAAGCTCGACGCCGTGCATGACC-3’
MJ5	5’-CGCGAATTCAGCCGGATCCGGTTCGCGAGGG CCTGAGGGCCATG-3’
MJ6	5’-GGCGAATTCGCCCAAGCTTCCTGGTCGAAAGT TTAAACTTATTTGCCGACTACCTTGGTG-3’
Primers for real-time quantitative PCR	
FrtRecJ	5’-AAAGGCATGAAATACAGCGA-3’
RrtRecJ	5’-CACTCGTTGAGGGCAAGTT-3’
FrtRecD	5’-CGAAGACGACCCACAGAAG-3’
RrtRecD	5’-CCAACTGCTCACCATCTTGT-3’

3.2.6 Growth Assay

About 10 ml of overnight cultures of wild type and *recJ* mutant # 31 were diluted into 100 ml TGY medium without antibiotic. Cells were grown at 30°C with shaking at 250 rpm for 30 hours. Cell density was monitored at OD_{600} using a UV spectrophotometer. Aliquots of the cultures were diluted and plated to ensure that optical density reflected viable cell numbers. Genomic DNA was isolated from the wild type and the *recJ* heterozygous mutant cultures at the end of the growth assay and subjected to non-quantitative PCR based genotyping as described in the previous section.

3.2.7 *recJ* Mutant Phenotype in Various DNA Damaging Treatments

Overnight cultures of *D. radiodurans* wild type R1 strain and *recJ* mutant # 31 grown in TGY medium (5 μg/ml streptomycin added in *recJ* mutant # 31) were diluted 1:10 into 15 ml fresh TGY without antibiotic. The resulting cultures grown to mid-log phase (OD_{600} = ~0.5, corresponding to ~1 $\times 10^9$ CFU/ml) were treated with different DNA damaging agents including gamma irradiation, hydrogen peroxide, UV irradiation and MMS, in exactly the same ways as described for *helD* mutant assays in chapter 2 (except that the dose rate of gamma irradiation was increased to 3.7 kGy/hour in *recJ* mutant assay).

After various DNA damaging treatments, both wild type and mutant cells were properly diluted with TGY medium and plated on triplicate TGY plates without streptomycin. The plates were incubated at 30°C for 2 to 3 days and colonies were counted. Cell survival fraction was plotted against dosages of different DNA damaging agents.

3.2.8 Bradford Assay

The Bradford assay is a fast and accurate way to estimate protein concentration within its sensitivity range (50 μg/ml to 2,000 μg/ml). The assay is based on the observation that the absorbance maximum for an acidic solution of Coomassie Brilliant Blue G-250 shifts from 465 nm to 595 nm when binding to protein occurs (111). One milliliter of Bradford reagent mixed with 20 μl of protein sample was incubated at room temperature for 10 minutes before its absorbance at 595 nm was determined by a UV spectrometer. A linear standard curve was created by plotting the absorbance of serially diluted BSA protein (250, 500, 1000, 1500 and 2000 μg/ml) against BSA concentrations. The equation for the linear standard curve was obtained in Microsoft Excel using its linear regression program. The concentration of an unknown protein sample can be calculated by solving the linear equation after plugging in the absorbance at 595 nm.

One liter of Bradford reagent contains 100 mg Coomassie Brilliant Blue G-250, 50 ml 95% ethanol, 100 ml 85% (w/v) phosphoric acid and 850 ml deionized water. When the dye has completely dissolved, the 1 liter of Bradford reagent has to be filtered using 0.45 μm filtration paper (Whatman) and stored at 4°C.

3.2.9 Single-Strand DNA Substrate Radiolabeling

The oligonucleotides HMC 1 (32-nt) and HMC 3 (20-nt) (Table 3 in chapter 2) were labeled at their 5'-ends with [γ-^{32}P] ATP by T4 polynucleotide kinase and purified as described in the previous chapter. The resulting radiolabeled oligonucleotide concentrations were determined by TLC and scintillation counting as described in last chapter. The 20 nM ssDNA substrates were prepared by mixing 10 nM ^{32}P-labeled

oligonucletides with 10 nM unlabeled oligonucleotides of the same type in annealing buffer containing 50 mM NaCl, 20 mM Tris-HCl, pH 7.5, 1 mM $MgCl_2$.

3.2.10 Nuclease Assay with Crude Cell Extract

10 ml overnight cultures that were started separately with single colonies from *D. radiodurans* wild type and *recJ* mutant # 31 plates were diluted into 100 ml fresh TGY (5 μg/ml streptomycin added for the *recJ* mutant) and grown at 30°C. When OD_{600} reached 1.5, the cells were harvested by centrifugation at 5,000 ×G for 20 minutes and stored at -80°C.

The wild type and mutant frozen cells were resuspended with 20 ml of 20 mM potassium phosphate buffer (pH 7.5) containing 1 mM EDTA and 1 mM PMSF. The cells were then lysed by passage through a French press five times at 1,000 PSI (pounds per square inch) and the soluble cell lysates were separated from cell debris by centrifugation at 10,000 ×G, 4°C for 2 hours. Total protein concentration of the crude cell lysates was determined by Bradford assays.

The nuclease reaction mixture (40 μl) included: 50 mM Tris-HCl, pH 7.5, 2 mM $MgCl_2$, 1 mM DTT, 0.1 mg/ml BSA, 1 nM of 5'-labeled HMC 1 and 1.2 μg of total proteins from cell extracts. After incubation in a 30°C water bath for the indicated time periods, 10 μl aliquot were placed on ice and mixed with 3 μl of 4 × quench buffer (40% glycerol, 2.4% SDS, 100 mM EDTA, 0.12% bromophenol blue).

Non-denaturing 15% polyacrylamide gels were loaded with 10 μl of quenched reaction samples in each lane and run in 1 × TBE buffer at 150 V (constant voltage). The

gels were then dried, exposed and scanned as described in chapter 2. Quantification of undegraded HMC 1 substrates on images was done using the ImageQuant software.

3.2.11 Construction of RecJ Expression Plasmids

The *recJ* cloning plasmid PCRblunt-recJ was digested with *BamH*I and *Nde*I restriction enzymes at 37°C overnight. The *recJ* gene insert (2.1 kb) was then purified and ligated into the expression vector pET15b digested with the same enzymes. The ligation mixture was used to transform *E. coli* strain Top 10 and the transformants were selected by LB plates with ampicillin (100 μg/ml). The resulting plasmid pET15-recJ was confirmed by double digestion with *BamH*I and *Nde*I restriction enzymes. This pET15-recJ plasmid can express N-terminal His-tagged RecJ protein with a molecular weight of 71 kDa.

The same *recJ* cloning plasmid PCRblunt-recJ with two *EcoR*I restriction sites located on each side of the *recJ* insert was also digested by *EcoR*I and ligated into the expression vector pGEX-4T-1 (GE Healthcare) cut with the same enzyme. Before ligation, the *EcoR*I digested pGEX-4T-1 was treated with Shrimp Alkaline Phosphatase (SAP) (Promega) at 37°C for 1 hour in the recommended conditions according to the manufacturer's instruction, to prevent vector self-ligation. SAP was then inactivated at 65°C for 15 minute incubation. Because of single digestion used, the *recJ* insert could be ligated into the vector in two possible directions (figure 3.2). The orientation of *recJ* inserts in the resulting plasmid pGEX-recJ was verified by a single digestion with *BamH*I: plasmid with the desired insert orientation produces 2.1 kb and 4.9 kb fragments; plasmids with the wrong orientation produce 6.9 kb and 0.1 kb fragments. The

pGEX-recJ with correctly oriented *recJ* insert can express N-terminal GST-tagged (26 kDa) RecJ protein with a molecular weight of 97 kDa.

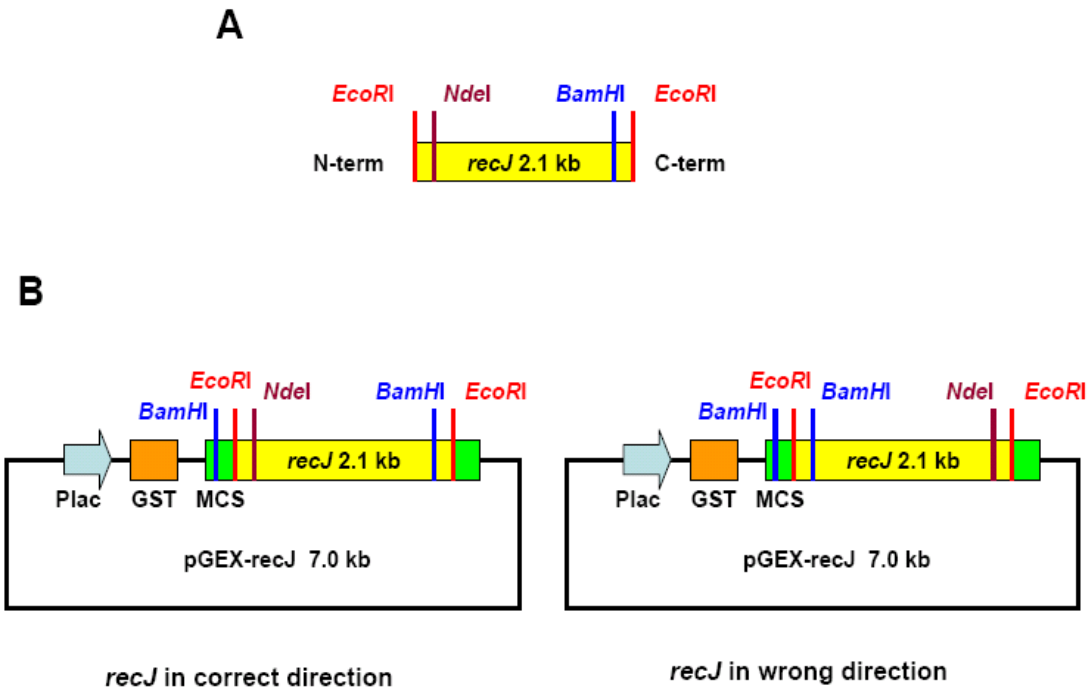

Figure 3.2 Schematic picture for construction of GST-tagged RecJ expression plasmid pGEX-recJ. (A) The 2.1 kb *recJ* insert cut from PCRblunt-recJ by *Eco*RI. (B) Two possible pGEX-recJ constructs with differently-oriented *recJ* insert: the one on the left has *recJ* in correct direction and can produce a 2.1 kb and a 4.9 kb fragments when digested with *BamH*I; the one the right with *recJ* in wrong direction and produces a 6.9 kb and a 0.1 kb fragments when digested with *BamH*I.

The *recJ* insert was cut from the correctly-oriental pGEX-recJ plasmid by *BamH*I and ligated into the expression vector pSmt3 (112) digested with the same enzyme. Similarly, the single enzyme digested pSmt3 was pre-treated with SAP to remove phosphate groups from both 5'termini of DNA, to prevent vector self-ligation. The resulting plasmid pSmt-recJ with two possible *recJ* orientations was further digested by *Nde*I to determine the insert direction: plasmid with correct insert direction should produce 7.3 kb and 0.3 kb fragments; plasmid with wrong direction should produce 5.3 kb and 2.3 kb fragments (figure 3.3). The pSmt-recJ can express N-terminal Smt3-tagged (12 kDa) RecJ protein with a molecular weight of 83 kDa. Smt3 protein is the homolog of human SUMO-1 protein in yeast (112).

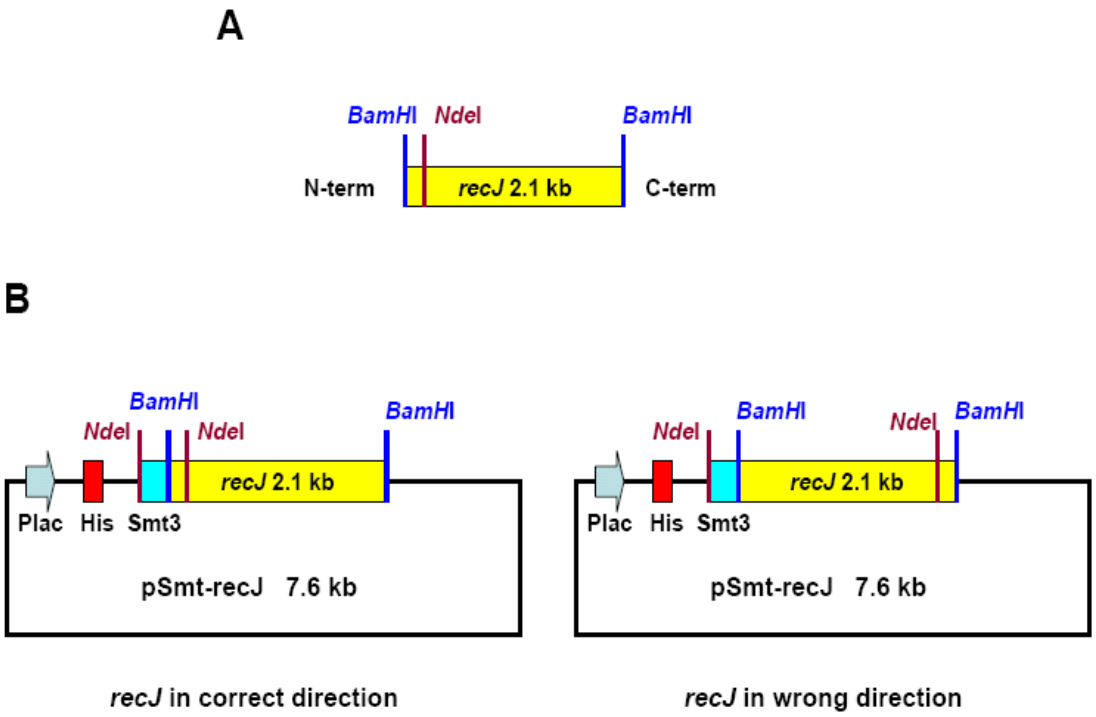

Figure 3.3 Schematic picture for construction of Smt3-tagged RecJ expression plasmid pSmt-recJ. (A) The 2.1 kb *recJ* insert cut from pGEX-recJ by *BamH*I. (B) Two possible pSmt-recJ constructs with differently-oriented *recJ* insert: the left one has *recJ* in correct direction and can produce a 7.3 kb and a 0.3 kb fragments when digested with *Nde*I; the right one with *recJ* in wrong direction and produces a 2.3 kb and a 5.3 kb fragments when digested with *Nde*I.

3.2.12 Expression of Differently Tagged RecJ Proteins

Single colonies of *E. coli* strain BL21(DE3) (Novagen) containing pET15-recJ, pGEX-recJ or pSmt-recJ separately were used to inoculate 10 ml of LB medium containing 200 μg/ml ampicillin (for pET15-recJ and pGEX-recJ) or 50 μg/ml kanamycin (for pSmt-recJ) and grown at 37°C overnight. The overnight culture was diluted 1:100 into 1 liter of ZYP-5052 medium containing 100 μg/ml ampicillin or 50 μg/ml kanamycin, as described in chapter 2. The cultures were grown at 23°C (room temperature) with vigorous shaking for 20 hours for auto-induction of differently tagged proteins. The cells were harvested by centrifugation at 5,000 ×G and stored at -80°C.

In RecJ expression solubility test, cells from 2 ml of each auto-induction culture was spun down and incubated at room temperature for 1 hour with 200 μl Bugbuster™ (Novagen), which is formulated to gently disrupt the cell wall of *E. coli* and liberate soluble proteins. The soluble portion of cellular proteins was separated from cell debris by centrifugation at 10,000 ×G for 3 minutes in 1.5 ml microcentrifuge tubes. Both the soluble and insoluble (resuspended with 200 μl water) proteins were mixed with loading buffer and analyzed by 10% SDS-PAGE.

3.2.13 RecJ Protein Purification via Denaturation-Refolding

About 9 grams of frozen cell pellet (from 1 liter auto-induced BL21(DE3) cells containing pET15-recJ plasmid) were resuspended in 50 ml native buffer A (20 mM Tris-HCl, pH 7.5, 500 mM NaCl, 10% glycerol, 20 mM imidazole and 1 mM PMSF) and lysed by sonication. The insoluble portion containing the N-terminal His-tagged RecJ protein in form of inclusion body was collected by centrifugation at 10,000 ×G, 4°C for 1

hour. The insoluble pellet was resuspended and incubated with buffer B (buffer A containing 6 M urea) at room temperature for 1 hour. After another centrifugation step at 10,000 ×G, 4°C for 2 hour, the denatured RecJ protein solution in 6 M urea was applied to a 5 ml nickel-NTA column (equilibrated with buffer B). The column was washed with 30 ml of buffer B and eluted with a 60 ml gradient of 20-300 mM imidazole in buffer B. The fractions containing RecJ protein (analyzed by 10% SDS-PAGE) were first dialyzed at 4°C against buffer A containing 1 M urea for 3 hours and then overnight against buffer C (20 mM Tris-HCl, pH 7.5, 100 mM NaCl, 10% glycerol, 1 mM DTT and 1 mM EDTA) to allow RecJ to refold. The precipitated protein was removed by centrifugation and the soluble refolded RecJ protein was further purified by the anion exchange chromatography on a 5 ml DEAE-cellulose (DE-52, Whatman) column. The column was washed with 40 ml buffer C and eluted with a 60 ml gradient of 0.2 -1.0 M NaCl in buffer C. The refolded RecJ protein concentration was determined by Bradford assays described in previous section.

3.2.14 Exonuclease Assay with Refolded RecJ Protein

Standard exonuclease reaction mixture (20 µl for single time point reaction and 60 µl for time course reaction) included: 50 mM Tris-HCl, pH 7.5, 2 mM $MgCl_2$, 1 mM DTT, 0.1 mg/ml BSA, 1 nM of 5'-labeled ssDNA substrate (HMC 1 or 3) and refolded RecJ. In assays with *D. radiodurans* SSB, various amount of purified SSB protein (0 to 100 nM) was included in above standard reaction mixture. Refolded RecJ and SSB proteins were diluted with enzyme dilution buffer (25 mM potassium phosphate, pH 7.5, 0.1 mM EDTA, 0.1 mM DTT, 0.1 mg/ml BSA and 10% glycerol) if necessary. In the RecJ time

course nuclease assays for the kinetic parameters estimation, the standard reaction conditions were used except that the substrate concentration was increased to 10 nM (prepared by mixing ^{32}P labeled HMC 1 with unlabeled HMC 1 in 1: 10 ratio).

After incubation in a 30°C water bath for the indicated time periods, 10 µl aliquots were taken out and mixed with 3 µl of 4 × quench buffer (40% glycerol, 2.4% SDS, 100 mM EDTA, 0.12% bromophenol blue) on ice.

About 10 µl of each quenched reaction sample was loaded onto non-denaturing 15% PAGE gels which were run in 1 × TBE buffer at 150 V (constant voltage). The gels were then dried, exposed and scanned as described in the previous chapter. Quantification of remaining substrate and degraded product on images was done using the ImageQuant software.

The concentration of degraded ssDNA was plotted as a function a time. The slope of each plotted reaction time course was determined by linear regression to give the reaction rate. In our assays, the substrate was mixed with 30-300 fold excess of the refolded RecJ protein. A variation of Michaelis-Menten equation was applied to calculate the kinetic parameters of the RecJ nuclease reaction (113). Assume that the enzyme and substrate react according to the schematic pathway.

$$\mathrm{E+S} \underset{k_{-1}}{\overset{k_1}{\leftrightarrow}} \mathrm{ES} \xrightarrow{k_{cat}} \mathrm{E+P}$$

In the initial reaction time, the equation $[\mathrm{S}]_0 = [\mathrm{S}] + [\mathrm{ES}]$ is assumed, where $[\mathrm{S}]_0$ is the initial total substrate concentration and $[\mathrm{S}]$ is the concentration of free substrate. In our assays, the enzyme concentration was in excess of that of the substrates, thus the equation $[\mathrm{E}]_0 = [\mathrm{E}] + [\mathrm{ES}] \approx [E]$ is assumed. With the steady state assumption, the term

K_S is defined as $K_S = \frac{k_{cat} + k_{-1}}{k_1}$ in the following initial reaction rate equation (113) (the K_s has the same expression as the K_m from the original Michaelis-Menten equation (114)):

$$V = k_{cat}[ES] = \frac{k_{cat}[S]_0[E]}{K_S + [E]}, \text{ where } V_{max} = k_{cat}[S]_0 .$$

The kinetic parameters of RecJ nuclease reactions were calculated by fitting the data to the above reaction rate equation via the non-linear regression program provided in the SigmaPlot software.

3.3 Results

3.3.1 *recJ* Gene Cloning and Sequencing Results

A 2064 bp *recJ* gene (locus DR1126, GenBank accession number NC_001263) fragment was amplified from genomic DNA of wild type R1 and BAA-816 strains of *D. radiodurans* respectively, as shown in figure 3.4. The two *recJ* inserts were both ligated into PCRblunt cloning vector. The resulting plasmids PCRblunt-recJ-R1 and PCRblunt-recJ-BAA816 were sequenced for *recJ* inserts with the three primers M13Rev, M13 (-21) and DRJ mid.

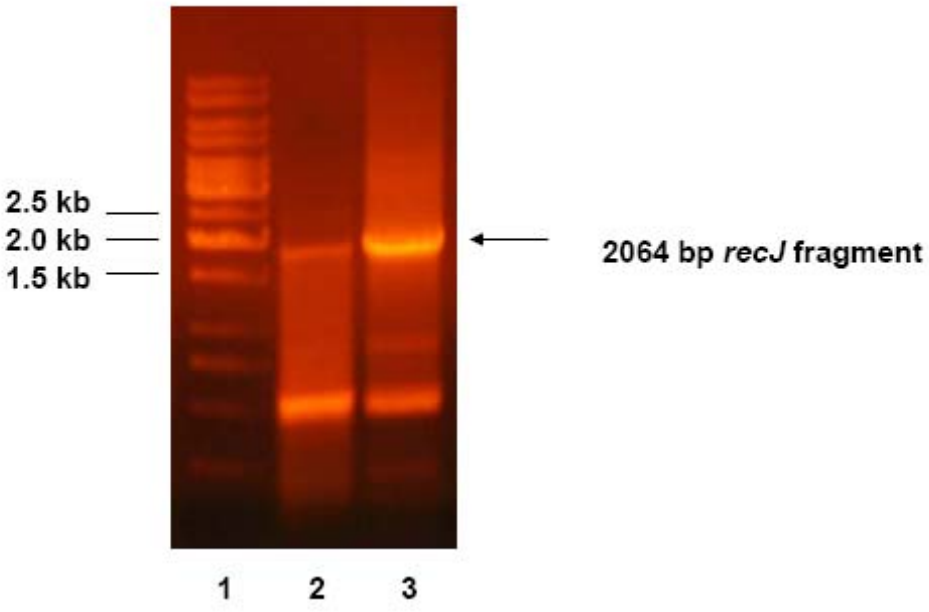

Figure 3.4 PCR products of *recJ* gene cloning on 0.8% agarose gel. Lane 1: Fermentas 1kb ladder; lane 2: *recJ* gene amplified from genomic DNA of *D. radiodurans* wild type BAA-816 strain; lane 3: *recJ* gene amplified from genomic DNA of wild type R1 strain.

The sequencing results indicated that both of the inserts amplified from different sources of wild type genomic DNA matched the *D. radiodurans recJ* sequence in GenBank, except for the presence of an additional G which is not found in the GenBank sequence. The additional G was found right after the 1894th residue (about 170 bp upstream of the stop codon) in both *recJ* inserts sequence (between bp # 1,136,609 to 1,136,610 in the genome). With the additional G, a resulting frameshift alters the predicted RecJ protein sequence. The corrected RecJ protein has 641 amino acids (in the same open reading frame) which is 44 amino acids shorter than the GenBank predicted sequence (Appendix 2).

3.3.2 Genotyping of *D. radiodurans* Δ*recJ::str* by Non-Quantitative PCR

The *recJ* gene was replaced by a streptomycin resistance gene *aadA* by homologous recombination. Genomic DNA was extracted from *recJ* mutants that were selected from TGY (5 μg/ml streptomycin added) transformation plates. Two pairs of primers were used in the *recJ* mutants genotyping by non-quantitative PCR. Primers MJ1 and MJ4 are complementary to the 5' of the *recJ* upstream fragment and 3' of the *recJ* downstream fragment, respectively. In amplification reactions with MJ1 and MJ4, the product expected from wild type genome is 3.9 kb while that from the *recJ* mutant is 3.2 kb. The second pair of primers is DRJ mid and MJ4. DRJ mid anneals to the internal region of the *recJ* gene. The reaction with wild type genomic DNA should produce a 2.2 kb fragment and reaction with mutant should not have any product, if all *recJ* genes from the mutant genome have been completely deleted (figure 3.5).

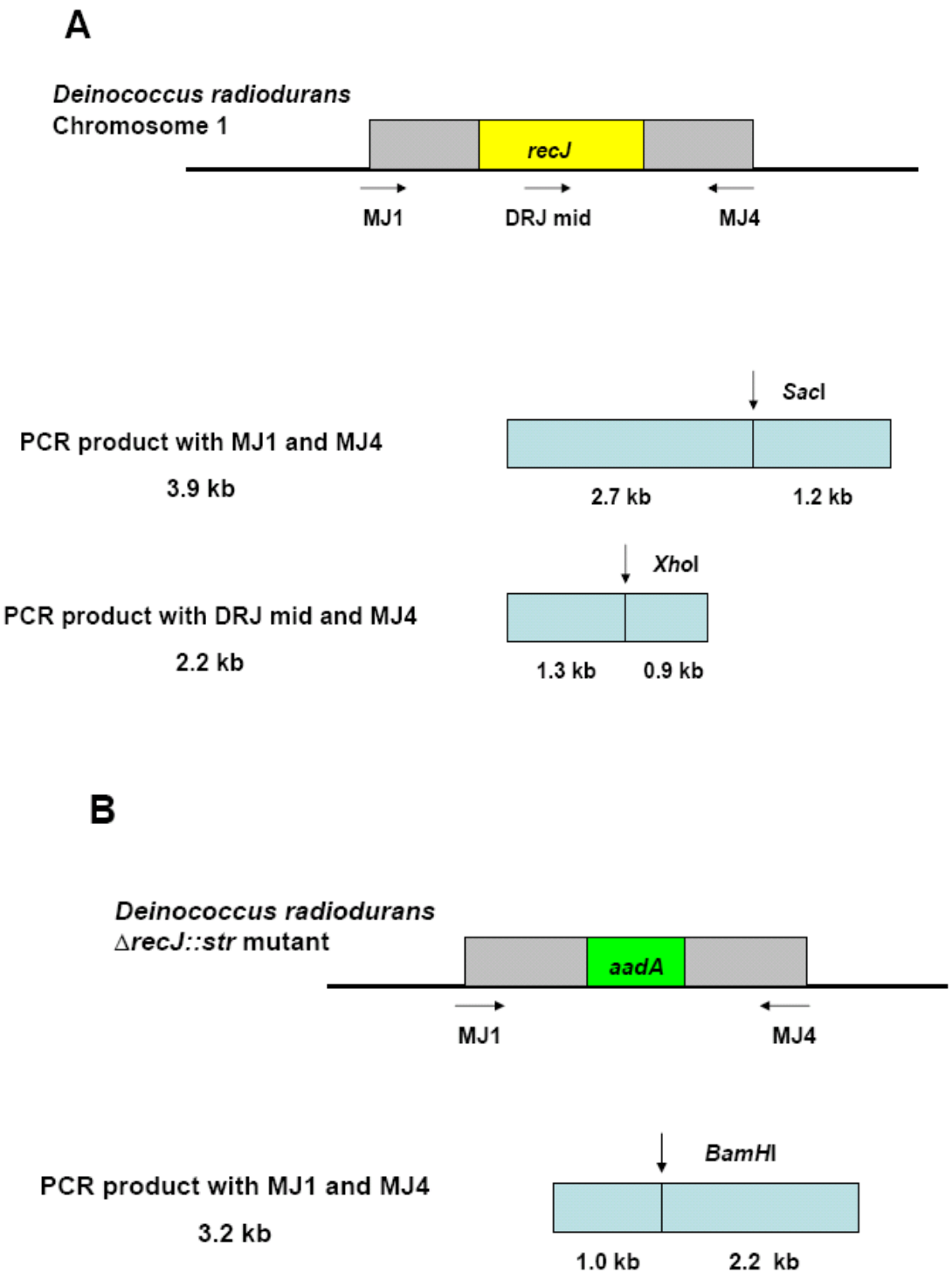

Figure 3.5 Schematic view of genotyping *recJ* mutant via non-quantitative PCR. (A) The two expected PCR products amplified from wild type genome: a 3.9 kb product that produces a 2.7 kb and a 1.2 kb fragments when digested with *Sac*I; a 2.2 kb product that produces a 1.3 kb and a 0.9 kb fragments when digested with *Xho*l. (B) The only expected 3.2 kb PCR product that produces a 1.0 kb and a 2.2 kb fragments when digested with *BamH*I.

As shown in figure 3.6, in PCRs with MJ1 and MJ4 primers, a single expected 3.9 kb band was found for the wild type, but 3.9 kb and 3.2 kb fragments were both found for the *recJ* mutant. The presence of 3.9 kb products in the mutant indicated that some wild type *recJ* genes still remained. In reactions with DRJ mid and MJ4 primers, a 2.2 kb band was observed in reactions with both wild type (lane 6) and *recJ* mutant (lane 7) gDNA. The unexpected 2.2 kb product in mutant reaction also suggested that the *recJ* mutant analyzed here was a heterozygote which partially kept the *recJ* gene in its genome.

To look further for a homozygous *recJ* mutant, genomic DNA for a total of 25 isolated transformants obtained from five different batches of transformations were tested by the same PCR verification methods. No homozygous *recJ* mutant was found, suggesting the *recJ* is essential for viability in *D. radiodurans*.

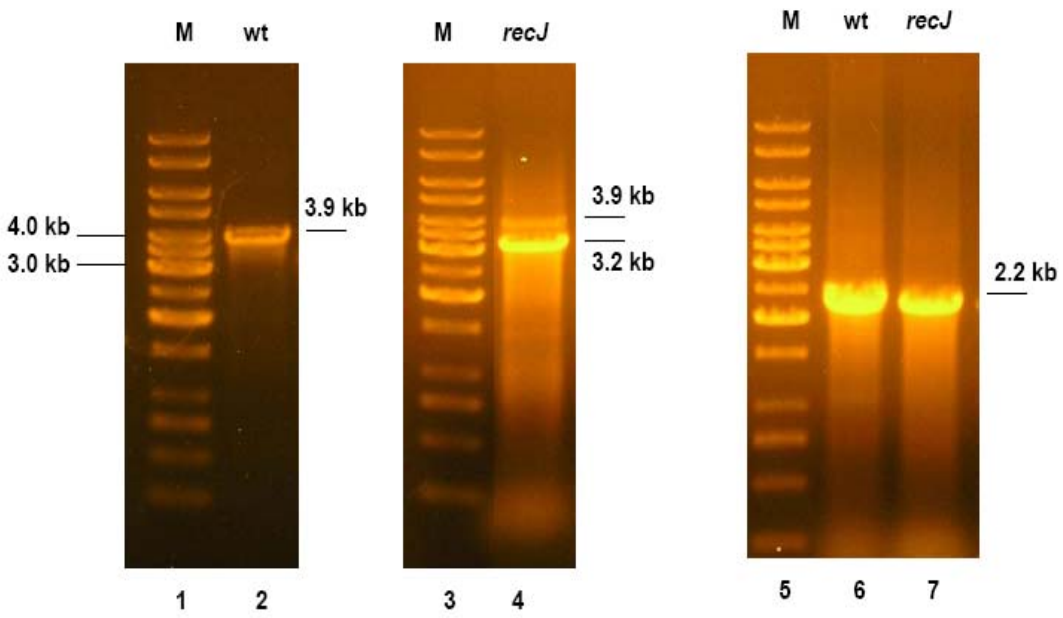

Figure 3.6 PCR genotyping products on 0.8% agarose gels. Lane 1, 3, 5: Fermentas 1kb ladder; lane 2: 3.9 kb fragment amplified from wild type genome with MJ1 and MJ4; lane 4: 3.9 kb and 3.2 kb fragments amplified from *recJ* mutant genome with MJ1 and MJ4; lane 6: 2.2 kb fragment amplified from wild type with DRJ mid and MJ4; lane 7: 2.2 kb fragment amplified from *recJ* mutant genome with DRJ mid and MJ4.

3.3.3 Digestions of PCR Products in *recJ* Mutants Genotyping

In the *recJ* mutant PCR genotyping reactions, two unexpected products (3.9 kb fragment with MJ1 and MJ4 primers; 2.2 kb fragments with DRJ mid and MJ4 primers) were found, suggesting the mutant was heterozygous. To rule out the possibility of non-specific PCR products and verify the heterozygous mutant conclusion, incomplete digestions with restriction enzymes specific to each of the three genotyping PCR products were performed (figure 3.7).

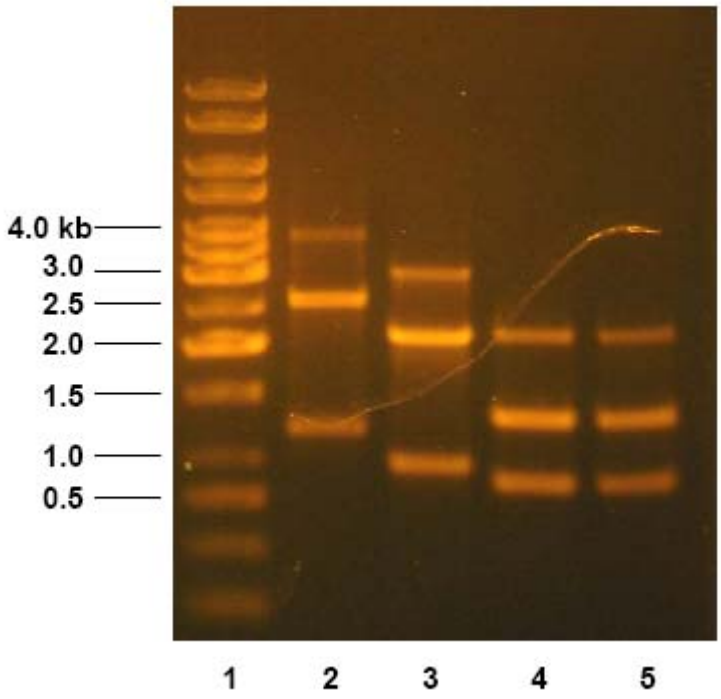

Figure 3.7 PCR genotyping products partially digested with different restriction enzymes on 0.8% agarose gel. Lane 1: 1 kb ladder; lane 2: 3.9 kb (amplified from wild type) product digested with *Sac*I; lane 3: 3.2 kb (amplified from *recJ* mutant) product digested with *BamH*I; lane 4 and 5: 2.2 kb (amplified from wild type and mutant respectively) products digested with *Xho*I.

As shown in figure 3.7, the expected partial digestion products for all reactions were found on the gel: in lane 2, 2.7 kb and 1.2 kb *Sac*I digestion products of the 3.9 kb fragment; in lane 3, 1.0 kb and 2.2 kb *BamH*I digestion products of the 3.2 kb fragment; in both lanes 4 and 5, 1.3 kb and 0.9 kb *Xho*I digestion products of the 2.2 kb fragment.

3.3.4 Relative *recJ* Gene Copy Number Determined by Quantitative PCR

Quantitative Real-Time PCR (RT-PCR) was performed to estimate the relative *recJ* gene copy number in mutant #31 strain (the same *recJ* mutant used in later *in vivo* assays) compared to wild type R1strain, on the MyiQ PCR Detection System (figure 3.8 and 3.9).

Two pairs of primers were used in RT-PCR: the FrtRecJ and RrtRecJ primers amplify a 77 bp fragment from the *recJ* gene and the FrtRecD and RrtRecD primers amplify a 76 bp fragment from the *recD* gene. Although genomic DNA analyzed in RT-PCR was quantified by UV, it is necessary to use a reference gene (*recD*) to calibrate the relative amount of gDNA used in each reaction. The quality and specificity of the two pairs of primers were monitored by the PCR products melting curves. If there is no mis-pairing or primer-dimer, each pair of primers should only amplify a single product (76 bp or 77 bp) from either gDNA template (wild type or *recJ* mutant #31). In figure 3.8 A, there was a weak non-specific band (smaller than 77 bp product) observed in reactions with *recJ* primers. But in figure 3.8 B, the two melting curves for the RT-PCR products with *recJ* primers were almost overlapped with each other and their Tm values were not distinguishable in the graph (~85.5°C). Similar results were found in melting curves for the RT-PCR products with *recD* primers. The melting curve graph suggested that the both pairs of primers used in RT-PCR were good in quality and specificity.

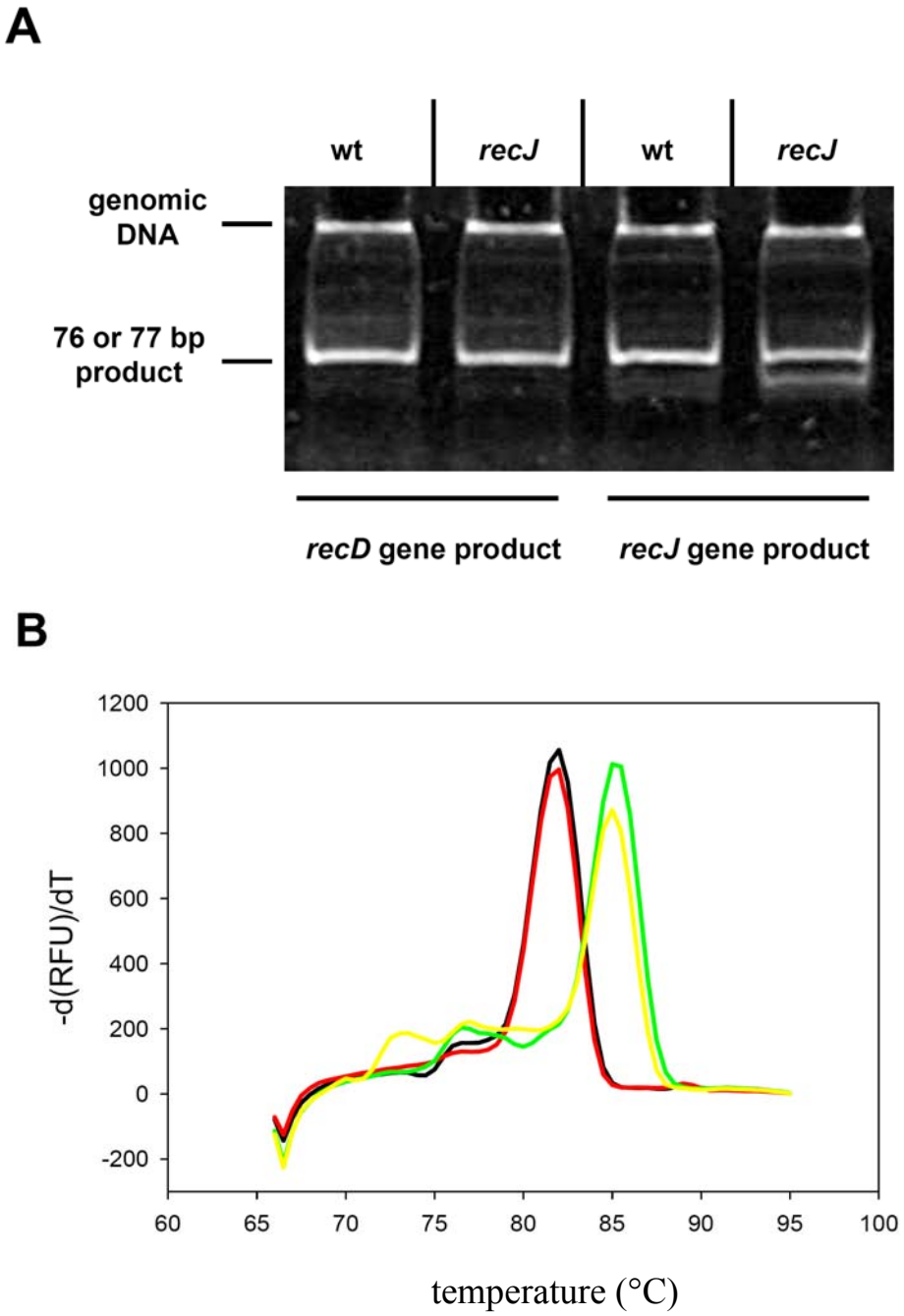

Figure 3.8 The products (A) and melting curves (B) of the four amplification reactions in quantitative Real-Time PCR. (A) The RT-PCR products on an agrose gel. (B) The change of fluorescence signal as a function of temperature (-dRFU/dT, RFU: relative fluorescence unit; T: temperature) reflects how fast the SYBR green bound dsDNA denatures. The temperature at which melting curve peaks is the Tm for this DNA. Black line: *recD* gene fragment (77 bp) amplification from wild type genome; red line: *recD* gene fragment amplification from *recJ* mutant #31 genome; green line: *recJ* gene fragment (76 bp) amplification from wild type genome; yellow line: *recJ* gene fragment amplification from *recJ* mutant #31 genome.

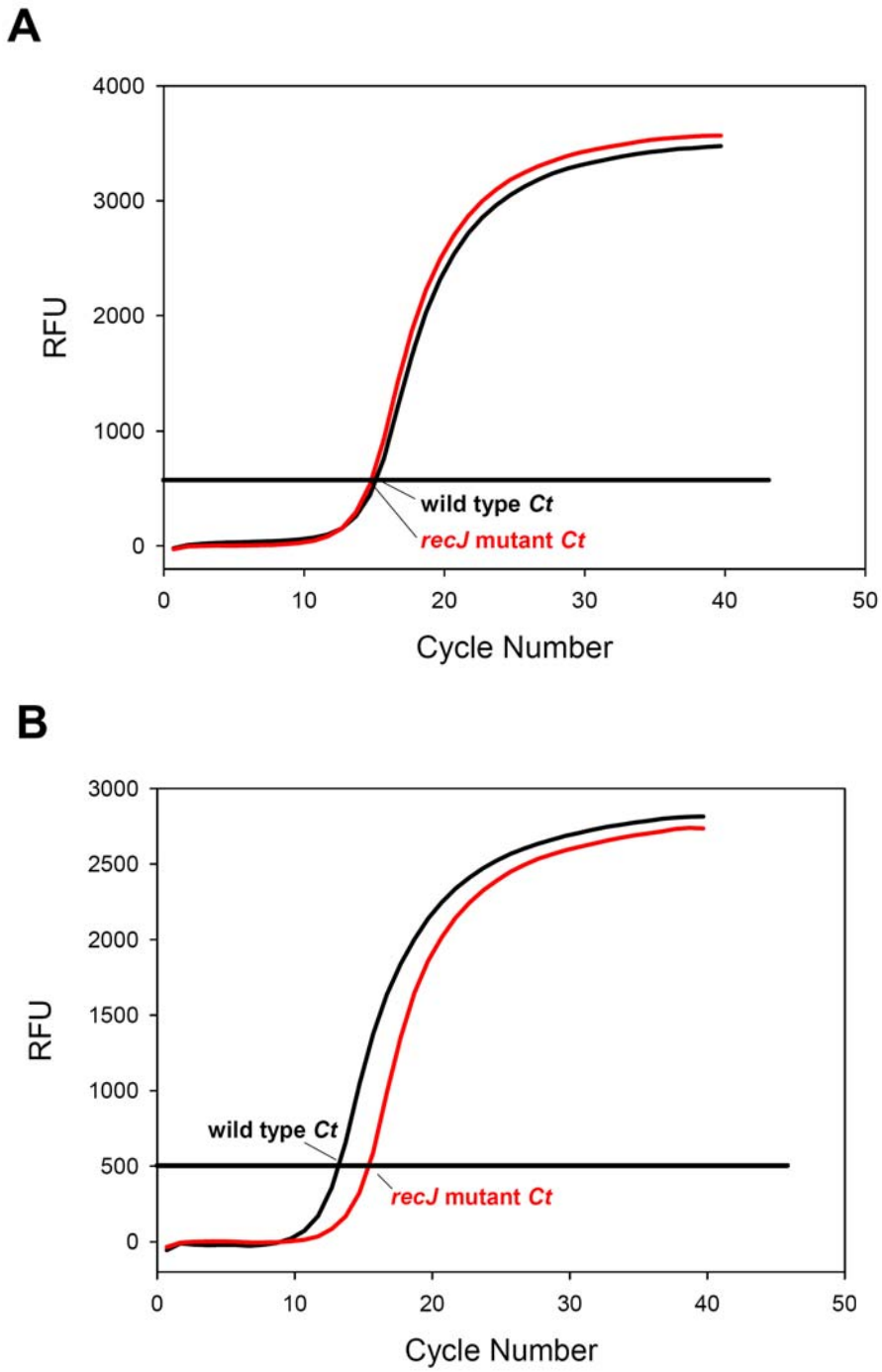

Figure 3.9 Fluorescence plots as a function of cycle number from selected RT-PCR reactions with *recD* primers (A) and *recJ* primers (B). RFU: relative fluorescence units. Black horizontal lines: MyiQ system determined threshold for cycle numbers (*Ct*) of all reactions. Cycle number (*Ct*): determined by the cycle number of the intersections between horizontal threshold line and the fluorescence curves in the same graphs. Black curves (RFU *vs* Cycle Number): reactions with wild type genomic DNA; red curves (RFU *vs* Cycle Number): reactions with *recJ* mutant #31 genomic DNA.

At the end of the RT-PCR amplification cycles, *Ct* values (figure 3.9) and amplification efficiency *E* were determined automatically by the MyiQ system internal software. The mutant relative *recJ* gene copy number (normalization based on *recJ* gene copy number in wild type) was calculated using the equation given in Materials and Methods in this chapter. The whole experiment was repeated twice. As seen in Table 7, the *recJ* mutant #31 is indeed heterozygous, which agrees with the conclusion drawn from non-quantitative PCR genotyping results. The *recJ* mutant #31 initially had about 50% *recJ* gene left in its genome; after about 12 passages (3 months), the relative *recJ* gene copy was decreased to less than 15%, suggesting at least no more *recJ* gene was gained back in the mutant.

3.3.5 Growth Assay

The growth of *recJ* mutant #31 in liquid TGY medium without streptomycin was compared to that of wild type R1 strain. As shown in figure 3.10 A, the heterozygous mutant clearly grew more slowly than wild type, although eventually at the end of growth curve (28^{th} hour) they both reached roughly the same cell density. The *recJ* mutant #31 was delayed for 3-4 hours to be able to enter the exponential phase compared to wild type. In the growth curve plotted in logarithmic scale (figure 3.10 B), the slope of the linear region of each grow curve was determined by linear regression in SigmaPlot software. In figure 3.10 B, the slope of the growth curves for both mutant #31 strains was 0.117 /hour whereas the slope of wild type growth was 0.137 /hour. In logarithmic scale, cell doubling refers to a change of 0.303 ($10^{0.303} = 2$) in $\log OD_{600}$. Thus, the cell doubling time for wild type strain is 0.303/0.137 = 2.2 hours; doubling time for mutant #31 is

0.303/0.117 = 2.6 hours. PCR results based the genomic DNA extracted after the growth assay showed that the *recJ* mutant #31 maintained the heterozygous genotype. The growth defect of the mutant #31, combined with the fact that the *recJ* genes could not be completely removed from the genome, suggested the RecJ plays a role in cell viability under ordinary growth conditions.

Table 7 Relative *recJ* copy number by RT-PCR

Cell genotype	Relative *recJ* copy number [c]		
	1st	2nd	Average
wild type R1	1.0	1.0	1.0
recJ #31 initial [a]	0.39	0.55	0.47
recJ #31 12th pass [b]	0.13	0.12	0.13

[a] *recJ* #31 initial: the *recJ* mutant #31 genomic DNA was extracted from the culture started with the original transformant colony.
[b] *recJ* #31 12th pass: the *recJ* mutant #31 genomic DNA was extracted from the culture that had been grown for 12 passages (3 months) on TGY plates (5 μg/ml streptomycin added); 1 passage (it was done once per week): overnight culture started from a single *recJ* mutant colony on previous passage plate was used to streak the new plate to keep colonies fresh.
[c] The relative *recJ* gene copy number was normalized based on that in wild type; in one experiment, all amplification reactions were done in triplicate. The whole experiment was repeated twice.

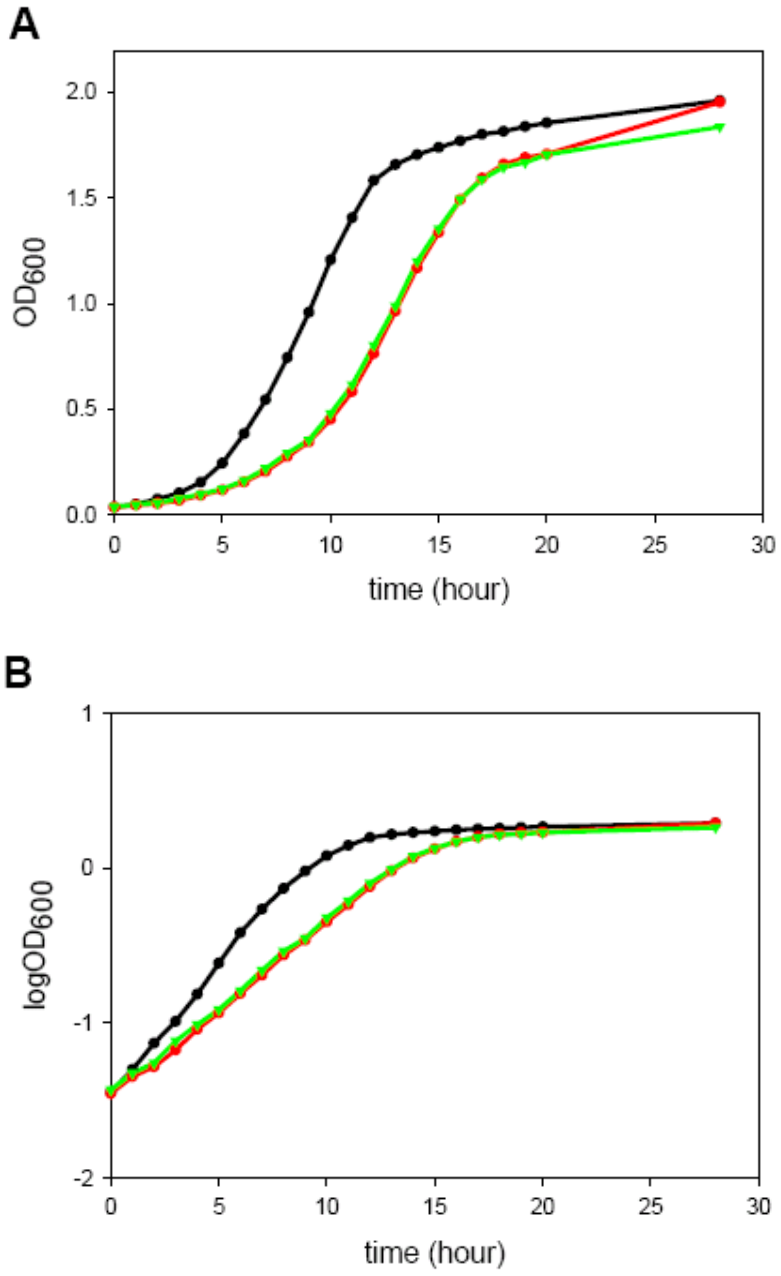

Figure 3.10 Growth curves of wild type and Δ*recJ::str* mutant *D. radiodurans* strains. Cells were grown at 30°C in TGY medium, without antibiotic for the mutant. Samples were removed at the indicated times, and the OD_{600} was measured. One wild type culture and two *recJ* mutant #31 cultures (A, B: started from different colonies on the *recJ* mutant #31 plate) were assayed. (A) The growth curves were plotted using OD_{600} vs. time. (B) The growth curves were plotted using $logOD_{600}$ vs. time. Black dots, wild type strain R1; red dots, *recJ* mutant #31 strain A; green triangles, *recJ* mutant #31 strain B. Results are from one experiment with single OD_{600} determination. This experiment was performed three times (the other two assays with *recJ* mutant #1 and #21 respectively) with comparable results.

3.3.6 *recJ* Mutant Phenotype in Various DNA Damaging Treatments

Mid-log phase cultures of wild type R1 strain and *recJ* mutant #31 were tested for cell survival abilities under the treatments with various DNA damaging agents.

The *recJ* mutant #31 showed significantly higher sensitivity in the tests using gamma irradiation (figure 3.11) and hydrogen peroxide (figure 3.12) than wild type. Both gamma rays and hydrogen peroxide can generate high oxidative stress inside of cells and cause DNA damage including base damage and strand breaks. These two assays indicated that RecJ could be an important player in the DNA repair pathways that cells use to deal with the massive DNA damage. The *recJ* mutant was moderately more sensitive than wild type to UV irradiation, which also causes DNA damage and strand breaks in cells, suggesting a role of RecJ in resistance to UV in *D. radiodurans*. Presumably, a mutant with a complete deletion of *recJ* would exhibit greater sensitivity to UV (figure 3.13).

In the test with MMS, which is a DNA methylating reagent and causes DNA base methylation at multiple positions, the *recJ* mutant #31 was as resistant as wild type, indicating that RecJ was not involved in DNA methylation related repair pathway (figure 3.14).

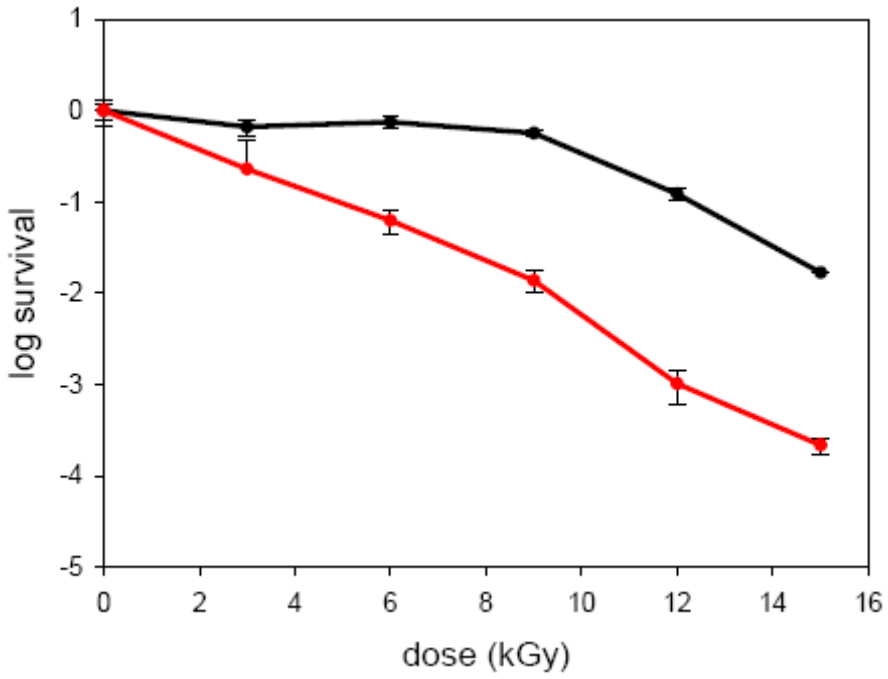

Figure 3.11 Sensitivity of wild-type and Δ*recJ::str* mutant *D. radiodurans* strains to gamma irradiation. Gamma irradiation was performed on ice, from a ^{60}Co source at 3.7 kGy/hour, for indicated doses. Black dots, wild type strain R1; red dots, *recJ* mutant #31. Results are from one experiment, with error bars generated from three independent determinations (triplicate plating results). The whole experiment was performed twice with comparable results.

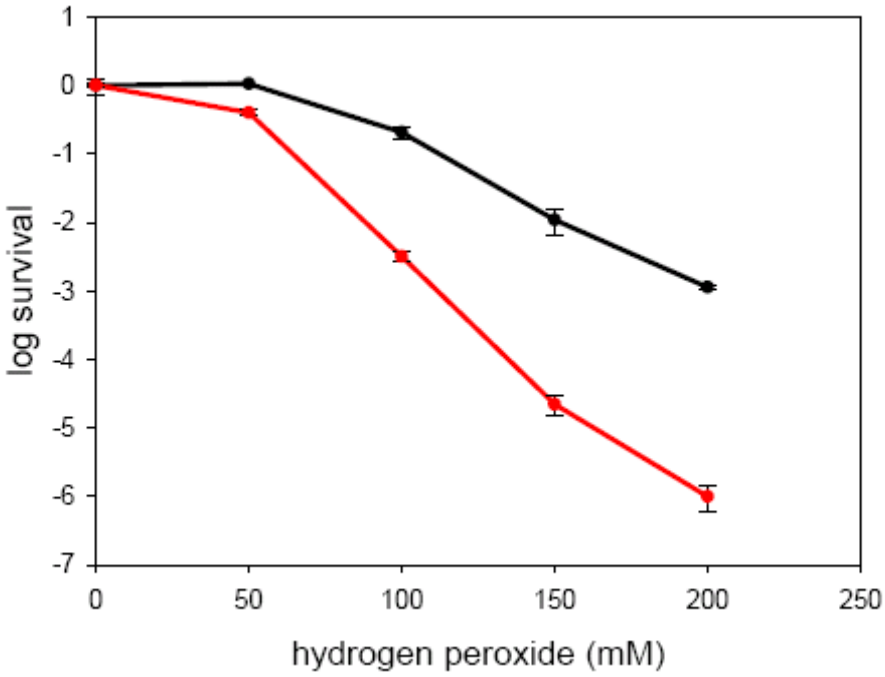

Figure 3.12 Sensitivity of wild-type and Δ*recJ::str* mutant *D. radiodurans* strains to hydrogen peroxide at 30°C. Cells were treated with hydrogen peroxide for one hour without shaking at 30°C, serially diluted and plated on TGY agar plates. Black dots, wild-type strain R1; red dots, *recJ* mutant #31. Results are from one experiment, with error bars generated from three independent determinations (triplicate plating results). The whole experiment was performed three times with comparable results.

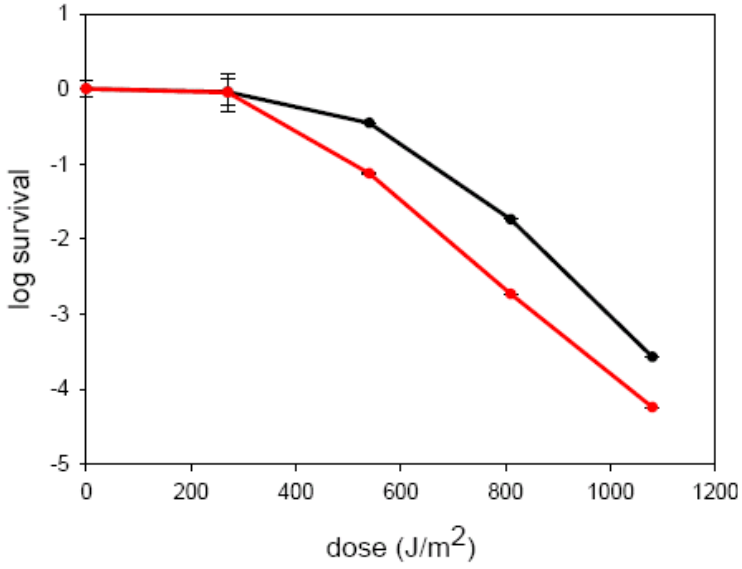

Figure 3.13 Sensitivity of wild-type and Δ*recJ::str* mutant *D. radiodurans* strains to UV irradiation. Cells grown to log phase were spread onto TGY plates and irradiated with UV light from a germicidal lamp at 90 J/m^2/min. Black dots, wild type strain R1; red dots, *recJ* mutant #31. Results are from one experiment, with error bars generated from three independent determinations (triplicate plating results). The whole experiment was performed four times with comparable results.

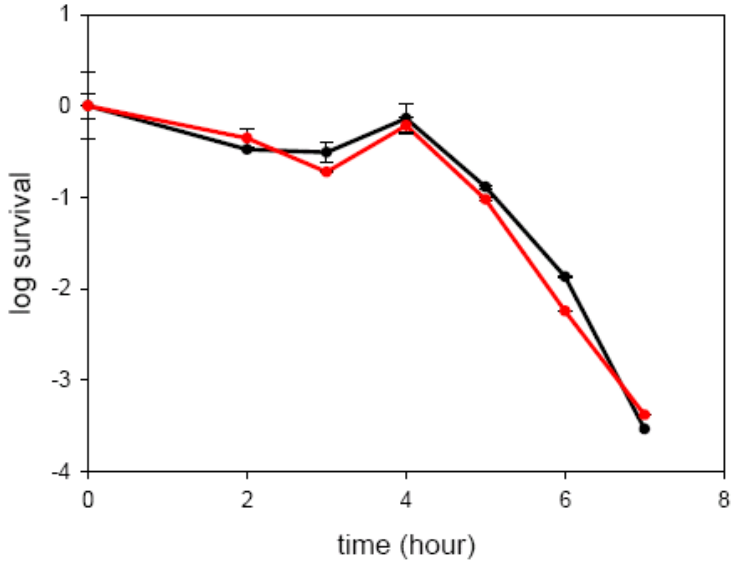

Figure 3.14 Sensitivity of wild-type and Δ*recJ::str* mutant *D. radiodurans* strains to MMS. Cells were treated with 30mM MMS for indicated times, serially diluted and plated on TGY agar plates. Black dots, wild-type strain R1; red dots, *recJ* mutant #31. Results are from one experiment, with error bars generated from three independent determinations (triplicate plating results). The whole experiment was performed twice with comparable results.

3.3.7 Nuclease Assay with Crude Cell Extracts

The stationary phase cells of wild type and the *recJ* mutant #31 were lysed by French press and the soluble portion of the cell lysates was extracted by centrifugation. Total protein concentrations of wild type and mutant cell extracts were determined by the Bradford assay as described in Materials and Methods.

Nuclease assays were carried out with the extracts of wild type and *recJ* mutant using the 5'-labeled ssDNA substrate HMC 1. As shown in figure 3.15, the nuclease activity in reactions with *recJ* mutant extract was lower than that in reactions with the same amount of wild type extract added. The small nuclease activity reduction in the mutant implies that RecJ as an exonuclease does contribute to cell's total nuclease activity.

3.3.8 Differently Tagged RecJ Proteins in Expression Tests Are Highly Insoluble

The three different expression plasmids pET15-recJ, pGEX-recJ and pSmt-recJ were constructed as described in Materials and Methods (data not shown). They were used to express N-terminal His-tagged, GST tagged and Smt3-tagged RecJ protein in *E. coli* strain BL21(DE3) respectively. The relatively large GST tag (26 kDa) is widely used in protein expression system in *E. coli*. Besides being an affinity tag, the GST may also increase solubility and stability of target protein (115). The Smt3 tag (SUMO tag) has recently emerged as an important alternative method to increase protein solubility and expression level (112,116).

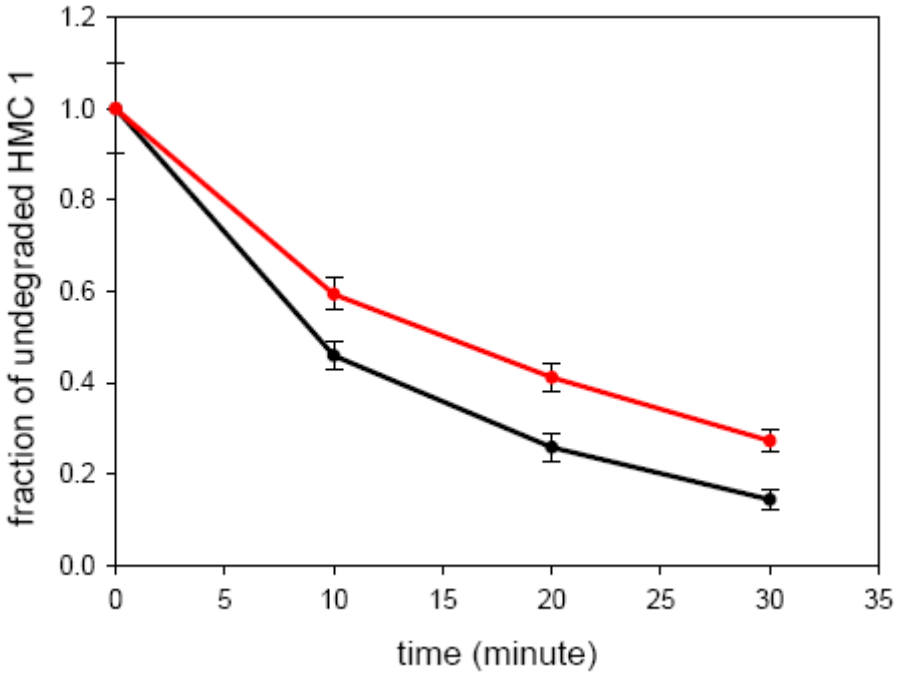

Figure 3.15 Nuclease assays with crude cell extracts. Reactions mixtures contained 50 mM Tris-HCl, pH 7.5, 2 mM $MgCl_2$, 1 mM ATP, 1 mM DTT, 0.1 mg/ml BSA, 1.2 µg of total proteins from cell extracts and 1 nM of ^{32}P 5'- labeled 32-nt ssDNA HMC 1. Reactions were incubated at 30°C for indicated time and then analyzed on native 15% polyacrylamide gels as described in Materials and Methods. Black dots: cell extract of wild type R1; red dots: cell extract of *recJ* mutant #31. Results are from one experiment, with error bars generated from three independent determinations (triplicate-reaction results). The experiment was performed four times with comparable results.

As shown in figure 3.16, in the solubility tests, the three differently tagged RecJ proteins from the auto-induction cultures grown at room temperature were all highly insoluble. The extremely low solubility of differently tagged RecJ proteins made it unlikely to be able to purify enough native RecJ protein for subsequent *in vitro* biochemical assays

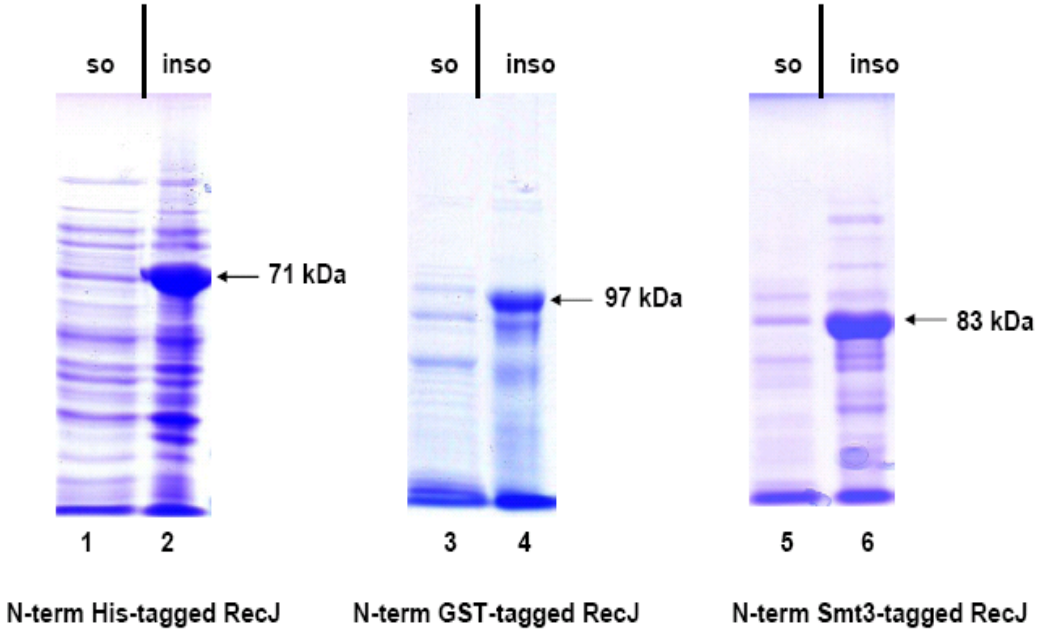

Figure 3.16 10% SDS-PAGE for RecJ solubility tests with different expression tags. The plasmids pET15-recJ, pGEX-recJ and pSmt-recJ were used to express N-terminal His-tagged, GST-tagged and Smt3-tagged RecJ proteins respectively in *E. coli* BL21(DE3) strain. After growth at room temperature in auto-induction medium, soluble and insoluble samples were prepared as described in Materials and Methods. Lane 1, 3 and 5: soluble portions of N-terminal His-tagged, GST-tagged and Smt3-tagged RecJ expression cell lysates respectively; lane 2, 4 and 6: insoluble portions of N-terminal His-tagged, GST-tagged and Smt3-tagged RecJ expression cell lysates.

3.3.9 N-Terminal His-Tagged RecJ Purification via Denaturation-Refolding

Because of the low solubility of N-terminal His-tagged RecJ protein, a denaturation-refolding pathway was employed to purify soluble RecJ.

RecJ protein expressed as inclusion body was first denatured and solubilized by 6 M urea. The re-dissolved RecJ protein was then purified by a nickel column under the same denaturing condition (6 M urea). As shown in figure 3.17, the denatured RecJ bound to nickel column relatively tightly and the majority of the protein was eluted off the column with 100 to 200 mM imidazole. On the same gel, many impurities (some of which could be fragments of RecJ) were also found in the nickel column fractions containing RecJ.

The denatured RecJ protein after nickel column was dialyzed against 1 M urea buffer A and subsequently native buffer C at 4°C, to remove denaturing reagent urea and let RecJ refold. After overnight refolding step, based on the SDS-PAGE (figure 3.18), about 40-50% of total RecJ was soluble.

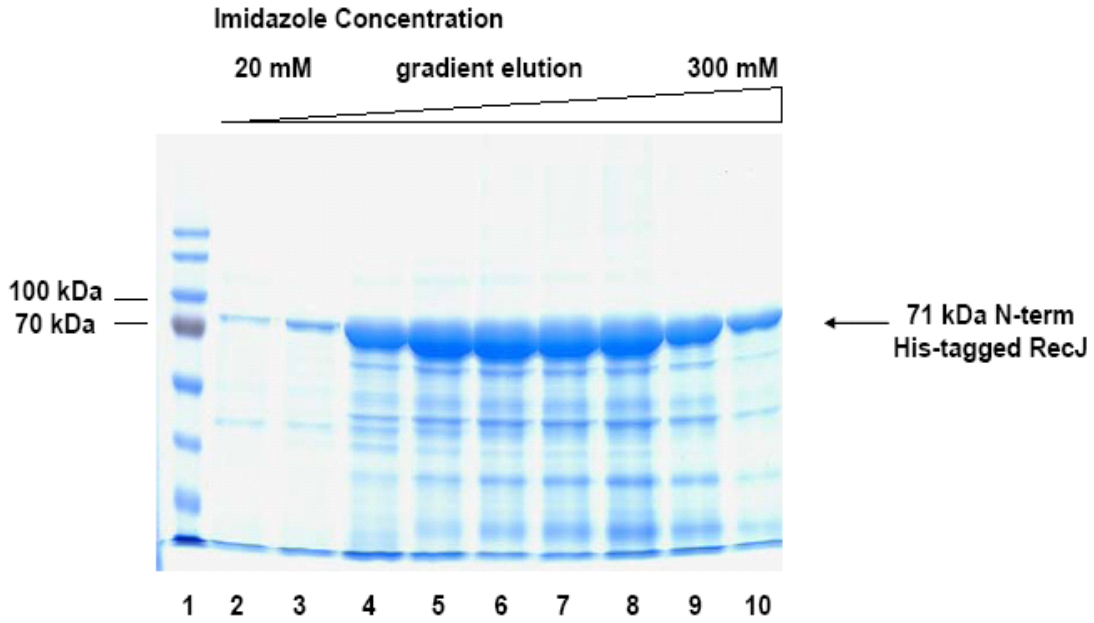

Figure 3.17 10% SDS-PAGE for denatured N-terminal His-tagged RecJ purification from a nickel column in presence of 6 M urea. Re-dissolved (denatured) N-term His-tagged RecJ was applied to a 5 ml nickel column. The column was washed and eluted by an imidazole gradient in presence of 6 M urea as described in Materials and Methods. Lane 1: Fermentas Pageruler prestained protein marker; lane 2-10: elution fractions 1-9 (corresponding to imidazole gradient from 20 mM to 300 mM).

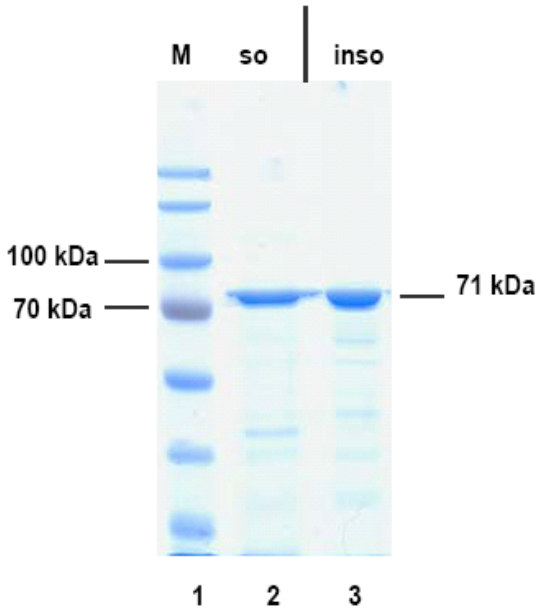

Figure 3.18 10%SDS-PAGE for refolded RecJ protein. The denatured RecJ from nickel column fractions was dialyzed against 1 M urea buffer A first and against native buffer C, to remove urea and refold. Soluble and insoluble RecJ was separated by centrifugation as described in Materials and Methods. Lane 1: Prestained protein marker; lane 2: soluble RecJ after refolding; lane 3: insoluble RecJ after refolding.

The soluble refolded RecJ protein was applied to a DEAE (anion exchange) column at pH 7.5 for further purification. The column was eluted by a 0.2 to 1.0 M NaCl gradient and the DEAE fractions were analyzed on SDS-PAGE. As seen in figure 3.19 A, relatively well purified RecJ protein was found in the early DEAE column fractions, and most of the impurities seen after nickel column were not detectable in these fractions.

The RecJ protein from DEAE fractions was tested for exonuclease activity on a linear 20-nt 5'-^{32}P-labeled ssDNA. In figure 3.19 B, the 5'-3' exonuclease activity was

consistent with the expectation based on the study of RecJ exonuclease from *E. coli* (105). There was only a small ^{32}P-labeled product observed with no apparent intermediates. The distribution of the relative exonuclease activity overlapped with that of refolded RecJ protein across all the DEAE fractions, indicating the exhibited nuclease activity was from RecJ.

3.3.10 Effects of Metal Ions and SSB on RecJ Exonuclease Activity

In following exonuclease assays, the refolded RecJ was incubated separately with different divalent cations including Mg^{2+}, Mn^{2+} and Ca^{2+} at 30°C for 30 minutes. As shown in figure 3.20 (lane 1 to 5), RecJ nuclease activity was clearly dependent on certain metal ions. The highest activity was observed in the reaction with Mg^{2+} (lane 2) and the second highest was with Mn^{2+} (lane 3). There was no detectable nuclease activity in reactions with Ca^{2+} (lane 4) and in no metal ion control reaction (lane 5).

In *E. coli* system, it is reported that *in vitro* SSB can significantly stimulate RecJ exonuclease activity (117). *D. radiodurans* SSB forms a dimer that occupies about 50 nucleotides on ssDNA, which means 2 nM SSB monomer (or 1 nM SSB dimer) are able to potentially coat 1 nM 50-nt ssDNA (118). In our experiment, 1 nM 20-nt ssDNA was included in each reaction and it required 2 nM SSB to possibly cover all the ssDNA substrates. In figure 3.20 (lane 6-10), however, *D. radiodurans* SSB bound the substrate and prevented RecJ to work on it. As a result, an inhibition effect of SSB was observed in RecJ nuclease assays.

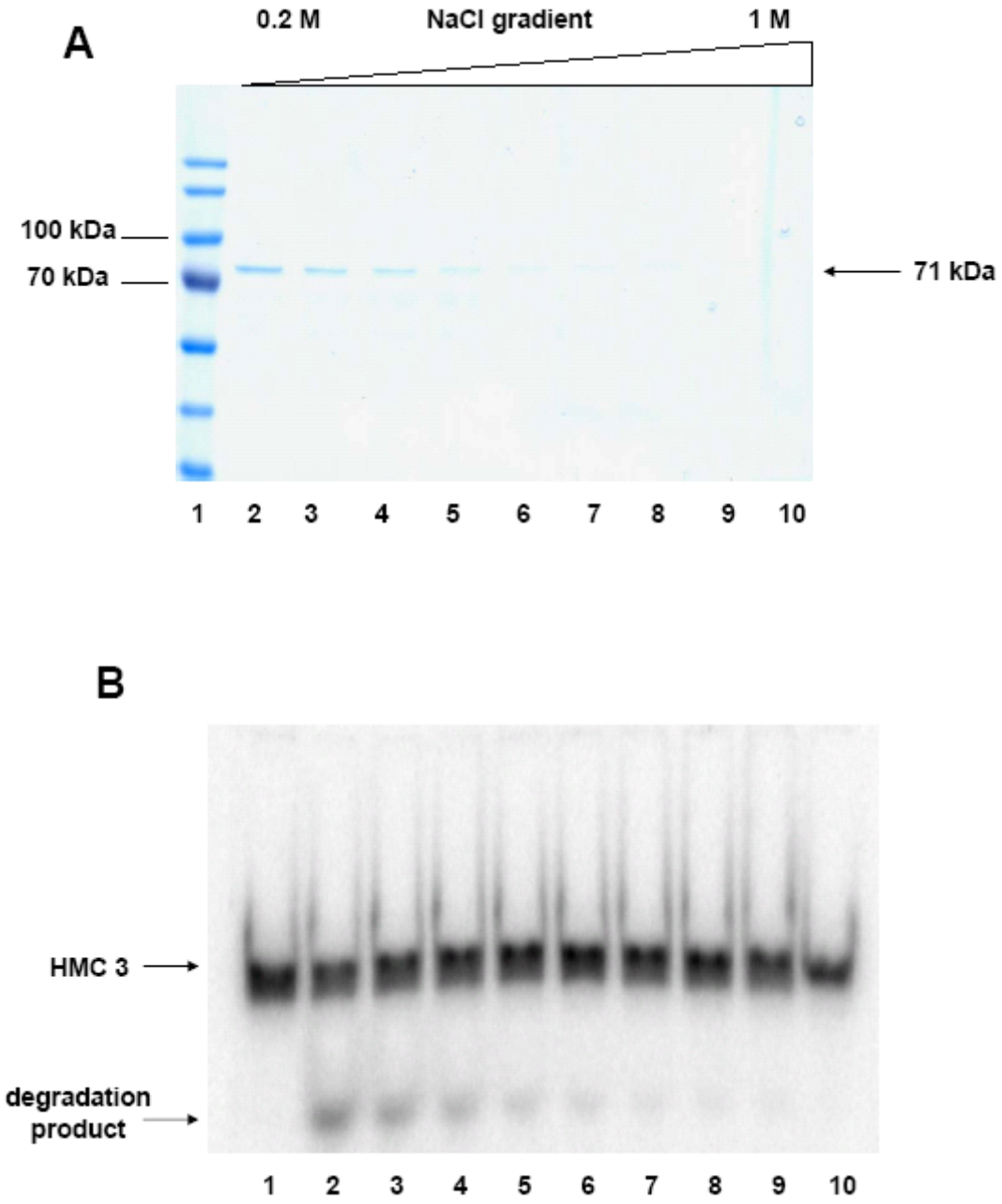

Figure 3.19 Refolded RecJ DEAE column fractions on 10% SDS-PAGE (A) and assays of exonuclease activity for each DEAE fraction (B). The soluble refolded RecJ protein was further purified by a 5 ml DEAE (anion exchange) column. The column was eluted by a NaCl gradient and the resulting fractions were tested for exonuclease activity on the 20-nt 5'-labeled HMC 3 at 30°C for 1 hour. (A) 10% SDS-PAGE for RecJ DEAE fractions: lane 1: prestained protein marker; lane 2-10: fraction 3-11. (B) Exonuclease activity assays with DEAE fractions: lane 1: no enzyme control; lane 2-10: exonuclease assays with DEAE fraction 3-11.

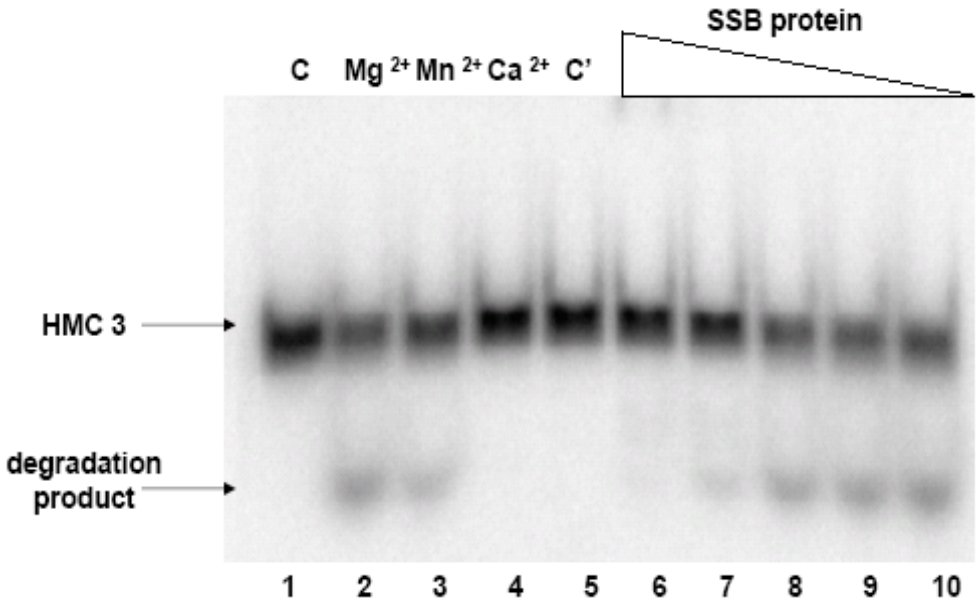

Figure 3.20 Effects of different cations and SSB protein on refolded RecJ exonuclease activity. Reaction mixtures contained 50 mM Tris-HCl, pH 7.5, 1 mM ATP, 1 mM DTT, 0.1 mg/ml BSA, 0.46 μM refolded RecJ and 1 nM of ^{32}P 5'-labeled 20-nt ssDNA HMC 3. Reactions were incubated at 30°C for 30 minutes. Three different cations were tested for metal ion effect assays (lane 1-5); in the SSB effect nuclease assays, 2 mM $MgCl_2$ was added to all reactions (lane 6-10). Lane 1: no RecJ and metal ion added control; lane 2: 2 mM $MgCl_2$ added; lane 3: 2 mM $MnCl_2$ added; lane 4: 2 mM $CaCl_2$ added; lane 5: no metal ion added; lane 6: 100 nM SSB added; lane 7: 10 nM SSB added; lane 8: 1 nM SSB added; lane 9: 0.1 nM SSB added; lane 10: no SSB added.

3.3.11 Kinetic Parameters of Refolded RecJ Exonuclease Reactions

Under the standard exonuclease reaction conditions described in Materials and Methods, the refolded RecJ protein (0.3 – 3 μM) was in large excess over the ssDNA HMC 1 substrate (10 nM). We plotted the degraded substrate concentration versus time. During the entire reaction period (60 minute), nearly linear curves were observed for each time course with different RecJ concentrations, indicating the reaction rates were almost unaltered during each reaction (figure 3.21 A). Linear regression was applied to the plotted data in figure 3.21 A to determine the slopes and initial reaction rates. The reaction rates was calculated by the equation:

$$\text{V(pM/s)} = \text{slope(nM/min)} \times \frac{1000\ \text{pM/nM}}{60\ \text{s/min}}.$$

In figure 3.21 B, the reaction rates were plotted against the concentration of refolded RecJ protein. The two kinetic parameters were determined by non-linear regression program: the value of K_s was 8.3 ($\pm$ 4.2) μM and the value for k_{cat} was 1.3 ($\pm$ 0.5) $\times$ 10^{-4} s^{-1} (the errors for both values were determined by the non-linear data fitting program).

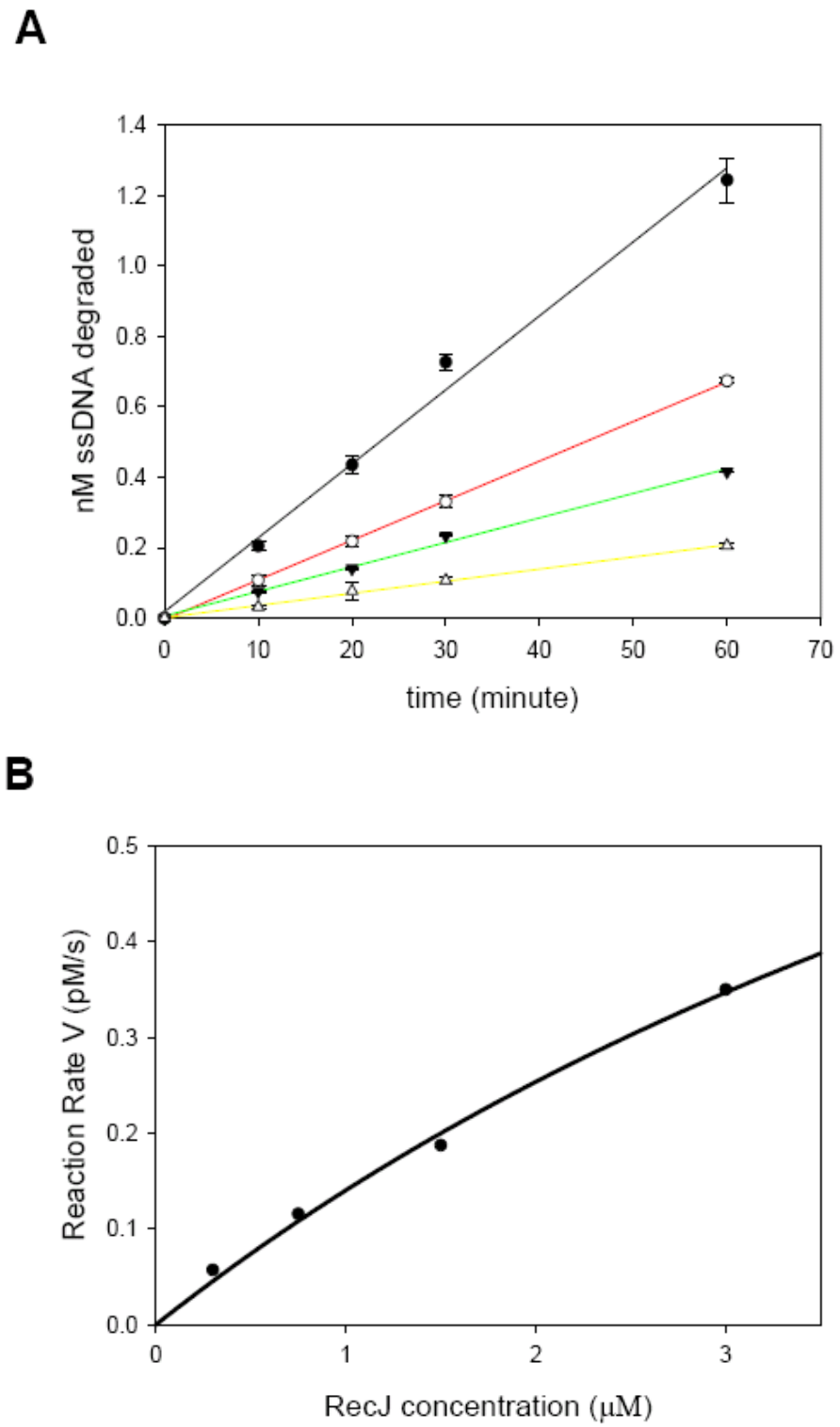

Figure 3.21 Determination of kinetic parameters of RecJ exonuclease reaction. Various amount of refolded RecJ protein was incubated with 10 nM ^{32}P labeled HMC1 in time course reactions. (A) Degraded substrate concentration was plotted in time scale, with linear regression of each reaction curve. (B) The initial reaction rate was plotted against RecJ concentration. Non-linear regression was applied to the data based on the reaction rate equation given in Materials and Methods.

3.4 Discussion

3.4.1 Primary Sequence of *D. radiodurans* RecJ

Based on the sequencing results for different *recJ* clones amplified from either *D. radiodurans* wild type strain R1 or from BAA-816, there is an additional G residue found in the same position close to the 3' terminus of the protein coding region.. With this extra nucleotide, the predicted new RecJ sequence in the same reading frame is 44-amino acids shorter in length, compared with the RecJ annotated by GenBank.

In BLASTp homologous RecJ sequence alignment (data not shown), the RecJ from *Thermus thermophilus* has the highest sequence identity (50%) to *D. radiodurans* RecJ, in addition to those homologues from other *Deinococcus* species. In contrast, the RecJ from *E. coli* only shares 33% sequence identify with that from *D. radiodurans*. The relatively close RecJ sequences of *D. radiodurans* and *T. thermophilus* are not surprising. *Deinococcus spp*. and *Thermus spp*. belong to a distinct branch of bacteria called the *Deinococsue- Thermus* group with a common origin. This is supported by the fact the two organisms consistently form a clade in phylogenetic trees of ribosomal RNAs and several conserved proteins (119). Thus the comparison of the RecJ protein properties from the two bacteria is discussed in several places below.

Another noticeable feature of the *D. radiodurans* RecJ protein sequence is that the predicted protein is somewhat shorter at the N-terminal end than the RecJ sequences from three other close relatives (figure 3.22), including *D. geothermalis*, *D. deserti* and T. *thermophilus*. The computer-predicted translation product of the upstream sequence of *D. radiodurans* RecJ protein aligns well with those of other relatives (figure 3.22).

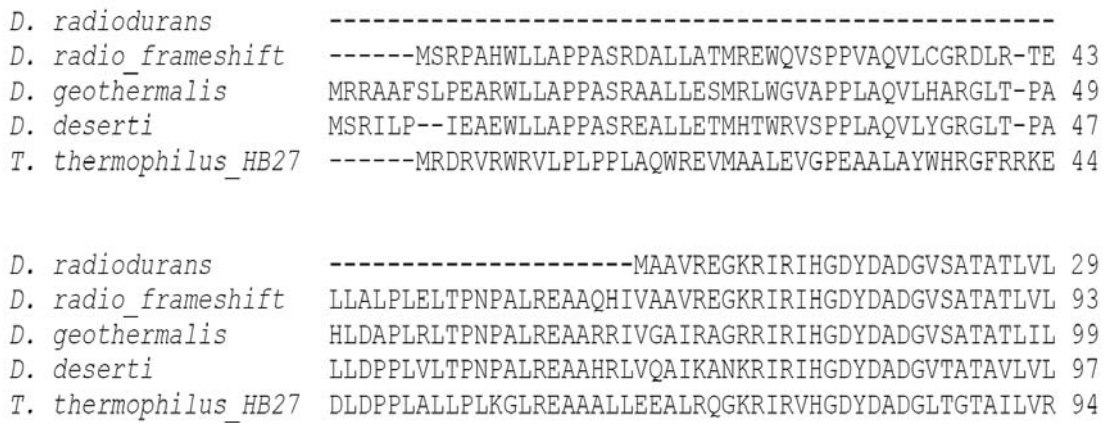

Figure 3.22 Alignment of RecJ proteins from *Deinococcus* and *Thermus thermomphilus.* The N-terminal amino acid sequences of RecJ homologues from *D. radiodurans* (locus DR_1126, GenBank accession # AAF10698), *D. geothermalis* (locus Dgeo_1599, acc. # ABF45894), *D. deserti* (locus Deide_07130, acc. # ACO45570), and *T. thermophilus* (locus TT_C0803, acc. # AAS81149) were aligned using ClustalW2 (http://www.ebi.ac.uk/Tools/clustalw2/index.html). A hypothetical form of *D. radiodurans* RecJ (*D. radio_frameshift*), in which an upstream start codon and frameshift were assumed (see text), was also used in the alignment.

The GenBank annotated *D. radiodurans* RecJ protein is translated from the putative start codon (GTG, at bp # 1,134,718). The hypothetical polypeptide (*D. radio_frameshift*) starts at an upstream ATG (bp #1,134,527). However, the upstream polypeptide is translated in a different reading frame compared to that of the annotated RecJ. Therefore a frameshift would be required to make the upstream hypothetical protein and the annotated RecJ can be translated in the same reading frame. The new resulting RecJ protein, containing the upstream polypeptide, woud align well with other RecJ homologues throughout its entire sequence. To test the above idea, we sequenced the 1 kb region that is directly upstream of the annotated RecJ start codon. The sequence we

obtained agrees unambiguously with that of GenBank and no frameshift was found in that region.

3.4.2 Inability to Obtain Homozygous *recJ* Mutants

We attempted to replace the *D. radiodurans recJ* gene on the chromosome with a streptomycin-resistant cassette via homologous recombination. This approach has been used successfully to completely delete many *D. radiodurans* genes in previous studies (56,88,120,121). However, our PCR-genotyping analysis of the resulting *recJ* mutants (25 different transformants obtained from five batches of mutants construction) showed that they were all heterozygous mutants. Quantitative RT-PCR was used to estimate the relative remaining *recJ* copies in three heterozygous mutant strains #21, 31, and 32 (RT-PCR data were not shown for #21 and 32 in the results section). A range of 30% to 45% remaining *recJ* was observed from the results of RT-PCR.

The limit of using RT-PCR to estimate the RecJ level is obvious: it cannot reflect the *recJ* cellular transcriptional or translational level. However, the amount of *recJ* mRNA or RecJ protein was almost unaltered after IR treatment in either transcriptome (70) or proteome analysis (122). This means our RT-PCR determined *recJ* gene copy number can roughly reflect the RecJ protein level in the following *in vivo* assays, if its transcription or translation is not increased as a response to low level of RecJ protein in the mutant cells.

3.4.3 Phenotype of Heterozygous *recJ* Mutants

The heterozygous *recJ* mutant #31 grew much more slowly than wild type strain even in the absence of streptomycin in growth assays. The growth defect of the *recJ*

mutant, combined with the fact we were unable to obtain a homozygous mutant, indicates RecJ has an essential role in cell viability under ordinary growth conditions. Although no extensive DNA damage is induced in growth assays, spontaneous damage can be generated as by-products of cellular metabolism (19). Damage that blocks DNA replication or transcription can be lethal if not repaired. It is likely that the remaining *recJ* gene copies in the mutant are not sufficient to efficiently remove some potentially lethal damage.

In assays where cells were treated with various DNA damaging agents, the heterozygous *recJ* mutant #31 displayed significantly higher sensitivity (10^3-10^4 fold more sensitive at high doses) than that of wild type strain to gamma rays and hydrogen peroxide. In contrast, the same mutant was only 10-fold more sensitive to UV irradiation and no more sensitive to MMS, compared to wild type strain. Comparable results were observed using *recJ* mutant #21, which is a different transformant obtained from a different batch of mutant construction. Gamma rays and hydrogen peroxide can cause massive amount of DSBs as well as single-strand breaks and base damage (19). UV irradiation primarily causes pyrimidine dimers and requires nucleotide excision repair to fix the damage. The agent MMS methylates bases at different positions and the resulting damage is repaired via base excision repair. Both UV and MMS can indirectly cause DSBs as a result of unsealed gaps after damaged nucleotide removal on opposite strands (21).

In *D. radiodurans* which lacks RecBCD, the enzymes responsible for the initiation and processing of the 3' tailed RecA substrate in DSBs repair are unknown. In *E. coli*, the

RecF pathway can catalyze RecA-dependent DSBs repair in the genetic background *recBC sbcB sbcC* (or *sbcD*). Two of the RecF pathway proteins RecQ (helicase) and RecJ (5'-3' exonuclease) are believed to work together to unwind dsDNA and process one strand from 5'-3' direction, to produce the 3' tailed intermediate (9). It has been experimentally shown that RecJ is able to binding affinity-tagged RecQ inside of *E. coli* cell (123). Recently, a seven-protein (five RecF pathway proteins, RecA and SSB) reaction that recapitulates the early steps of RecF-protein catalyzed DSB repair in *E. coli* has been reconstituted *in vitro*. This *in vitro* reaction system showed that RecJ and RecQ work together to resect dsDNA, which is a necessary step for subsequent RecA-mediated strand exchange (44). Similarly, in *D. radiodurans*, RecJ could be a key protein for DSB repair to process dsDNA ends to expose 3' ssDNA tail.

In addition to RecF pathway-mediated DSB repair, *E. coli* RecJ is also required to help resume DNA replication after the replication fork stalls at sites of UV damage without involving recombination. RecJ exonuclease and RecQ together unwind and selectively degrade newly synthesized lagging strand to generate a ssDNA gap on lagging strand template (108). The resulting gap can be loaded with RecA via RecFOR and the RecA-ssDNA filament can recruit DNA replication machinery and resume replication through an unknown mechanism (124). Therefore, it is likely that the *D. radiodurans* RecJ homologue could also be involved in rescuing arrested replication fork with other RecF pathway proteins.

In nuclease assays carried out with protein from cell extracts, a small reduction (about 20%-30%) in nuclease activity was observed in reaction with the *recJ* mutant

extract compared to that of wild type extract. This small reduction in nuclease activity could result from the fact that the mutant is heterozygous. It is also likely that other nucleases in the extract besides RecJ contribute to the observed activity.

In contrast to the strong phenotype of the *D. radiodurans recJ* mutant, *E. coli recJ* mutant has much weaker phenotype in a wild type genetic background (125) in which there are usually redundant DNA repair pathways or functionally overlapping proteins (126). The *recJ* mutation effect is usually more evident if some redundant pathways or exonucleases are inactivated. For example, the *recJ* mutation in *recBC sbcB sbcC* (or *sbcD*) background causes higher UV sensitivity and reduced recombination efficiency. Another example comes from mismatch repair, in which RecJ, ExoI, ExoVII and ExoX are the four redundant exonucleases of this repair pathway. The cells with mutations on all four nucleases grew poorly and were completely deficient in methyl-directed mismatch repair (109). *D. radiodurans* only encodes three of the five exonucleases (four mismatch repair exonucleases and sbcCD) encoded in *E. coli*, including RecJ, ExoVII and SbcCD (3). The more severe effect of *recJ* deletion in *D. radiodurans* than that of *recJ* deletion in *E. coli* could be partially due to the absence of the other exonuclease homologues.

3.4.4 *In Vitro* Characterization of RecJ

Like its close relative T. *thermophilus* RecJ (ttRecJ) (113), *D. radiodurans* RecJ (drRecJ) was highly insoluble with different affinity tags. The drRecJ in the initial form of inclusion body after expression was purified via denaturation-refolding pathway. This

is a relatively reliable method to purify drRecJ and more than three batches of refolded soluble RecJ with similar quality were reproducibly made with this method.

The soluble refolded drRecJ exhibited exonuclease activity on a 5' labeled linear ssDNA. On the nuclease reaction gels, only a small ^{32}P-labeled product was observed, with no apparent partially degraded intermediate (figure 3.19). There was no reaction with blunt ended linear double-stranded DNA (HMC 3+ 2) nor with 12 nt-3' tailed dsDNA (HMC1 + 2) (data not shown). The results indicated that drRecJ specifically degraded ssDNA in a 5'-3' direction, which is the same as that of ttRecJ (113) and RecJ in *E. coli* (117). However, we are not certain about the exact form of the drRecJ nuclease products. The RecJ of *E. coli* degrades ssDNA completely into mononucleotides (117). The drRecJ nuclease products could be verified by running the reaction mixtures on TLC plates along with mononucleotides as markers.

In addition, the drRecJ exhibited approximately the same exonuclease activity with Mg^{2+} or Mn^{2+} whereas no activity could be detected with Ca^{2+}, suggesting the highly concentrated cellular antioxidant Mn^{2+} is not specifically required for the nuclease activity. We also tested the interaction between *D. radiodurans* SSB and drRecJ in nuclease reaction. In *E. coli*, DNA binding and nuclease activity of RecJ is specifically enhanced by the pre-addition of *E. coli* SSB (117). It is proposed that the interaction between the two proteins may help recruitment of RecJ onto the substrates (117). In our assays, however, addition of increasing amount of SSB leads to inhibition of of drRecJ nuclease activity (figure 3.20). The inhibitory interaction could be caused by the incorrect folding of drRecJ or the His-tag interference.

Similar to the refolded ttRecJ, the exonuclease reaction with the refolded drRecJ is very slow and requires a large amount of enzyme and long reaction time to detect product formation. Our drRecJ has a K_s of 8.3 ($\pm$ 4.2) μM at 30°C, which is comparable to the K_s (4.0 $\pm$ 1.4 μM) of refolded ttRecJ at 50°C (the optimal temperature for ttRecJ activity) (113). However, the k_{cat} of drRecJ is 1.3 ($\pm$ 0.5) $\times$ 10^{-4} s^{-1}, which is 30-times less than that obtained with refolded ttRecJ. We do not know the fraction of refolded drRecJ or ttRecJ that is actually active in either study. The reaction rates of both refolded enzymes are much lower than the native core domain of ttRecJ or native RecJ from *E. coli*. The core domain of ttRecJ identified by sequencing the stable ttRecJ fragment resistant to limited proteolysis is soluble. Their subsequent far-UV circular dichroism spectra showed that both refolded ttRecJ and its native core domain were properly folded (113). In our situation, we do not know if the drRecJ is properly folded as we don't have a native drRecJ (or core domain) to compare.

To conclude, the phenotype of heterozygous *D. radiodurans recJ* mutants suggests that RecJ has an important role in DNA repair, especially in RecF pathway catalyzed DSB repair. I propose that *D. radiodurans* RecJ works together with a helicase, perhaps with RecQ, to unwind dsDNA (by helicase), resect one strand with its 5'-3' exonuclease and produce a 3' tailed ssDNA intermediate for RecA binding in the HR or ESDSA pathway.

CHAPTER 4 *DEINOCOCCUS RADIODURANS* RECD PROTEIN BINDING PARTNER INVESTIGATION

4.1 Introduction

The isolated RecD homolog protein encoded in *D. radiodurans* has been characterized both *in vivo* and *in vitro*. The *D. radiodurans* RecD protein is a DNA helicase with 5'-3' polarity and low processivity (17). The *recD* mutant is significantly more sensitive to gamma rays, UV, and hydrogen peroxide than wild type cells (46) indicating its important role(s) in some unidentified DNA repair pathway(s). In contrast, the RecD protein in *E. coli* associates with the RecB and RecC proteins *in vitro* to form a heterotrimeric complex (127). In addition to the physical association, the subunits of RecBCD complex are functionally interdependent as all three subunits are required for the complex to possess its multi-biochemical activities and substrate specificity (18).

Although *D. radiodurans* is naturally devoid of *recB* and *recC*, it is still very possible that the RecD functions as part of a multiprotein complex other than RecBCD in the cell or that it transiently interacts with other proteins for a specific function. Thus the *D. radiodurans* RecD cellar binding partner identification could be very helpful to have better understanding of the function of RecD in a specific DNA repair pathway.

To test this idea, *D. radiodurans* RecD was overexpressed and purified as described in Materials and Methods of this chapter. The purified RecD was used as a ligand in protein affinity chromatography to fish out possible binding partners from *D. radiodurans* crude cell extract. The potential RecD-binding candidates (identified later as RNA polymerase core enzyme) were sent for identification via mass spectrometry. The

interaction between the RecD and the partially purified RNA polymerase were repeated with protein affinity column, nickel column and far western blot *in vitro*.

4.2 Materials and Methods

4.2.1 *D. radiodurans* RecD Expression and Purification

The *D. radiodurans recD* gene (2.2kb) has been inserted to the protein expression vector pET21a (Novagen). The resulting plasmid pDr-recD-21 which encodes the RecD protein with a His-tag appended to its C terminus was stored in the *E. coli* host strain Top 10 (Invitrogen). The plasmid pDr-recD-21 freshly extracted from 5 ml overnight culture of Top 10 cells was transformed into *E. coli* strain BL21(DE3) (Novagen) and the transformants were selected on LB agar plates with 100 μg/ml ampicillin added.

A single colony of pDr-recD-21in BL21(DE3) from above transformation plates was used to start overnight culture in 10 ml LB medium containing 200 μg/ml ampicillin at 37°C. The next day the 10 ml overnight culture was diluted with 1 liter (1:100 dilution) fresh LB medium added with 100 μg/ml ampicillin and shaken at 37°C. During the growth, cell density was monitored at OD_{600} using a UV spectrophotometer. After OD_{600} of the culture reached 0.4 – 0.6, 0.2 mM final concentration of IPTG was added to the culture to induce expression of RecD at 30°C for 3 hours with vigorous shaking. The cells with RecD protein overexpressed were harvested by centrifugation at 6,000 ×G, 4°C for 20 minutes and stored at -80°C.

The strategy applied to purify *D. radiodurans* RecD protein was close to that used in HelIV proteins purification. The frozen cell pellet (~6-8 grams of wet cells per liter

culture) stored at -80°C was thawed on ice and then suspended with 50 ml of native buffer (20 mM sodium phosphate, 500 mM NaCl, pH 7.8) supplemented with 20 mM imidazole, 1 mM PMSF and 50 µl /g cells protease inhibitor cocktail (Sigma-Aldrich). After cells were lysed by sonication, the supernatant including soluble RecD protein was separated and saved from cell debris by centrifugation at 10,000 ×G, 4°C for 2 hours.

The crude cell lysate obtained from the previous step was loaded onto a 5-ml Ni^{2+}-NTA column which was pre-equilibrated with 10 column-volumes of native buffer. The column was washed with 10 column-volumes of native buffer containing 60 mM imidazole, and then eluted with a 60 ml gradient of 60-500 mM imidazole in native buffer.

The nickel column fractions containing RecD protein (based on the results of 10% SDS-PAGE) were combined and dialyzed against Buffer A (20 mM potassium phosphate, pH 7.5, 1 mM EDTA, 1 mM DTT, 10% (v/v) glycerol) containing 50 mM NaCl at 4°C overnight. The precipitated proteins were removed by centrifugation and the soluble portion was applied to a 5-ml ssDNA cellulose column. The ssDNA column was washed with 50 ml of Buffer A containing 50 mM NaCl and then eluted stepwise with 30 ml 0.6 M NaCl, 30 ml 1.0 M NaCl and 30 ml 1.5 M NaCl in Buffer A. The fractions containing purified RecD protein were pooled and dialyzed against Buffer A containing 100 mM NaCl, to decrease the high NaCl concentration applied in elution steps. The dialyzed RecD protein was concentrated by ultrafiltration and stored at -80°C in Buffer A with 50% (v/v) glycerol.

RecD protein concentration was determined from the absorbance at 280 nm, using ε_{280} = 53860 M^{-1} cm^{-1} for C-terminal His-tagged 78 kDa RecD (calculated with the program ProtParam at ca.expasy.org/tools/protparam.html).

4.2.2 Conjugation of Purified RecD Protein onto Affi-Gel 15 Resin

RecD *in vivo* binding partners investigation was first assayed by affinity chromatography using Affi-Gel 15 affinity support (BioRad). Affi-Gel 15 is a type of activated affinity supports that have N-hydroxysuccinimide esters crosslinked to agarose gel bead (figure 4.1 B). They can rapidly and efficiently form covalent amide bonds with all ligands with a primary amine group including proteins (figure 4.1 A). Besides, Affi-Gel 15 resin is slightly positively charged in the physiological pH range (6.5-8.5), which is to enhance coupling process with the negatively charged RecD protein (pI 6.2).

About 1.0 ml slurry of activated Affi-Gel 15 matrix was washed with 5 ml of ice-cold deionized water three times and then equilibrated with 5 ml of coupling buffer (25 mM HEPES, pH 7.5, 10% glycerol (v/v), 50 mM NaCl). The purified RecD protein (~ 2 mg) stored at -80°C in 50% glycerol was dialyzed against coupling buffer at 4°C overnight and then mixed with 0.2 ml of the pre-treated Affi-Gel resin. The coupling reaction was incubated at 4°C overnight with gentle agitation. After overnight coupling, soluble (unbound) RecD remaining in the coupling buffer was assayed by measuring the OD_{280} after mixing with equal volume of 0.1 M HCl. The HCl is supposed to bring down the pH of protein samples as the N-hydroxysuccinimide released during coupling will absorb at 280 nm at neutral or basic pH.

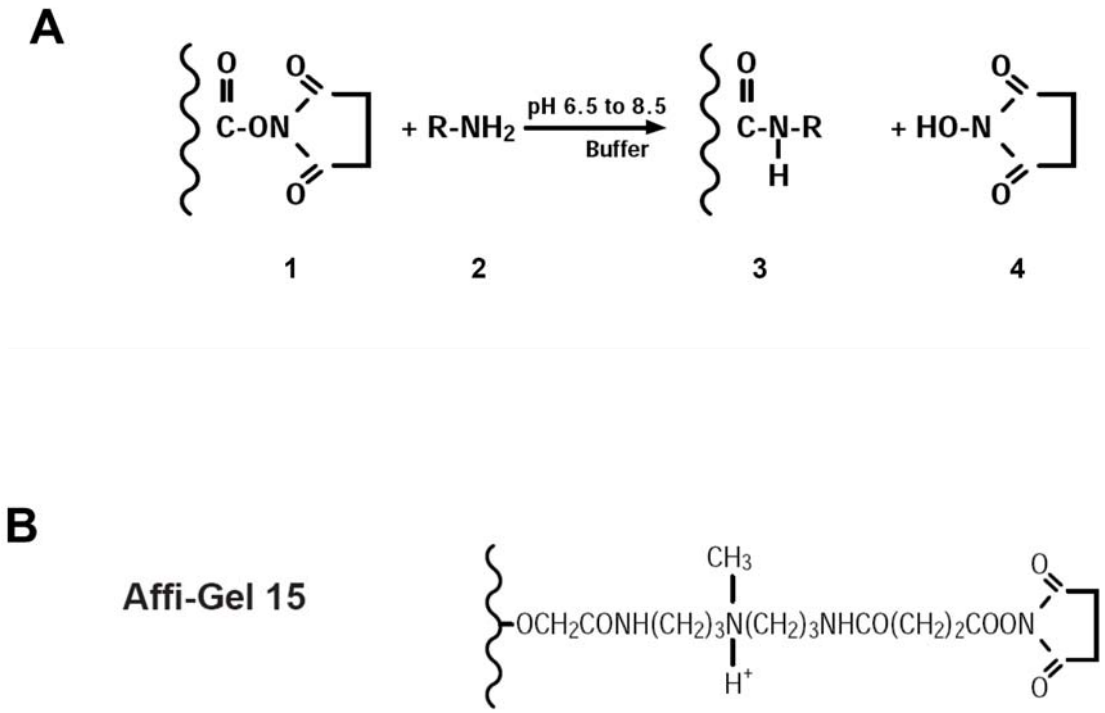

Figure 4.1 Coupling reaction of Affi-Gel supports with ligand containing primary amine groups (A) and the structure of Affi-Gel 15 supports (B). (A) The chemical conjugation reaction that happens between Affi-Gel supports and its ligand. 1- N-hydroxysuccinimide ester cross-linked to agrose bead; 2- protein ligand with a primary amine group; 3- ligand protein chemically conjugated to Affi-Gel support via formation of an amide bond; 4- N-hydroxysuccinimide released after reaction. Figure is adapted from Cline and Hanna, 1987 (128). (B) The schematic structure of Affi-Gel 15 support with a positively charged 15-atom spacer and an active N-hydroxysuccinimide ester. Figure is adapted from Cuatrecasas and Parikh, 1972 (129).

Due to the relative large binding capacity of Affi-Gel 15 (35 mg protein per milliliter resin) and limited amount of purified RecD available, after the first RecD coupling step, 10 mg BSA protein (Sigma Aldrich) dissolved in water was added to the same reaction and incubated at 4°C for another four hours with gentle agitation. The amount of unbound BSA after coupling was calculated from its OD_{280} using ε_{280} = 46238 M^{-1} cm^{-1}. According to the Affi-Gel 15 manufacturer's instruction, a precautionary step of blocking any remaining active ester site with 1 M ethanolamine-HCl (pH 8.0) was applied for 1 hour incubation, after the second coupling step with BSA was performed.

A BSA control column was prepared in a similar way: 10 mg of BSA (the only ligand) dissolved in water was coupled with 0.2 ml Affi-Gel slurry followed by ethanolamine blocking step.

4.2.3 RecD-Based Protein Affinity Chromatography

Around 1.5 grams of *D. radiodurans* wild type BAA-816 strain cells (grown at 30°C, harvested at OD_{600} = 1.0) were resuspended with 20 ml loading buffer (coupling buffer supplemented with 1 mM EDTA, 1 mM DTT and 100 µl/g cells protease inhibitor cocktail). The cells were subsequently lysed by passing through a French press five times at 1,000 PSI. The cell lysate was then centrifuged at 10,000 ×G, 4°C for 1 hour to remove cell debris. The soluble portion of the cell lysate then was incubated at 37°C for 1 hour with 8 units/ml Benzonase® nuclease (Novagen) which can degrade all forms of DNA and RNA into oligonucleotides 2-5 bases in length. After the treatment with nuclease, the total soluble protein concentration was determined by Bradford assay reagents. The 10 ml of clear cell lysate was loaded onto the 0.2 ml RecD-BSA based protein affinity column

which was already equilibrated with 5 ml of loading buffer. The same volume of cell lysate was applied to the BSA-based control column. Both of the RecD-BSA column and the BSA control column were washed and eluted in the same following steps. Each of the columns was washed with 15 ml loading buffer and eluted with a 30 ml gradient of 50-500 mM NaCl dissolved in loading buffer. As the final wash step, 10 ml of 2 M NaCl in loading buffer was applied to each affinity column to clean off any remaining protein that was still associated with the column.

4.2.4 Silver Staining of 10% SDS-PAGE

The elution fractions from RecD-BSA column and BSA control column were analyzed by 10% SDS-PAGE followed by silver staining which is more sensitive to low-concentration protein on the gel than regular coomassie staining.

After electrophoresis was finished, SDS-PAGE gels were first soaked in water based solution containing 50% methanol and 5% acetic acid for 20 minutes. Gels were then incubated in 50% methanol in water to remove remaining acetic acid. Then gels were sensitized by 1 minute incubation with 0.02% $Na_2S_2O_3$ (sodium thiosulfate) in water followed by two rinses of distilled water. Gels were submerged in 0.1% $AgNO_3$ at 4°C for 20 minutes and then transferred to distilled water for 1 minute to rinse off extra $AgNO_3$ left on the gels. The gels were developed on a shaker in 0.04% formaldehyde water solution with 2% $NaCO_3$ until they turned yellow color. Development reaction was stopped by discarding the developing solution and transferring gels into 5% acetic acid water solution.

The SDS-PAGE that contained the bands of possible RecD binding partners was sent to the Genome Center Proteomic Facility at University of California, Davis for protein identification (by liquid chromatography combined with tandem mass spectrometry).

4.2.5 *D. radiodurans* RNA Polymerase (RNAP) Purification

The following method applied for *D. radiodurans* RNAP purification is modified from the protocol used for of *E. coli* RNAP core enzyme purification (130).

About 10 grams of *D. radiodurans* wild type BAA-816 strain cells (grown at 30°C, harvested at OD_{600} = 1.0) were resuspended with 50 ml lysis buffer (50 mM Tris-HCl, pH 8.0, 5% glycerol, 1 mM PMSF, 5 mM DTT, 50 µl/g cells protease inhibitor cocktail). The cells were lysed by passing through a French press five times at 1,000 PSI and the soluble portion of the cell lysate was separated from cell debris by centrifugation at 10,000 ×G, 4°C for 1 hour. The clear cell lysate from last step was added slowly with 10% (v/v) pH 7.9 polyethyleneimine (polymin P) (Sigma-Aldrich) to a final concentration of 0.5% polymin P. The highly positively charged polymer polymin P can precipitate negatively charged genomic DNA along with associated proteins including RNAP. The resulting mixture with polymin P added was slowly stirred with a magnetic bar for 15 minutes, followed by centrifugation at 10,000 ×G, 4°C for 1 hour. The pellet including genomic DNA and associated proteins was washed twice with 50 ml TGED buffer (10 mM Tris-HCl, pH 8.0, 0.1 mM EDTA, 5% glycerol, 1 mM DTT) containing 0.5 M NaCl, to remove relatively loosely DNA bound proteins. The pellet after previous two wash steps was then resuspended with 50 ml TGED buffer containing 1 M NaCl, which was a high enough NaCl concentration to elute *D. radiodurans* RNAP from genomic DNA. This

resuspension with 1 M NaCl was centrifuged at 10,000 ×G for 30 minutes and the supernatant containing eluted RNAP was saved for further purification. The RNAP was then salted out by slowly adding solid $(NH_4)_2SO_4$ up to 60% saturation in the supernatant obtained from last spinning step. The precipitated RNAP was collected by centrifugation 10,000 ×G for 30 minutes and re-dissolved in 20 ml TGED buffer containing 0.1 M NaCl.

The re-dissolved RNAP solution was subsequently loaded to a weak cation exchange column packed with 15 ml Bio-Rex 70® resin (BioRad) equilibrated with TGED buffer containing 0.2 M NaCl. The column was washed with 50 ml TGED buffer containing 0.2 M NaCl and eluted with a 90 ml gradient of 0.2-1.0 M NaCl in TGED buffer. The fractions containing RNAP (checked by 10% SDS-PAGE) were combined and concentrated using ultrafiltration. The concentrated RNAP solution was dialyzed against Buffer A with 50% glycerol (same storage buffer used for RecD) and stored at -80°C.

The concentration of purified *D. radiodurans* RNAP was determined by the total absorbance at 280 nm using $\varepsilon_{280} = 214605\ M^{-1}\ cm^{-1}$ which is the sum of each RNAP subunit's extinction coefficient. The *D. radiodurans* RNAP core enzyme subunits that were assumed to calculate total ε_{280} and molecular weight include beta prime, beta, alpha and omega (3).

4.2.6 Binding of Purified RNAP on RecD-BSA Protein Affinity Column

The preparations of a 0.2 ml RecD-BSA conjugated Affi-Gel 15 affinity colum and a 0.2 ml BSA control column were as described in previous Materials and Methods section of this chapter. The partially purified RNAP stored in Buffer A with 50% glycerol was dialyzed against the HEPES loading buffer (20 mM HEPES, pH 7.5, 50 mM NaCl, 10%

glycerol) at 4°C overnight. The RNAP molar concentration was determined by its OD_{280} reading and extinction coefficient.

About 0.2 nmole RNAP was loaded onto the RecD-BSA column and the BSA control column separately. Each of the columns was then eluted sequentially with 4 ×5 ml of loading buffer containing 50 mM, 100 mM, 200 mM and 2 M NaCl respectively. The resulting elution fractions were analyzed by silver-stained 10% SDS-PAGE.

4.2.7 RecD and RNAP *In Vitro* Binding Assays with Nickel Spin Column

The purified RecD can bind to nickel column via the interaction between its C-terminal His-tag and the Ni^{2+} cations on the resin. If a RecD-bound nickel column is prepared, RNAP can be applied to the RecD column to test their interaction.

The purified RecD and RNAP that were both stored in Buffer A with 50% glycerol were dialyzed against HEPES loading buffer (the same HEPES buffer as used in section 4.2.6) at 4°C overnight. Their molar concentrations were determined separately from their UV absorbance at 280 nm.

Ni^{2+}-NTA resin (25 µl) was equilibrated with HEPES loading buffer and packed in each mini-spin column (BioRad). Two slightly different ways were employed to set up binding assays involving RecD and RNAP.

Binding assay one: 0.18 nmole of purified RecD was mixed with the pre-treated 25 µl nickel resin in a mini column at 4°C for 30 minutes with gentle shaking. The mini column was spun at 10,000 ×G for 30 seconds to remove unbound RecD. The nickel resin bound with RecD was then incubated with 0.20 nmole purified RNAP at 4°C for 1 hour.

Binding assay two: roughly equal amout of RecD (0.18 nmole) and RNAP (0.20 nmole) mixed in a 1.5 ml microtube were incubated at 4°C for 10 minutes. Then the pre-mixed binding mixture was loaded to a nickel mini column and incubated at 4°C for 1 hour with gentle shaking.

In both of the binding assays, after the indicated reaction time, each mini column was washed with 40 mM imidazole in loading buffer five times and eluted with 400 mM imidazole in loading buffer three times. 10% silver-stained SDS-PAGE gels were used to analyze the samples prepared from loading flowthrough, wash and elution fractions of each mini-spin column.

4.2.8 Detecting RecD and RNAP Interaction Using "Far Western Blot"

Far western blot is a useful technique to study protein-protein interactions. This technique involves separating proteins on SDS-PAGE, blotting to PVDF membrane and probing the blot with a protein of interest. Although many protein-protein interactions are based on their tertiary or secondary structures which are disrupted under the reducing and denaturing condition in SDS-PAGE, some types of protein interactions can still occur and be detected using the far western blot technique even after one of the partners has been denatured (131).

About 2.3 μg of partially purified RNAP and 2.5 μg of RecD were heated in SDS loading buffer separately at 95°C for 2 minutes before they were applied to 10% SDS-PAGE. The proteins from SDS-PAGE were then transferred to a piece of PVDF membrane at 30 mA for 20 hours using a Bio-Rad transfer apparatus. Alternatively, the same amount of native RNAP was subjected directly to a small piece of PVDF membrane

which was then air dried at room temperature to fully absorb the applied proteins. The PVDF membrane with transferred RNAP (denatured or native) was blocked with 4% milk in 1 × t-TBS for 1 hour and incubated in the same milk blocking solution supplemented with 40 nM purified RecD (used as RNAP binding probe) for another hour. Free or loosely bound RecD was removed by rinsing the PVDF membrane with t-TBS buffer. The blot then was incubated with the monoclonal anti-RecD primary antibody (lab stock) and the secondary antibody (Novagen) conjugated with alkaline phosphatase, followed by visualization after reaction with ECF substrates as described in Materials and Methods in Chapter 2.

4.3 Results

4.3.1 RecD Protein Expression and Purification

The *D. radiodurans* C-terminal His-tagged RecD protein was expressed in *E. coli* strain BL21(DE3), with 0.2 mM IPTG induction at 30°C for 3 hours. Total 22 grams of cell pellet from 3 liters of IPTG-induced LB culture were lysed by sonication and the resulting clear cell lysate containing soluble RecD protein was separated first by a nickel column. As shown in figure 4.2, most of the C-terminal His-tagged RecD protein was eluted off the nickel column by 150-250 mM imidazole and it was mainly concentrated in 6 fractions (3 ml/fraction, total 22 fractions). The combined RecD nickel column fractions were dialyzed and applied to a ssDNA cellulose column in the second purification step. The ssDNA column bound with RecD protein was eluted stepwise using increased NaCl concentrations. In figure 4.3, RecD was majorly washed off the column at the 0.6 M NaCl

elution step. After two-step column purifications, the relatively well purified RecD protein with good quality and concentration (0.5 mg/ml) was stored in Buffer A with 50% glycerol at -80°C. The overall yield for RecD expression and purification was about 0.5 mg/liter IPTG-induced culture.

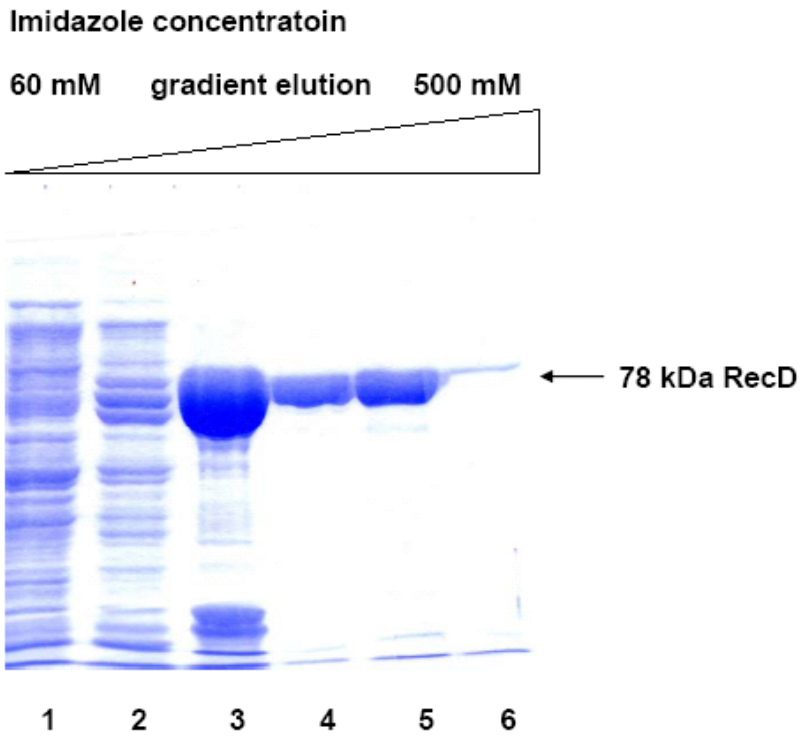

Figure 4.2 10% SDS-PAGE gels for C-terminal His-tagged RecD from a nickel column. The 22 grams of IPTG-induced cells were lysed by sonication and the soluble portion of cell lysate was loaded to a 5-ml Ni2+-NTA column. The column was washed and eluted as described in Materials and Methods. Selected nickel column fractions were analyzed on 10% SDS-PAGE. Lane1: column wash with 60 mM imidazole; lane 2: fraction No.1; lane 3: fraction No. 3; lane 4: fraction No. 6; lane 5: fraction No. 8; lane 6: fraction No. 10.

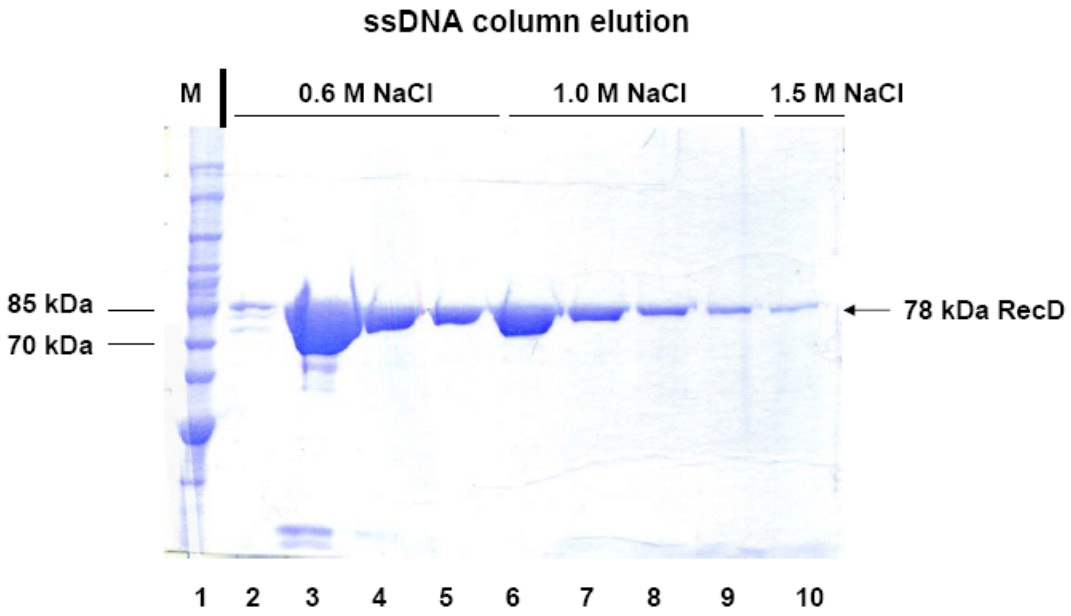

Figure 4.3 10% SDS-PAGE for the second step RecD purification using ssDNA column. The fractions from nickel column containing RecD protein were combined and dialyzed against Buffer A with 0.1 M NaCl. The soluble RecD portion after dialysis was applied to a 5-ml ssDNA column and the column was eluted as described in Materials and Methods. Lane 1: Fermentas Pageruler unstained protein marker; lane 2-9: fraction No. 7-14; lane 10: fraction No. 19.

4.3.2 Affi-Gel 15 Coupling Reactions with RecD and BSA Proteins

The protein affinity column resin Affi-Gel 15 has an activated terminal group (N-hydroxysuccinimide ester) that can react with any primary amine group including protein N-termini and side chain of lysine residues, to form a covalent amide bond. A protein affinity column saturated with ligands could become a very sensitive tool to investigate unknown protein interactions with the ligand.

Due to the large protein binding capacity of Affi-Gel resin (35 mg/ml) and relative low RecD expression yield, two modifications were made to construct RecD based protein affinity column: 1) as small column volume as 0.2 ml was used; 2) enough pure BSA protein was applied to occupy the remaining active sites on Affi-Gel after RecD coupling. BSA is an acidic protein (pI 4.9) with a close molecular weight (69 kDa) to 78 kDa RecD (pI 6.2) under physiological pH. To ensure any protein fished out by RecD-BSA column was because of its specific interaction with RecD rather than BSA, a control protein affinity column saturated by BSA protein was constructed and assayed in parallel with RecD conjugated column.

After up to 12 hours reaction time, 70% (1.4 mg) of the initially applied 2 mg RecD protein was conjugated to the 0.2 ml Affi-Gel 15 resin that had a 7 mg total protein binding capacity. About 4 mg out of 10 mg BSA protein was coupled to the remaining active sites in the RecD column. As a result, the 0.2 ml RecD-BSA Affi-Gel resin contained 20% RecD, 60% BSA and 20% ethanolamine (blocking reagent). In contrast, the BSA only based Affi-Gel resin had 90% of the active sites occupied by BSA protein and 10% blocked by ethanolamine.

4.3.3 RecD Based Protein Affinity Pull Down Assays

10 ml nuclease-treated *D. radiodurans* wild type cell extract (containing about 25 mg total proteins) was applied to the RecD-BSA protein affinity column. The column was eluted with a NaCl gradient and its elution fractions were visualized by silver-stained 10% SDS-PAGE. The BSA control column was eluted and analyzed in the same way. As shown in figure 4.4 A, there were quite some *D. radiodurans* cellular proteins interacting with RecD-BSA columns, although their binding affinity was not strong and most of the interacting bands were eluted off the column by 50-100 mM NaCl. In contrast, almost all *D. radiodurans* cellular proteins passed through BSA control column (figure 4.4 B) without any even weak binding to BSA. This result indicated that at least some of the proteins found in RecD-BSA column elution fractions truly interacted with RecD protein on the column. We were especially interested in those four bands (number Band 1-4) located above the RecD position on SDS-PAGE. Unlike the other possible RecD interacting proteins positioned below RecD, the upper four bands were definitely not from RecD fragmentation.

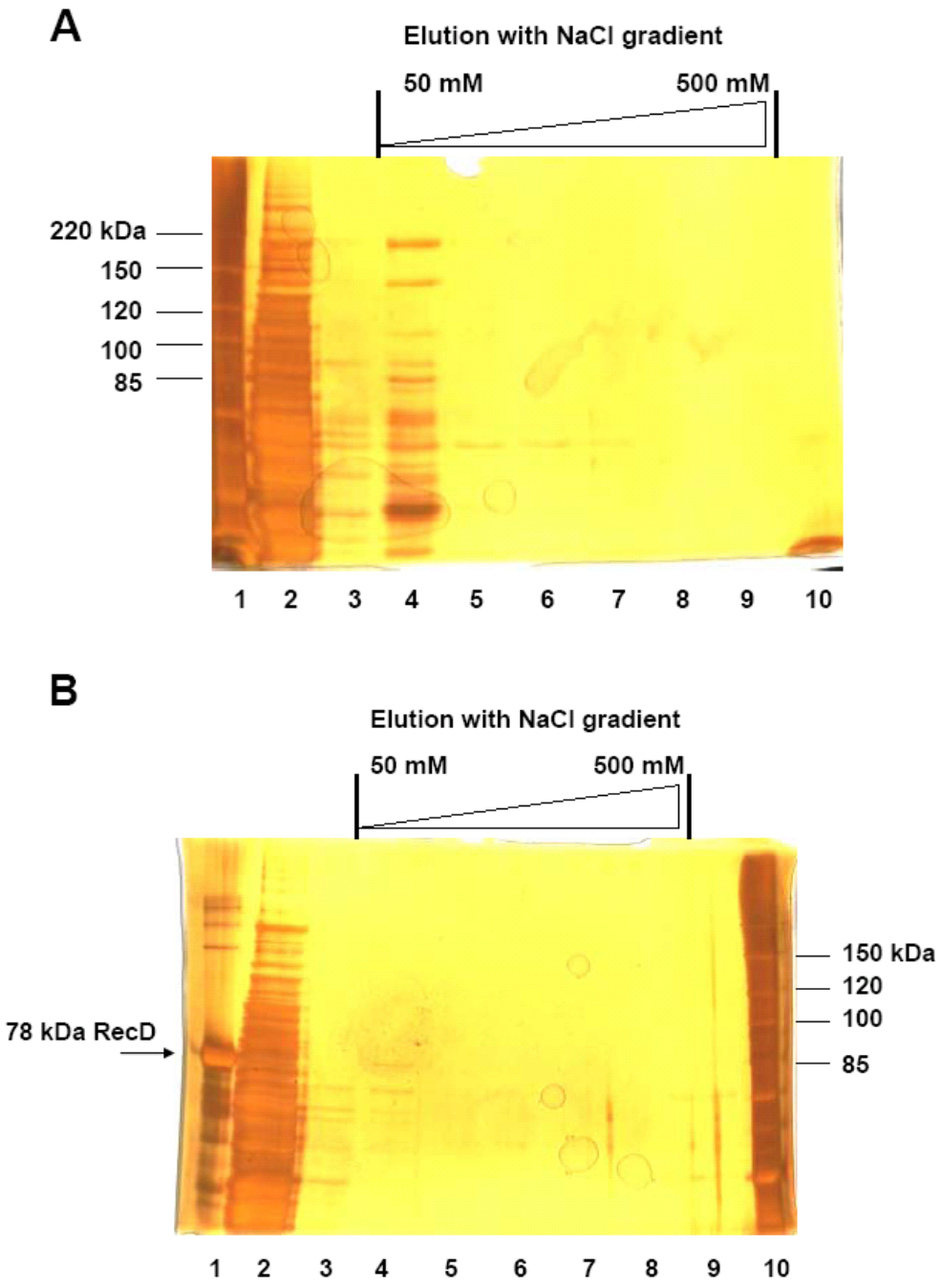

Figure 4.4 Silver-stained 10% SDS-PAGE gels for the fractions from the RecD (A) and BSA (B) based protein affinity columns. Wild type *D. radiodurans* cell crude lysate was applied to RecD-BSA and BSA conjugated Affi-Gel columns separately. Each of the columns was washed and eluted in the same way as described in Materials and Methods. (A) The fractions were eluted from RecD-BSA column. Lane 1: Fermentas unstained protein marker; lane 2: loading flowthrough; lane 3: wash step; lane 4-9: elution fractions 1-6; lane 10: final wash with 2 M NaCl. (B) The fractions were from BSA control column. Lane 1: purified RecD; lane 2: loading flowthrough; lane 3: wash step; lane 4-8: elution fractions 1-5; lane 9: final wash with 2 M NaCl; lane 10: Fermentas unstained protein marker.

As shown in figure 4.5, the parallel elution fractions from RecD and control column were re-run in another silver-stained 10% SDS-PAGE in which more samples were loaded to each lane. The four bands as labeled on the gel were sent to Genome Center Proteomic Facility at University of California, Davis for protein identification.

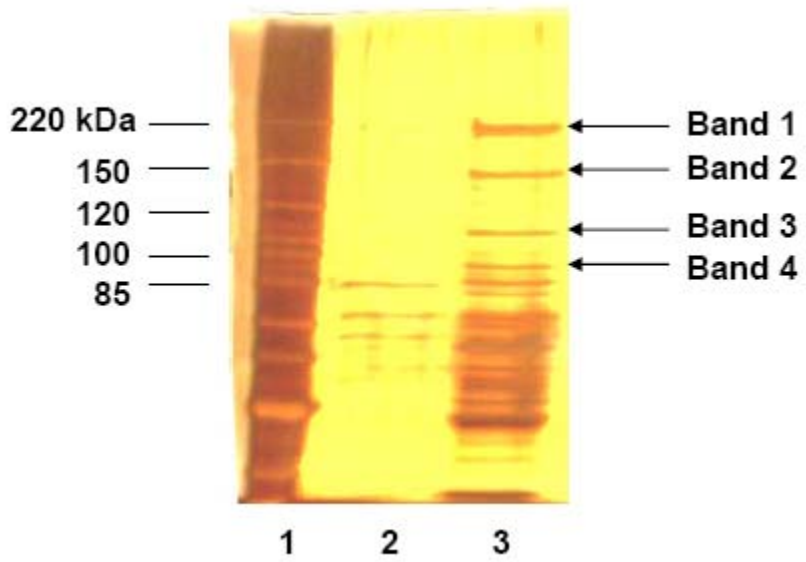

Figure 4.5 The four RecD binding candidates sent for protein identification on a silver-stained 10% SDS-PAGE. Lane 1: Fermentas unstained protein marker; lane 2: elution fraction No.1 from BSA control column; lane 3: elution fraction No.1 from RecD-BSA affinity column.

The mass spectrometry sequencing results shows that the proteins in Band 1 are indentified as DNA-directed RNA polymerase (RNAP) beta prime subunit with a molecular weight of 171 kDa. Band 2 is identified as RNAP beta subunit with a molecular weight of 131 kDa and Band 3 is a fragment of RNAP beta subunit. Band 4, however, is representing the protein of elongation factor G with a molecular mass of 76 kDa. The proteins identified by mass spectrometry are all from *D. radiodurans*.

4.3.4 *D. radiodurans* RNAP Purification

Although the protocol was modified from that applied to *E. coli* RNAP purification, *D. radiodurans* RNAP was still able to be partially purified from *D. radiodurans* wild type crude cell lysate.

In the protocol as described in Materials and Methods, there were three major steps involved in RNAP purification. RNAP was first co-precipitated with negatively charged genomic DNA by a highly positively charged polymer, polymin P. The DNA-tightly associated RNAP was eluted at a high NaCl concentration and was further purified by $(NH_4)_2SO_4$ precipitation. The re-dissolved RNAP were finally applied to a Bio-Rex 70 (ion exchange) column which was eluted by a NaCl gradient. The overall yield for RNAP purification was about 0.5 mg per liter of *D. radiodurans* wild type culture (OD_{600} = 1.0).

As shown in figure 4.6, RNAP core enzyme which should include beta prime, beta, alpha and omega was partially purified, since only two (beta prime and beta) out of four subunits were able to be identified on the SDS-PAGE. A third band positioned between 40 kDa and 50 kDa (which may or may not be the 37 kDa alpha subunit) was not separable from the two RNAP subunits.

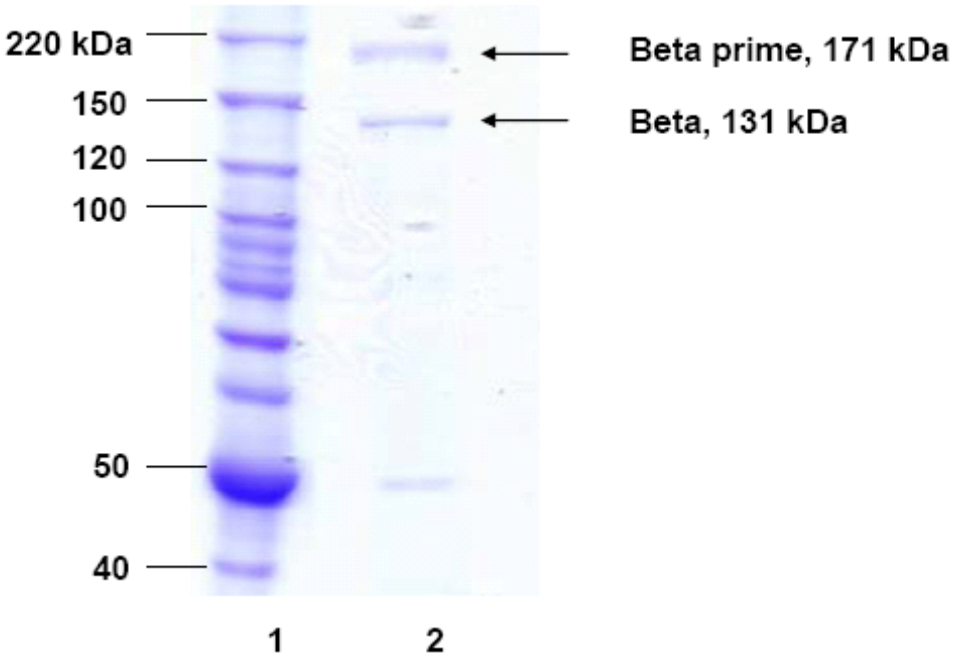

Figure 4.6 10% SDS-PAGE of partially purified *D. radiodurans* core RNA polymerase. Lane 1: Fermentas unstained protein marker; lane 2: partially purified RNAP core subunits (beta prime, beta).

4.3.5 Binding of Purified RNAP on RecD-BSA Protein Affinity Column

The interaction between partially purified RNAP and RecD was first tested on the RecD-BSA conjugated protein affinity column. Equal amounts of RNAP proteins were subjected to a RecD-BSA affinity column as well as a BSA control column. After incubation with RNAP, both of the columns were washed and eluted with exactly the same steps as described in Materials and Methods. The resulting parallel fractions were analyzed by silver-stained SDS-PAGE, as shown in figure 4.7. Comparing the strength of the interaction of RNAP on RecD and BSA columns, based on the gel results, no significant difference was observed. Most of the RNAP directly passed through both columns under the conditions for loading. A small fraction of residual RNAP was able to stay on both columns unless eluting NaCl concentration was greater than 0.2 M. A 69 kDa band representing BSA was seen in all the elution fraction lanes on the gel (figure 4.7). This is because BSA can stay in higher oligomeric states such as dimer and high salt concentration is able to, at least partially, break down BSA oligomers.

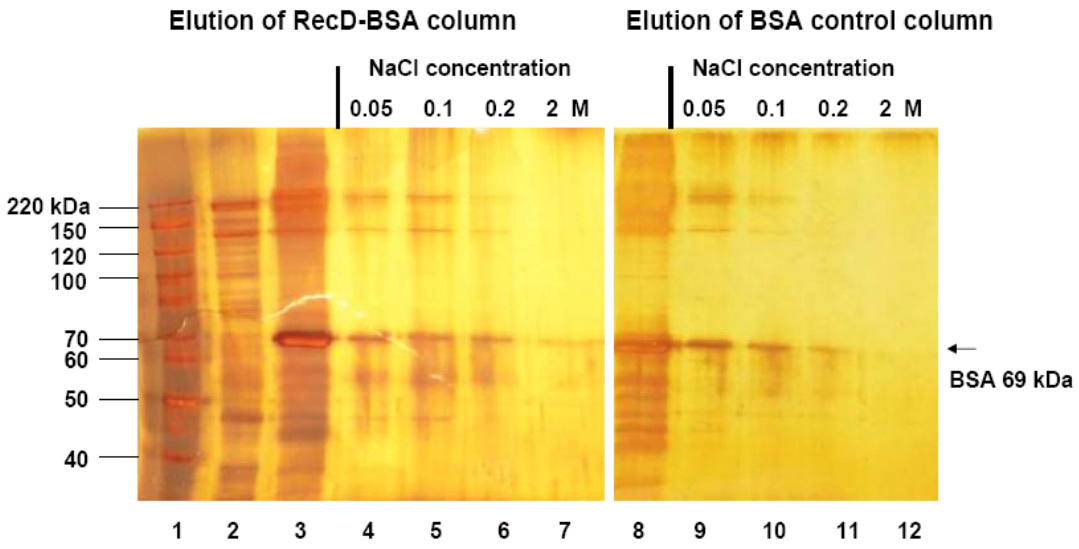

Figure 4.7 Silver-stained 10% SDS-PAGE for the elution fractions from RNAP binding on RecD-BSA column (lane 1-7) and BSA control (lane 8-12). To test the *in vitro* binding affinity with RecD, equal amount of partially purified RNAP was applied to a RecD-BSA based protein affinity column and a BSA control column. The two columns were eluted in the same conditions as described in Materials and Methods. Lane 1: Fermentas protein marker; lane 2: purified RNAP; lane 3, 8: RNAP loading flowthrough; lane 4-6 and 9-11: wash with 50, 100 and 200 mM NaCl; lane 7, 12: final wash with 2 M NaCl.

4.3.6 RecD-RNAP Interaction on Nickel Mini-Spin Columns

Two slightly different ways were designed to assay the interaction between purified RecD and RNAP on nickel (25 µl bed volume) mini-spin columns. In assay one, a mini nickel column already charged with RecD protein was incubated with roughly equal amount of RNAP proteins. In assay two, equal moles of RecD and RNAP were pre-incubated for 10 minutes and then the pre-mixture was applied to a mini nickel column. Both mini columns were subsequently eluted with exactly the same steps and their fractions were analyzed by silver-stained 10% SDS-PAGE (figure 4.8).

From the gel's image below, we can tell that over half of the applied RecD was able to bind the mini column (lane 8 and 11). However, as happened in RNAP-RecD interaction on protein affinity columns, most of the RNAP was found in loading flowthrough in both of the two binding assays, indicating that there was no strong interaction between RNAP and RecD.

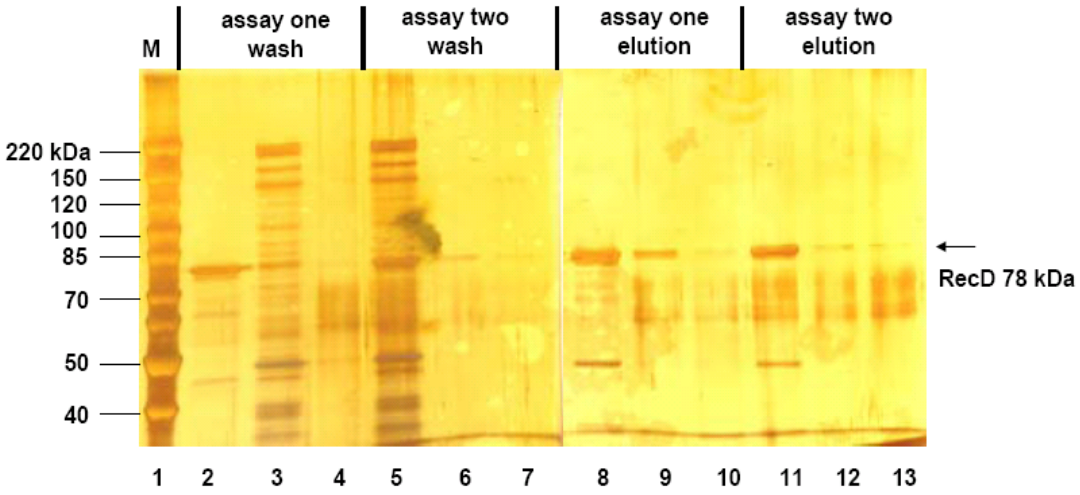

Figure 4.8 Silver-stained 10% SDS-PAGE for the samples from RNAP and RecD binding assays using mini-spin nickel columns. Two different ways were used to set up RNAP and RecD binding assays: in assay one, RecD was loaded to bind a nickel mini column first and then RNAP was incubated with the RecD-bound nickel resin; in assay two, equal moles of RecD and RNAP were pre-incubated together before the mixture was applied to a nickel mini column. Lane 1: Fermentas protein marker; lane 2-4 (assay one): RecD loading flowthrough, RNAP loading flowthrough and the first wash; lane 5-7 (assay two): RecD-RNAP mixture loading flowthrough, first and third wash; lane 8-10 (assay one): elution 1-3; lane 9-12 (assay two): elution 1-3.

4.3.7 Detecting RecD-RNAP Interaction by Far Western Blot

The partially purified RNAP fractionated by 10% SDS-PAGE was transferred to a regular western blotting PVDF membrane (or native RNAP was directly added to PVDF). The membrane was incubated with purified RecD protein (probe), followed by recognition of the anti-RecD primary and the phosphatase-conjugated secondary antibodies.

As shown in figure 4.9, RecD protein was not able to interact with any of the denatured RNAP subunits. No interaction was detected either between RecD and native RNAP on PVDF membrane (data not shown.).

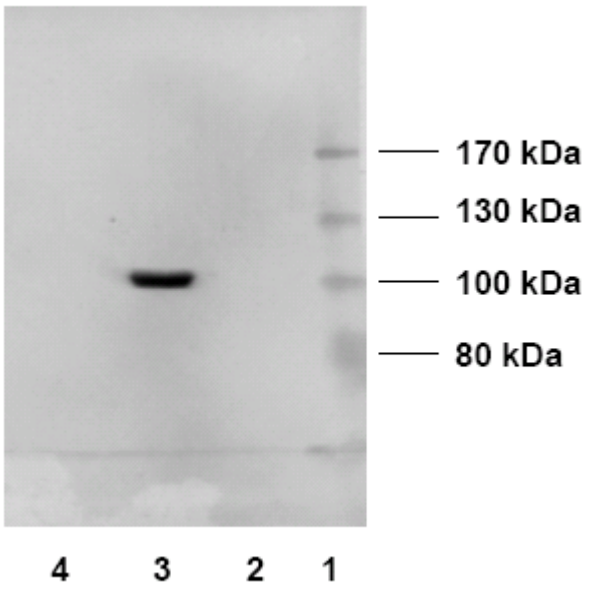

Figure 4.9 Far western blot using purified RecD protein as a probe to detect its interaction with RNAP fractionated on 10% SDS-PAGE. After RNAP on PAGE gel was transferred to PVDF membrane, the membrane was incubated with RecD probe followed by anti-RecD primary, secondary antibodies recognition and visualization as described in Materials and Methods. Lane 1: Fermentas Pageruler pre-stained protein marker; lane 2: empty lane; lane 3: purified RecD (positive control); lane 4: partially purified RNAP.

4.4 Discussion

Protein affinity chromatography, a very sensitive protein-protein interaction technique, was applied to probe any possible RecD binding partners from crude cell extract of *D. radiodurans*. The technique has been successfully used for identifying the components or interacting proteins of some important cellular protein complex (132-134). It is especially useful for detecting relatively weak interactions since a large amount of ligand protein can be immobilized to the column material. For example, the binding capacity of Affi-Gel 15 resin that was used in this study is as large as 35 mg protein per milliliter column bed volume.

In our RecD pull down assays, purified RecD protein was covalently conjugated to Affi-Gel 15 resin. Because of limited RecD expression and low purification yield, we were only able to build the Affi-Gel column with 20% active sites conjugated with RecD. As shown in figure 4.4 and 4.5, it seemed that many cellular proteins from *D. radiodurans* cell extract specifically interacted with RecD/BSA protein affinity column and they had much lower affinity to the BSA control column, assuming each band on the gel represented a different protein. We sequenced the top four bands that were all located above RecD position on the gel. Three of the four bands were identified as the two subunits (beta prime and beta) of *D. radiodurans* RNA polymerase core enzyme. The fourth band identified as the elongation factor G is a little surprising as the DNA helicase RecD is unlikely to have tight interaction with translation machinery. We think the elongation factor binding to RecD is an artifact as a lot of elongation factors may be required in exponential phase cells which involve extensive protein synthesis.

It could be a very interesting result if the observed *in vitro* physical association between RecD and RNAP is real and functionally significant in the cell. In *E. coli* and other bacteria, compared to the global nucleotide excision repair (NER) pathway, there is a special NER called transcription coupled repair (TCR) pathway (135). During transcription elongation, if the RNAP progression is blocked by DNA damage posed on the transcribed strand, TCR can be initiated. The helicase superfamily 2 protein Mfd can bind to the DNA upstream of a transcription bubble and promote the forward translocation of RNAP, to eventually dissociate RNAP and recruit NER pathway proteins to fix the damage (135,136). Thus, the DNA repair helicase RecD could be involved in TCR pathway and act as what Mfd does in *E. coli*, although there is already a Mfd homologue identified in *D. radiodurans* (3).

The interaction between partially purified RNAP (including subunits of beta, beta prime and maybe alpha) and RecD was assayed with three different methods including protein affinity column, nickel column and far western blotting. In protein affinity column, the RecD was covalently linked to Affi-gel resin via its primary amine groups (128) including the lysine side chains, which should be distributed over the protein surface. Thus the RecD ligand on the Affi-gel column was presented in a variety of orientations, which presumably should have a better chance to be recognized by its binding partner. In nickel column, RecD ligand was non-covalently chelated with nickel ion on the column via its C-terminal His-tag. However, the partially purified RNAP did not interact with either RecD column.

Far western blotting derived from standard western blotting is a convenient way to detect *in vitro* protein-protein interactions (131). The partially purified RNAP was reduced and denatured after separation on SDS-PAGE. During the 20-hour long protein transferring (to PVDF) step, the RNAP might be partially refolded in the native buffer conditions. A modified far western blotting involving a denaturing/renaturing step after transferring denatured prey protein has been reported recently. This extra step mimics the standard *in vitro* protein refolding procedure carried out in dialysis bag. In this method, the prey protein on PVDF membrane is completely denatured by 6 M Guanidine–HCl and refolded in buffers with gradually reduced Guanidine–HCl concentration (137). In our assays, native RNAP was also directly subjected to PVDF membrane for RecD binding. Unfortunately, the RecD probe protein failed to interact with either native or SDS-PAGE-transferred RNAP on the PVDF membrane. The hypothesis that the failure to detect RecD-RNAP interaction in far western blotting was caused by inappropriate RNAP refolding could not be excluded.

To conclude, the RecD-RNAP association was able to be detected in the preliminary pull down assays. However, the interaction between purified RecD and partially purified RNAP could not be repeated in these three ways we tried. It is possible that RecD-RNAP interacting requires extra protein(s) or other molecules that are missing in binding assays with purified RNAP. Another possibility is that inside of cell the binding between RecD and RNAP requires all the subunits of RNAP core or even holoenzyme. Our partially purified RNAP is not sufficient to interact tightly with RecD *in vitro*.

CHAPTER 5 CONCLUSIONS

5.1 *D. radiodurans*: a Model Organism for DNA Repair Study

The bacterium *D. radiodurans* exhibits an exceptionally strong ability to recover from DNA strand/base damage caused by various agents and to maintain the integrity of its chromosome. It is especially impressive that this bacterium can withstand a much higher dose of ionizing radiation (IR) without losing survivability, compared to most other organisms including both prokaryotes and eukaryotes (10). It has already been shown that the DNA in *D. radiodurans* is as fragile as that in radio-sensitive bacteria such as *E. coli* and is not specifically protected from being damaged during IR or other DNA damaging treatments (85). Daly and his colleagues believe that the accumulation of cellular antioxidant Mn^{2+} should take up most of the credit accounting for efficient DNA repair in *D. radiodurans* (10,81). However, it is not deniable that a potent DNA repair system would also be indispensable for *D. radiodurans* to survive and fix extensive DNA damage.

After its complete genome was sequenced and made accessible in 1999, there have been a lot of molecular biology and biochemical studies performed on the genes predicted to be involved in *D. radiodurans* DNA repair (4). Although the genome sequence of *D. radiodurans* reveals that it does not have an apparent novel DNA repair system (78), this tough organism still has some unique aspects in terms of enzymes involved in DNA repair. Its DSB repair is a good example. After IR treatment that causes hundreds of DSBs, the transcription level of 72 genes are up-regulated and only a limited number of well defined DNA repair genes are found among them. The five most highly IR-induced

genes encode proteins with unknown function (70). Combined with the fact that *D. radiodurans* is naturally devoid of the most common prokaryotic DSB repair complex, RecBCD, it implies that the DSB repair in this bacterium could involve a mechanism different from currently known pathways.

5.2 Helicase and Nuclease: in the Center Stage of DSB Repair

Homologous recombination (HR) mediated DSB repair is fundamental to cell survival in both prokaryotes and eukaryotes. This process involves two essential steps: the generation of recombinogenic 3' single-stranded DNA tail and the resolution of recombination intermediates, where both helicase and nuclease are considered to be the key players (138). *D. radiodurans* lacks RecBCD and the enzymes involved in formation of 3' ssDNA tailed in the initiation step of HR or ESDSA model are unknown. Therefore the study of DNA repair related helicase and nuclease *D. radiodurans* is important to advance our understanding of DSB repair in this organism.

5.3 Conclusions

In *D. radiodurans*, a recent DSB repair model termed ESDSA mainly involves extended DNA synthesis and RecA-dependent recombination. The initiation step of this model is the same as that in classic homologous recombination repair, involving helicase and nuclease activities to produce the 3' ssDNA tail (12). However, the potential helicase and nuclease are still not identified.

To contribute to the understanding of DSB repair in *D. radiodurans*, the novel helicase HelIV and nuclease RecJ from this organism were characterized both *in vivo* and *in vitro*.

The HelIV *in vitro* exhibits ATPase activity independent of ssDNA and helicase activity with a 5'-3' polarity. Its helicase activity is ATP dependent and requires the N-terminal region preceding the helicase domain of the protein. A truncated version of HelIV whose N-terminal region is missing has no detectable DNA unwinding activity. The *helD* null mutant cells are more sensitive to MMS and hydrogen peroxide but not sensitive to gamma rays, UV irradiation and MMC, compared to wild type *D. radiodurans* cells. This moderate phenotype of the *helD* mutant makes it difficult to predict its function in DNA repair. In *E. coli*, the double mutant of *helD uvrD* and the triple mutant *recQ helD uvrD* can significantly reduce cell resistance to UV, in the genetic background where RecF pathway is operative (*recBC sbcB sbcC*). It is suggested that RecQ, HelIV and UvrD with somewhat overlapping function are all involved in RecF pathway in *E. coli* (99,100). *D. radiodurans* has homologues of RecQ and UvrD and it is genetically devoid of RecBC and SbcB. Thus it could be interesting to construct similar double or triple mutants of *recQ*, *helD* and *uvrD* and test them with UV radiation or other DNA damaging agents. It could probably tell us if RecQ, HelIV and UvrD also have an overlapping role in *D. radiodurans.*

In contrast to the moderate phenotype of *helD* mutant, even partial deletion of *recJ* gene in *D. radiodurans* renders cells with defect in growth and high sensitivity to gamma rays, hydrogen peroxide and UV irradiation. The *recJ* gene is so important to cell survival and growth that the cells with complete removal of *recJ* are not viable.

The *D. radiodurans* RecJ protein is highly insoluble *in vitro* and has to be purified via a denaturation-refolding pathway. The refolded RecJ displays very low exonuclease

activity with a 5'-3' direction. The nuclease activity of refolded RecJ is not enhanced by adding SSB from *D. radiodurans*. A stimulation effect on nuclease activity is observed for *E. coli* RecJ incubated with SSB (117). In the *E. coli* RecF DSB repair pathway, RecJ with a 5'-3' exonuclease activity works with helicase RecQ to produce a 3' ssDNA tail, which is the suitable substrate for RecFOR catalyzed RecA loading (9). Thus in *D. radiodurans*, I propose that in the initiation step of ESDSA repair model, RecQ unwinds dsDNA ends and RecJ degrades one strand from the 5'-3' direction to produce the 3' ssDNA tail. Recently, a reconstituted *in vitro* reaction system, which involves RecF pathway proteins, RecA and SSB, has been shown to be able to recapitulate the early steps of RecF pathway-mediated DSB repair *in vivo* (44). If a similar *in vitro* system can be set up with *D. radiodurans* RecF pathway proteins, RecA and SSB, many remaining questions about RecF pathway in this bacterium can be solved directly from the *in vitro* reaction.

The isolated *D. radiodurans* RecD has already been studied both *in vivo* and *in vitro*. RecD protein exhibits ATP dependent 5'-3' helicase activity in biochemical assays (17). The *recD* null mutant is more sensitive to gamma rays, UV irradiation and hydrogen peroxide (46). Because *D. radiodurans* has no RecBC homologue, it is not clear what DNA repair pathway RecD is involved in with the current results. Thus the study of RecD binding partner would be helpful to predict its biological functions. The core technique in RecD binding study is protein affinity chromatography. In the Affi-Gel column coated with purified RecD, a relatively strong binding with *D. radiodurans* RNA polymerase (RNAP) is detected. Then the RNAP is partially purified and its interaction with RecD is

probed *in vitro*. However, their interactions cannot be repeated *in vitro* with any of the three methods: protein affinity column, nickel column and far western blotting. If all subunits of *D. radiodurans* RNAP are cloned to expression plasmid and overexpressed in *E. coli*, purer RNAP with good yield can be obtained. It might in turn enhance the interaction between RNAP and RecD *in vitro*, if the binding is real in the cell.

APPENDICES

Appendix 1 *D. radiodurans* Corrected *helD* Gene and Protein Sequence

```
   1   M  Q  A  T  P  D  K  R  R  A  Y  A  T  F  F  S  D  S  T  C
   1  ATGCAGGCCACTCCAGATAAAAGGCGCGCGTATGCAACGTTCTTCAGTGACTCGACCTGC

  21   R  F  T  S  L  R  A  V  Q  R  P  R  R  A  M  L  L  F  M  S
  61  CGTTTCACTTCTCTGAGAGCGGTTCAGCGGCCACGACGCGCTATGCTGCTCTTTATGTCT

  41   L  A  E  P  P  V  K  T  H  P  D  F  E  A  E  S  S  H  L  A
 121  CTGGCAGAACCACCCGTCAAAACCCATCCTGATTTCGAGGCCGAATCTAGTCATCTGGCG

  61   G  T  V  Q  A  M  I  R  Q  I  G  S  W  E  D  R  D  R  N  T
 181  GGCACCGTCCAGGCCATGATTCGCCAGATCGGGAGCTGGGAAGACCGCGACCGCAACACG

  81   G  A  D  L  E  T  S  V  T  M  A  D  T  A  E  E  H  A  A  M
 241  GGCGCCGACCTCGAAACCTCGGTGACGATGGCCGACACCGCCGAGGAACATGCCGCGATG

 101   L  S  V  H  V  H  Q  P  Y  F  G  S  L  K  V  R  V  G  G  R
 301  CTGAGCGTGCATGTCCACCAGCCCTACTTCGGCAGCCTGAAAGTACGCGTCGGCGGGCGC

 121   E  Q  T  L  Y  I  G  K  H  A  F  R  D  V  G  G  P  H  H  V
 361  GAGCAGACCCTCTATATCGGCAAGCACGCCTTCCGCGACGTGGGCGGGCCGCACCACGTG

 141   V  S  W  D  S  E  V  G  S  L  F  Y  S  D  A  L  D  W  V  P
 421  GTGAGCTGGGACAGCGAGGTCGGCAGCCTCTTTTACTCCGACGCTCTGGACTGGGTGCCC

 161   R  R  G  S  K  G  Q  I  R  R  R  R  Q  L  D  V  A  Q  K  A
 481  CGGCGTGGCAGCAAGGGCCAGATTCGGCGGCGGCGCCAGCTCGACGTGGCGCAAAAAGCG

 181   L  L  R  V  T  D  L  Y  D  D  E  Q  G  G  D  T  G  G  R  E
 541  CTGCTGCGCGTCACCGACCTCTACGACGATGAGCAGGGCGGCGACACCGGCGGACGCGAG

 201   E  V  L  L  R  R  L  K  E  Q  S  T  A  G  M  R  D  V  V  E
 601  GAAGTGCTGCTGCGGCGCCTGAAAGAGCAGAGCACCGCCGGGATGCGCGACGTGGTGGAG

 221   T  L  Q  P  E  Q  N  E  A  M  R  F  P  A  G  T  P  V  I  I
 661  ACGCTGCAACCCGAGCAGAACGAGGCGATGCGCTTTCCCGCCGGCACGCCGGTCATCATT

 241   Q  G  A  A  G  S  G  K  T  T  I  G  F  H  R  L  A  W  M  T
 721  CAGGGGGCTGCCGGGTCGGGCAAGACGACCATCGGCTTTCACCGCCTTGCCTGGATGACG

 261   S  G  D  R  G  P  H  Q  A  R  P  E  A  C  M  V  L  M  P  N
 781  AGCGGCGACCGAGGCCCGCATCAGGCGCGGCCCGAGGCATGCATGGTTCTGATGCCCAAC

 281   R  V  L  A  A  Y  A  A  R  I  L  P  E  L  G  I  G  G  V  S
 841  CGGGTGCTGGCGGCTTACGCGGCGCGCATCCTGCCCGAACTCGGCATCGGCGGCGTCAGC

 301   V  T  T  P  E  A  W  A  T  A  L  L  G  L  E  K  L  E  I  T
 901  GTGACCACGCCCGAAGCCTGGGCCACCGCGCTGCTGGGCCTCGAAAAACTGGAAATCACC

 321   D  R  T  L  S  L  L  L  T  D  T  D  N  G  R  R  A  L  A  W
 961  GACCGCACACTCTCGCTGCTGCTCACCGATACCGACAACGGACGCCGGGCGCTGGCGTGG

 341   R  R  A  K  L  L  G  D  A  R  M  L  D  V  V  R  T  H  L  W
1021  CGGCGGGCCAAGCTGCTCGGCGACGCCCGGATGCTCGACGTGGTGCGGACCCACCTCTGG
```

```
 361   N  K  F  G  A  A  I  T  G  Q  S  L  Q  E  N  I  E  V  A  G
1081  AACAAGTTCGGGGCGGCCATCACCGGCCAGAGCTTGCAGGAAAACATCGAGGTGGCGGGG

 381   R  G  L  L  T  F  S  L  S  E  S  D  L  A  D  K  L  H  D  V
1141  CGCGGGCTGCTGACCTTCAGCCTGAGCGAGAGCGACCTCGCCGACAAGCTGCACGACGTG

 401   F  A  Q  D  P  L  D  G  Y  R  A  G  F  R  R  L  V  E  E  E
1201  TTCGCGCAAGACCCCCTCGACGGCTACCGCGCCGGCTTCCGGCGGCTGGTGGAGGAAGAA

 421   A  V  S  R  L  R  V  P  E  E  E  E  A  S  V  R  R  Q  L  S
1261  GCCGTCTCGCGCCTGCGGGTGCCCGAGGAAGAGGAAGCGAGCGTGCGGCGGCAACTCAGC

 441   K  P  L  T  T  L  L  G  R  I  F  A  S  T  T  P  V  T  E  A
1321  AAGCCGCTCACCACGCTGCTGGGGCGCATTTTCGCCTCGACGACGCCCGTGACCGAGGCC

 461   R  R  L  L  A  D  A  D  A  L  A  A  S  G  L  L  S  D  K  E
1381  CGGCGCCTGCTCGCCGACGCGGACGCCCTGGCCGCGAGCGGACTGCTGAGCGACAAGGAA

 481   I  R  L  L  L  A  D  P  L  S  G  I  P  T  P  R  R  A  H  A
1441  ATCCGGCTGCTGCTCGCCGATCCGCTCAGCGGCATTCCGACCCCGCGCCGGGCTCACGCC

 501   D  V  T  E  L  P  I  M  L  A  V  Q  A  F  T  G  G  I  G  R
1501  GACGTGACCGAGCTGCCCATCATGCTGGCGGTGCAGGCGTTTACCGGCGGCATCGGGCGA

 521   A  V  G  R  T  L  E  P  F  D  H  V  V  L  D  E  A  Q  D  Y
1561  GCGGTGGGGCGCACGTTGGAGCCGTTCGACCATGTGGTGCTCGACGAGGCGCAAGACTAT

 541   S  P  L  L  Y  A  L  L  A  R  A  A  R  P  G  H  V  T  A  L
1621  TCGCCGCTGCTCTACGCCCTGCTCGCCCGCGCCGCGCGCCCGGGGCACGTCACTGCGTTG

 561   G  D  L  N  Q  G  M  H  G  Y  K  G  P  S  K  W  Q  D  V  Q
1681  GGCGACCTCAACCAGGGGATGCACGGCTACAAGGGGCCGAGCAAGTGGCAGGACGTGCAG

 581   D  Q  L  P  G  A  Q  V  L  T  L  S  R  T  Y  R  S  T  R  Q
1741  GACCAGTTACCGGGGGCACAGGTGCTGACGCTCTCGCGCACCTACCGCTCCACCCGGCAA

 601   I  T  E  L  G  A  R  I  A  E  T  Y  N  R  A  A  Q  V  Q  G
1801  ATCACCGAACTCGGCGCCCGGATTGCCGAAACCTACAACCGCGCCGCGCAGGTGCAGGGC

 621   V  D  R  E  G  A  E  V  Q  R  Y  E  G  G  D  E  R  A  L  I
1861  GTGGACCGCGAGGGGGCCGAGGTGCAGCGCTACGAGGGCGGTGACGAGCGCGCGCTGATT

 641   A  Q  A  V  K  D  A  Q  A  A  G  H  T  N  I  A  I  V  T  R
1921  GCCCAGGCCGTCAAGGACGCGCAGGCCGCCGGGCACACCAACATCGCCATCGTGACGCGG

 661   R  G  A  D  A  D  R  L  S  A  E  L  R  D  F  D  T  D  A  Q
1981  CGCGGGGCCGACGCCGACCGCCTGAGCGCCGAGCTGCGCGACTTCGACACCGACGCGCAG

 681   P  I  T  T  Q  E  H  R  F  K  G  G  L  V  I  L  P  V  S  L
2041  CCCATCACCACGCAGGAGCACCGTTTCAAGGGCGGGCTGGTCATTCTGCCGGTCAGCCTC

 701   A  K  G  L  E  F  S  A  A  I  V  T  G  A  N  Q  T  T  Y  D
2101  GCTAAAGGGCTGGAATTCAGCGCGGCGATTGTGACCGGAGCGAACCAGACGACGTATGAC

 721   E  S  T  E  Y  E  R  R  L  L  Y  V  A  A  S  R  A  L  H  W
2161  GAGAGCACCGAGTACGAACGGCGCCTGCTCTATGTCGCCGCCAGCCGCGCCCTGCACTGG

 741   L  G  L  V  S  G  G  A  E  L  H  P  L  V  R  -
2221  CTGGGGCTGGTGAGCGGTGGGGCGGAGCTGCACCCGCTGGTGCGCTGA
```

Appendix 1 *D. radiodurans* corrected *helD* gene and protein sequence. The DNA sequence corresponds to nt # 1,591,892 to 1,594,158 in the *D. radiodurans* chromosome I sequence, except for the additional G at position # 1492. The predicted ATG start codon for full length HelIV at position #1 and the ATG codon at position # 643 for the truncated HelIV protein are underlined.

Appendix 2 *D. radiodurans* Corrected *recJ* Gene and Protein Sequence

```
  1   M  A  A  V  R  E  G  K  R  I  R  I  H  G  D  Y  D  A  D  G
  1  ATGGCAGCGGTGCGCGAGGGAAAGCGCATCCGTATTCACGGTGACTACGACGCCGACGGG

 21   V  S  A  T  A  T  L  V  L  G  L  R  A  I  G  A  N  V  H  G
 61  GTGAGTGCGACTGCGACTCTGGTGCTGGGCCTGCGCGCCATCGGGGCGAATGTGCACGGG

 41   F  I  P  H  R  L  N  E  G  Y  G  I  H  P  D  R  V  P  E  H
121  TTCATTCCCCACCGATTGAACGAGGGCTACGGGATTCATCCTGACCGGGTGCCTGAGCAC

 61   A  A  A  A  D  L  V  V  T  V  D  C  G  V  S  N  L  D  E  V
181  GCCGCCGCTGCCGATCTGGTGGTCACGGTGGACTGTGGGGTGTCCAACCTCGACGAGGTG

 81   K  S  L  L  A  T  G  T  E  V  V  V  T  D  H  H  A  P  G  E
241  AAGTCGCTGCTGGCAACGGGCACTGAGGTCGTGGTCACCGACCACCACGCGCCGGGCGAG

101   N  F  P  E  C  L  V  V  H  P  H  L  T  P  D  Y  D  P  D  R
301  AACTTTCCCGAATGTTTGGTCGTCCACCCCCATCTGACGCCGGACTATGACCCCGACCGC

121   H  N  L  T  G  A  G  V  A  Y  H  L  L  W  A  V  Y  E  E  L
361  CACAATCTGACCGGGGCCGGAGTCGCCTATCACCTGCTGTGGGCGGTGTACGAGGAACTG

141   G  R  P  E  P  R  A  L  L  P  L  A  T  L  G  T  V  A  D  V
421  GGGAGGCCCGAGCCGCGTGCATTGTTGCCGCTGGCGACGCTGGGCACGGTGGCCGACGTG

161   A  P  L  L  G  E  N  R  A  L  V  R  A  G  L  A  E  M  A  R
481  GCGCCGCTGCTGGGTGAAAACCGTGCTCTGGTCCGCGCCGGGCTGGCCGAAATGGCCCGC

181   T  E  L  P  G  L  R  A  L  M  N  E  K  R  V  R  Q  P  T  A
541  ACCGAGTTGCCCGGTCTGCGCGCCCTGATGAACGAAAAGCGCGTGCGGCAGCCTACGGCG

201   R  D  V  A  F  I  L  A  P  R  I  N  A  A  G  R  M  G  E  A
601  CGTGACGTGGCCTTTATCCTCGCGCCGCGCATCAATGCGGCTGGGCGGATGGGGGAGGCG

221   D  R  A  L  E  L  L  T  T  P  S  D  H  E  A  K  S  L  A  A
661  GACCGGGCGCTGGAGCTGCTGACCACGCCCAGCGACCACGAAGCGAAGAGCCTGGCCGCC

241   Y  L  E  I  R  N  Q  E  R  R  K  I  Q  D  D  M  F  A  Q  A
721  TACCTGGAAATTCGCAACCAGGAGAGGCGCAAGATTCAGGACGATATGTTCGCGCAGGCG

261   L  Q  L  A  D  P  N  D  P  A  L  V  L  T  H  D  D  W  H  A
781  CTGCAACTCGCCGACCCGAACGACCCGGCGCTGGTGCTCACCCACGACGACTGGCATGCG

281   G  V  M  G  I  V  A  S  K  L  V  E  T  F  N  R  P  V  Y  I
841  GGCGTGATGGGCATCGTGGCGAGCAAGCTGGTGGAGACGTTCAACCGGCCCGTGTATATC

301   V  A  Q  G  K  G  S  V  R  S  T  P  G  I  S  A  V  Q  G  L
901  GTCGCGCAGGGCAAAGGCTCGGTGCGCTCCACCCCCGGCATCAGTGCGGTGCAGGGCCTC
```

```
 321   R  E  S  R  D  L  L  G  R  F  G  G  H  P  G  A  A  G  F  S
 961   CGCGAAAGCCGCGACCTCCTGGGGCGCTTCGGCGGGCACCCCGGCGCGGCGGGCTTTTCG

 341   L  D  P  Q  N  F  G  A  L  R  E  R  I  H  G  Y  V  R  Q  F
1021   CTGGACCCGCAGAATTTTGGCGCGCTGCGCGAGCGGATTCATGGGTATGTTCGGCAGTTT

 361   P  T  P  V  P  A  V  R  L  D  A  P  L  P  V  A  A  L  T  P
1081   CCGACCCCGGTCCCGGCAGTGCGGCTAGATGCCCCGCTGCCTGTGGCGGCCCTGACCCCC

 381   E  L  L  S  E  L  S  I  L  E  P  F  G  E  G  N  P  R  P  L
1141   GAGCTGCTGTCCGAGCTGAGCATTCTGGAACCCTTCGGCGAAGGCAACCCGCGCCCGCTG

 401   W  H  L  R  G  P  L  T  D  T  R  L  V  G  K  Q  G  D  V  L
1201   TGGCACCTGCGCGGGCCGCTGACTGACACCCGATTGGTGGGCAAGCAGGGCGACGTGCTG

 421   Q  F  R  F  G  G  V  K  G  M  K  Y  S  E  R  D  D  A  A  G
1261   CAATTCCGGTTCGGTGGCGTCAAAGGCATGAAATACAGCGAACGCGACGACGCTGCGGGC

 441   E  R  D  V  A  A  E  L  A  L  N  E  W  K  G  R  T  S  L  E
1321   GAACGTGACGTGGCGGCAGAACTTGCCCTCAACGAGTGGAAGGGCCGGACCTCCCTGGAA

 461   L  H  A  A  A  L  R  P  L  A  P  L  A  L  A  G  T  E  E  G
1381   CTGCACGCGGCGGCGCTGCGCCCGCTGGCTCCCCTCGCGCTGGCAGGAACTGAGGAGGGG

 481   L  P  T  L  P  R  L  N  P  R  E  A  M  T  F  L  K  T  G  A
1441   CTGCCCACCCTGCCCCGGCTCAATCCCCGTGAGGCGATGACCTTCCTGAAAACGGGCGCG

 501   A  A  Y  A  E  Q  G  V  A  T  Y  L  R  D  N  V  P  G  L  T
1501   GCGGCCTACGCCGAGCAGGGCGTCGCCACCTACCTGCGCGACAACGTACCGGGCCTCACC

 521   L  L  D  T  N  A  P  H  P  G  G  D  L  I  L  Y  G  L  P  P
1561   CTGCTGGACACGAACGCGCCGCACCCCGGCGGTGACCTGATCCTGTACGGTTTGCCCCCC

 541   E  S  A  L  R  R  W  L  H  E  A  Q  E  Q  G  G  R  V  A  F
1621   GAGTCGGCCCTGCGCCGCTGGCTGCATGAGGCGCAGGAGCAGGGAGGCCGGGTGGCGTTT

 561   A  L  G  P  K  T  L  A  E  L  D  A  A  L  T  L  A  K  L  L
1681   GCGCTGGGACCGAAGACGCTCGCAGAGCTCGACGCTGCCCTGACGCTGGCGAAGCTGTTG

 581   P  D  S  H  T  E  A  A  Q  E  A  A  A  D  A  Y  R  S  W  Q
1741   CCTGACTCTCACACCGAGGCCGCGCAGGAAGCTGCCGCTGACGCTTACCGCAGCTGGCAG

 601   W  A  H  H  Y  R  V  L  N  D  A  G  W  S  A  S  V  Y  A  M
1801   TGGGCGCACCATTACCGCGTGCTGAACGACGCGGGGTGGAGCGCCTCGGTCTACGCGATG

 621   L  G  L  P  V  P  A  A  L  P  K  A  A  E  A  L  A  L  A  A
1861   CTCGGGCTGCCTGTACCGGCAGCGCTCCCGAAGGCGGCGGAAGCGCTGGCGCTCGCTGCG

 641   G  -
1921   GGTTAA
```

Appendix 2 ***D. radiodurans*** **corrected** ***recJ*** **gene and protein sequence.** The DNA sequence shown corresponds to bp # 1134718 to 1136772 in chromosome I of the *D. radiodurans* genome sequence. The starting codon and the additional G found by DNA sequencing, at nucleotide position # 1894, are underlined.

BIBLIOGRAPHY

1. Anderson, A.W., Nordon, H. C., Cain, R. F., Parrish, G. & Duggan, D. (1956) Studies on a radio-resistant micrococcus. I. Isolation, morphology, cultural characteristics, and resistance to γ-radiation. *Food Technol.*, **10**, 575-578.
2. Cox, M.M. and Battista, J.R. (2005) *Deinococcus radiodurans* - the consummate survivor. *Nat. Rev. Microbiol.*, **3**, 882-892.
3. White, O., Eisen, J.A., Heidelberg, J.F., Hickey, E.K., Peterson, J.D., Dodson, R.J., Haft, D.H., Gwinn, M.L., Nelson, W.C., Richardson, D.L. *et al.* (1999) Genome sequence of the radioresistant bacterium *Deinococcus radiodurans* R1. *Science*, **286**, 1571-1577.
4. Blasius, M., Sommer, S. and Hubscher, U. (2008) *Deinococcus radiodurans*: what belongs to the survival kit? *Crit. Rev. Biochem. Mol. Biol.*, **43**, 221-238.
5. Minton, K.W. (1994) DNA repair in the extremely radioresistant bacterium *Deinococcus radiodurans*. *Mol. Microbiol.*, **13**, 9-15.
6. Battista, J.R. (1997) Against all odds: the survival strategies of *Deinococcus radiodurans*. *Annu. Rev. Microbiol.*, **51**, 203-224.
7. Battista, J.R., Park, M.J. and McLemore, A.E. (2001) Inactivation of two homologues of proteins presumed to be involved in the desiccation tolerance of plants sensitizes *Deinococcus radiodurans* R1 to desiccation. *Cryobiology*, **43**, 133-139.
8. Battista, J.R., Earl, A.M. and Park, M.J. (1999) Why is *Deinococcus radiodurans* so resistant to ionizing radiation? *Trends. Microbiol.*, **7**, 362-365.
9. Kowalczykowski, S.C. (2000) Initiation of genetic recombination and recombination-dependent replication. *Trends. Biochem. Sci.*, **25**, 156-165.
10. Daly, M.J. (2009) A new perspective on radiation resistance based on *Deinococcus radiodurans*. *Nat. Rev. Microbiol.*, **7**, 237-245.
11. Daly, M.J., Ouyang, L., Fuchs, P. and Minton, K.W. (1994) In vivo damage and *recA*-dependent repair of plasmid and chromosomal DNA in the radiation-resistant bacterium *Deinococcus radiodurans*. *J. Bacteriol.*, **176**, 3508-3517.
12. Zahradka, K., Slade, D., Bailone, A., Sommer, S., Averbeck, D., Petranovic, M., Lindner, A.B. and Radman, M. (2006) Reassembly of shattered chromosomes in *Deinococcus radiodurans*. *Nature*, **443**, 569-573.
13. Kuzminov, A. (1999) Recombinational repair of DNA damage in *Escherichia coli* and bacteriophage lambda. *Microbiol. Mol. Biol. Rev.*, **63**, 751-813.
14. Chedin, F. and Kowalczykowski, S.C. (2002) A novel family of regulated helicases/nucleases from Gram-positive bacteria: insights into the initiation of DNA recombination. *Mol. Microbiol.*, **43**, 823-834.
15. Kooistra, J., Haijema, B.J. and Venema, G. (1993) The *Bacillus subtilis addAB* genes are fully functional in *Escherichia coli*. *Mol. Microbiol.*, **7**, 915-923.

16. Makarova, K.S., Aravind, L., Wolf, Y.I., Tatusov, R.L., Minton, K.W., Koonin, E.V. and Daly, M.J. (2001) Genome of the extremely radiation-resistant bacterium *Deinococcus radiodurans* viewed from the perspective of comparative genomics. *Microbiol. Mol. Biol. Rev.*, **65**, 44-79.
17. Wang, J. and Julin, D.A. (2004) DNA helicase activity of the RecD protein from *Deinococcus radiodurans*. *J. Biol. Chem.*, **279**, 52024-52032.
18. Dillingham, M.S. and Kowalczykowski, S.C. (2008) RecBCD enzyme and the repair of double-stranded DNA breaks. *Microbiol. Mol. Biol. Rev.*, **72**, 642-671.
19. Friedberg, E.C., Walker, G. C., Siede, W., Wood, R. D., Schultz, R. A., Ellenberger, T. (2006) *DNA Repair and Mutagenesis*. ASM Press, Washington, D. C. .
20. Breen, A.P. and Murphy, J.A. (1995) Reactions of oxyl radicals with DNA. *Free Radic. Biol. Med.*, **18**, 1033-1077.
21. Bonura, T. and Smith, K.C. (1975) Enzymatic production of deoxyribonucleic acid double-strand breaks after ultraviolet irradiation of *Escherichia coli* K-12. *J. Bacteriol.*, **121**, 511-517.
22. Kuzminov, A. (1995) Collapse and repair of replication forks in *Escherichia coli*. *Mol. Microbiol.*, **16**, 373-384.
23. Kuzminov, A. (2001) DNA replication meets genetic exchange: chromosomal damage and its repair by homologous recombination. *Proc. Natl. Acad. Sci. U S A*, **98**, 8461-8468.
24. Michel, B., Grompone, G., Flores, M.J. and Bidnenko, V. (2004) Multiple pathways process stalled replication forks. *Proc. Natl. Acad. Sci. U S A*, **101**, 12783-12788.
25. Michel, B., Boubakri, H., Baharoglu, Z., LeMasson, M. and Lestini, R. (2007) Recombination proteins and rescue of arrested replication forks. *DNA Repair (Amst)*, **6**, 967-980.
26. McGlynn, P. and Lloyd, R.G. (2000) Modulation of RNA polymerase by (p)ppGpp reveals a RecG-dependent mechanism for replication fork progression. *Cell*, **101**, 35-45.
27. McGlynn, P. and Lloyd, R.G. (2002) Genome stability and the processing of damaged replication forks by RecG. *Trends. Genet.*, **18**, 413-419.
28. Thoms, B., Borchers, I. and Wackernagel, W. (2008) Effects of single-strand DNases ExoI, RecJ, ExoVII, and SbcCD on homologous recombination of *recBCD*$^+$ strains of *Escherichia coli* and roles of SbcB15 and XonA2 ExoI mutant enzymes. *J. Bacteriol.*, **190**, 179-192.
29. Wang, J.C. (1996) DNA topoisomerases. *Annu. Rev. Biochem.*, **65**, 635-692.
30. Roth, D.B. and Craig, N.L. (1998) VDJ recombination: a transposase goes to work. *Cell*, **94**, 411-414.
31. Wyman, C., Ristic, D. and Kanaar, R. (2004) Homologous recombination-mediated double-strand break repair. *DNA Repair (Amst)*, **3**, 827-833.

32. Paques, F. and Haber, J.E. (1999) Multiple pathways of recombination induced by double-strand breaks in *Saccharomyces cerevisiae*. *Microbiol. Mol. Biol. Rev.*, **63**, 349-404.
33. Kowalczykowski, S.C., Dixon, D.A., Eggleston, A.K., Lauder, S.D. and Rehrauer, W.M. (1994) Biochemistry of homologous recombination in *Escherichia coli*. *Microbiol. Rev.*, **58**, 401-465.
34. Dixon, D.A. and Kowalczykowski, S.C. (1991) Homologous pairing in vitro stimulated by the recombination hotspot, Chi. *Cell*, **66**, 361-371.
35. Dixon, D.A. and Kowalczykowski, S.C. (1993) The recombination hotspot chi is a regulatory sequence that acts by attenuating the nuclease activity of the *E. coli* RecBCD enzyme. *Cell*, **73**, 87-96.
36. Anderson, D.G. and Kowalczykowski, S.C. (1997) The recombination hot spot chi is a regulatory element that switches the polarity of DNA degradation by the RecBCD enzyme. *Genes Dev.*, **11**, 571-581.
37. Bianco, P.R. and Kowalczykowski, S.C. (1997) The recombination hotspot Chi is recognized by the translocating RecBCD enzyme as the single strand of DNA containing the sequence 5'-GCTGGTGG-3'. *Proc. Natl. Acad. Sci. U S A*, **94**, 6706-6711.
38. Anderson, D.G. and Kowalczykowski, S.C. (1997) The translocating RecBCD enzyme stimulates recombination by directing RecA protein onto ssDNA in a chi-regulated manner. *Cell*, **90**, 77-86.
39. West, S.C. (1996) DNA helicases: new breeds of translocating motors and molecular pumps. *Cell*, **86**, 177-180.
40. West, S.C. (1996) The RuvABC proteins and Holliday junction processing in *Escherichia coli*. *J. Bacteriol.*, **178**, 1237-1241.
41. Smith, G.R. (1989) Homologous recombination in *E. coli*: multiple pathways for multiple reasons. *Cell*, **58**, 807-809.
42. Nakayama, H., Nakayama, K., Nakayama, R., Irino, N., Nakayama, Y. and Hanawalt, P.C. (1984) Isolation and genetic characterization of a thymineless death-resistant mutant of *Escherichia coli* K12: identification of a new mutation (*recQ1*) that blocks the RecF recombination pathway. *Mol. Gen. Genet.*, **195**, 474-480.
43. Umezu, K., Chi, N.W. and Kolodner, R.D. (1993) Biochemical interaction of the *Escherichia coli* RecF, RecO, and RecR proteins with RecA protein and single-stranded DNA binding protein. *Proc. Natl. Acad. Sci. U S A*, **90**, 3875-3879.
44. Handa, N., Morimatsu, K., Lovett, S.T. and Kowalczykowski, S.C. (2009) Reconstitution of initial steps of dsDNA break repair by the RecF pathway of *E. coli*. *Genes Dev.*, **23**, 1234-1245.
45. Rocha, E.P., Cornet, E. and Michel, B. (2005) Comparative and evolutionary analysis of the bacterial homologous recombination systems. *PLoS Genet.*, **1**, e15.
46. Servinsky, M.D. and Julin, D.A. (2007) Effect of a *recD* mutation on DNA damage resistance and transformation in *Deinococcus radiodurans*. *J. Bacteriol.*, **189**, 5101-5107.

47. Kim, J.I., Sharma, A.K., Abbott, S.N., Wood, E.A., Dwyer, D.W., Jambura, A., Minton, K.W., Inman, R.B., Daly, M.J. and Cox, M.M. (2002) RecA Protein from the extremely radioresistant bacterium *Deinococcus radiodurans*: expression, purification, and characterization. *J. Bacteriol.*, **184**, 1649-1660.
48. Kim, J.I. and Cox, M.M. (2002) The RecA proteins of *Deinococcus radiodurans* and *Escherichia coli* promote DNA strand exchange via inverse pathways. *Proc. Natl. Acad. Sci. U S A*, **99**, 7917-7921.
49. Zaitsev, E.N. and Kowalczykowski, S.C. (2000) A novel pairing process promoted by *Escherichia coli* RecA protein: inverse DNA and RNA strand exchange. *Genes Dev.*, **14**, 740-749.
50. Gutman, P.D., Fuchs, P., Ouyang, L. and Minton, K.W. (1993) Identification, sequencing, and targeted mutagenesis of a DNA polymerase gene required for the extreme radioresistance of *Deinococcus radiodurans*. *J. Bacteriol.*, **175**, 3581-3590.
51. Daly, M.J. and Minton, K.W. (1996) An alternative pathway of recombination of chromosomal fragments precedes *recA*-dependent recombination in the radioresistant bacterium *Deinococcus radiodurans*. *J. Bacteriol.*, **178**, 4461-4471.
52. Misra, H.S., Khairnar, N.P., Kota, S., Shrivastava, S., Joshi, V.P. and Apte, S.K. (2006) An exonuclease I-sensitive DNA repair pathway in *Deinococcus radiodurans*: a major determinant of radiation resistance. *Mol. Microbiol.*, **59**, 1308-1316.
53. Killoran, M.P. and Keck, J.L. (2006) Three HRDC domains differentially modulate *Deinococcus radiodurans* RecQ DNA helicase biochemical activity. *J. Biol. Chem.*, **281**, 12849-12857.
54. Huang, L., Hua, X., Lu, H., Gao, G., Tian, B., Shen, B. and Hua, Y. (2007) Three tandem HRDC domains have synergistic effect on the RecQ functions in *Deinococcus radiodurans*. *DNA Repair (Amst)*, **6**, 167-176.
55. Leiros, I., Timmins, J., Hall, D.R. and McSweeney, S. (2005) Crystal structure and DNA-binding analysis of RecO from *Deinococcus radiodurans*. *EMBO. J.*, **24**, 906-918.
56. Xu, G., Wang, L., Chen, H., Lu, H., Ying, N., Tian, B. and Hua, Y. (2008) RecO is essential for DNA damage repair in *Deinococcus radiodurans*. *J. Bacteriol.*, **190**, 2624-2628.
57. Lee, B.I., Kim, K.H., Park, S.J., Eom, S.H., Song, H.K. and Suh, S.W. (2004) Ring-shaped architecture of RecR: implications for its role in homologous recombinational DNA repair. *EMBO. J.*, **23**, 2029-2038.
58. Koroleva, O., Makharashvili, N., Courcelle, C.T., Courcelle, J. and Korolev, S. (2007) Structural conservation of RecF and Rad50: implications for DNA recognition and RecF function. *EMBO. J.*, **26**, 867-877.
59. Kitayama, S., Kohoroku, M., Takagi, A. and Itoh, H. (1997) Mutation of *D. radiodurans* in a gene homologous to *ruvB* of *E. coli*. *Mutat. Res.*, **385**, 151-157.
60. Slade, D., Lindner, A.B., Paul, G. and Radman, M. (2009) Recombination and replication in DNA repair of heavily irradiated *Deinococcus radiodurans*. *Cell*, **136**, 1044-1055.

61. Zhou, Q., Zhang, X.J., Xu, H., Xu, B.J., and Hua, Y.J. (2006) RadA: A protein involved in DNA damage repair processes of *Deinococcus radiodurans* R1. *Chin. Sci. Bull.*, **51**, 2993-2999.
62. Narumi, I., Satoh, K., Cui, S., Funayama, T., Kitayama, S. and Watanabe, H. (2004) PprA: a novel protein from *Deinococcus radiodurans* that stimulates DNA ligation. *Mol. Microbiol.*, **54**, 278-285.
63. Hefferin, M.L. and Tomkinson, A.E. (2005) Mechanism of DNA double-strand break repair by non-homologous end joining. *DNA Repair (Amst)*, **4**, 639-648.
64. Pitcher, R.S., Wilson, T.E. and Doherty, A.J. (2005) New insights into NHEJ repair processes in prokaryotes. *Cell Cycle*, **4**, 675-678.
65. Weller, G.R., Kysela, B., Roy, R., Tonkin, L.M., Scanlan, E., Della, M., Devine, S.K., Day, J.P., Wilkinson, A., d'Adda di Fagagna, F. *et al.* (2002) Identification of a DNA nonhomologous end-joining complex in bacteria. *Science*, **297**, 1686-1689.
66. Shuman, S. and Glickman, M.S. (2007) Bacterial DNA repair by non-homologous end joining. *Nat. Rev. Microbiol.*, **5**, 852-861.
67. Aravind, L. and Koonin, E.V. (2001) Prokaryotic homologs of the eukaryotic DNA-end-binding protein Ku, novel domains in the Ku protein and prediction of a prokaryotic double-strand break repair system. *Genome Res.*, **11**, 1365-1374.
68. Weller, G.R. and Doherty, A.J. (2001) A family of DNA repair ligases in bacteria? *FEBS Lett.*, **505**, 340-342.
69. Nick McElhinny, S.A. and Ramsden, D.A. (2003) Polymerase mu is a DNA-directed DNA/RNA polymerase. *Mol. Cell. Biol.*, **23**, 2309-2315.
70. Tanaka, M., Earl, A.M., Howell, H.A., Park, M.J., Eisen, J.A., Peterson, S.N. and Battista, J.R. (2004) Analysis of *Deinococcus radiodurans*'s transcriptional response to ionizing radiation and desiccation reveals novel proteins that contribute to extreme radioresistance. *Genetics*, **168**, 21-33.
71. Blasius, M., Buob, R., Shevelev, I.V. and Hubscher, U. (2007) Enzymes involved in DNA ligation and end-healing in the radioresistant bacterium *Deinococcus radiodurans*. *BMC Mol. Biol.*, **8**, 69.
72. Blasius, M., Shevelev, I., Jolivet, E., Sommer, S. and Hubscher, U. (2006) DNA polymerase X from *Deinococcus radiodurans* possesses a structure-modulated 3'-->5' exonuclease activity involved in radioresistance. *Mol. Microbiol.*, **60**, 165-176.
73. Lecointe, F., Shevelev, I.V., Bailone, A., Sommer, S. and Hubscher, U. (2004) Involvement of an X family DNA polymerase in double-stranded break repair in the radioresistant organism *Deinococcus radiodurans*. *Mol. Microbiol.*, **53**, 1721-1730.
74. Burrell, A.D., Feldschreiber, P. and Dean, C.J. (1971) DNA-membrane association and the repair of double breaks in X-irradiated *Micrococcus radiodurans*. *Biochim. Biophys. Acta.*, **247**, 38-53.
75. Mortimer, R.K. (1958) Radiobiological and genetic studies on a polyploid series (haploid to hexaploid) of *Saccharomyces cerevisiae*. *Radiat. Res.*, **9**, 312-326.

76. Harsojo, Kitayama, S. and Matsuyama, A. (1981) Genome multiplicity and radiation resistance in *Micrococcus radiodurans*. *J. Biochem.*, **90**, 877-880.
77. Levin-Zaidman, S., Englander, J., Shimoni, E., Sharma, A.K., Minton, K.W. and Minsky, A. (2003) Ringlike structure of the *Deinococcus radiodurans* genome: a key to radioresistance? *Science*, **299**, 254-256.
78. Makarova, K.S., Omelchenko, M.V., Gaidamakova, E.K., Matrosova, V.Y., Vasilenko, A., Zhai, M., Lapidus, A., Copeland, A., Kim, E., Land, M. *et al.* (2007) *Deinococcus geothermalis*: the pool of extreme radiation resistance genes shrinks. *PLoS One*, **2**, e955.
79. Zimmerman, J.M. and Battista, J.R. (2005) A ring-like nucleoid is not necessary for radioresistance in the *Deinococcaceae*. *BMC Microbiol.*, **5**, 17.
80. Eltsov, M. and Dubochet, J. (2005) Fine structure of the *Deinococcus radiodurans* nucleoid revealed by cryoelectron microscopy of vitreous sections. *J. Bacteriol.*, **187**, 8047-8054.
81. Daly, M.J., Gaidamakova, E.K., Matrosova, V.Y., Vasilenko, A., Zhai, M., Leapman, R.D., Lai, B., Ravel, B., Li, S.M., Kemner, K.M. *et al.* (2007) Protein oxidation implicated as the primary determinant of bacterial radioresistance. *PLoS Biol.*, **5**, e92.
82. Domain, F., Houot, L., Chauvat, F. and Cassier-Chauvat, C. (2004) Function and regulation of the cyanobacterial genes *lexA, recA* and *ruvB*: LexA is critical to the survival of cells facing inorganic carbon starvation. *Mol. Microbiol.*, **53**, 65-80.
83. Hastings, J.W., Holzapfel, W.H. and Niemand, J.G. (1986) Radiation resistance of lactobacilli isolated from radurized meat relative to growth and environment. *Appl. Environ. Microbiol.*, **52**, 898-901.
84. Leibowitz, P.J., Schwartzberg, L.S. and Bruce, A.K. (1976) The in vivo association of manganese with the chromosome of *Micrococcus radiodurans*. *Photochem. Photobiol.*, **23**, 45-50.
85. Daly, M.J., Gaidamakova, E.K., Matrosova, V.Y., Vasilenko, A., Zhai, M., Venkateswaran, A., Hess, M., Omelchenko, M.V., Kostandarithes, H.M., Makarova, K.S. *et al.* (2004) Accumulation of Mn(II) in *Deinococcus radiodurans* facilitates gamma-radiation resistance. *Science*, **306**, 1025-1028.
86. Imlay, J.A. (2008) Cellular defenses against superoxide and hydrogen peroxide. *Annu. Rev. Biochem.*, **77**, 755-776.
87. Imlay, J.A. (2006) Iron-sulphur clusters and the problem with oxygen. *Mol. Microbiol.*, **59**, 1073-1082.
88. Mennecier, S., Coste, G., Servant, P., Bailone, A. and Sommer, S. (2004) Mismatch repair ensures fidelity of replication and recombination in the radioresistant organism *Deinococcus radiodurans*. *Mol. Genet. Genomics*, **272**, 460-469.
89. Cao, Z. and Julin, D.A. (2009) Characterization in vitro and in vivo of the DNA helicase encoded by *Deinococcus radiodurans* locus DR1572. *DNA Repair (Amst)*, **8**, 612-619.

90. Earl, A.M., Rankin, S.K., Kim, K.P., Lamendola, O.N. and Battista, J.R. (2002) Genetic evidence that the *uvsE* gene product of *Deinococcus radiodurans* R1 is a UV damage endonuclease. *J. Bacteriol.*, **184**, 1003-1009.
91. Davidson, R.C., Blankenship, J.R., Kraus, P.R., de Jesus Berrios, M., Hull, C.M., D'Souza, C., Wang, P. and Heitman, J. (2002) A PCR-based strategy to generate integrative targeting alleles with large regions of homology. *Microbiology*, **148**, 2607-2615.
92. Studier, F.W. (2005) Protein production by auto-induction in high density shaking cultures. *Protein. Expr. Purif.*, **41**, 207-234.
93. Wong, I. and Lohman, T.M. (1993) A double-filter method for nitrocellulose-filter binding: application to protein-nucleic acid interactions. *Proc. Natl. Acad. Sci. U S A*, **90**, 5428-5432.
94. Carrasco, B., Fernandez, S., Petit, M.A. and Alonso, J.C. (2001) Genetic recombination in *Bacillus subtilis* 168: effect of *ΔhelD* on DNA repair and homologous recombination. *J. Bacteriol.*, **183**, 5772-5777.
95. Lundin, C., North, M., Erixon, K., Walters, K., Jenssen, D., Goldman, A.S. and Helleday, T. (2005) Methyl methanesulfonate (MMS) produces heat-labile DNA damage but no detectable in vivo DNA double-strand breaks. *Nucleic. Acids. Res.*, **33**, 3799-3811.
96. Eggington, J.M., Haruta, N., Wood, E.A. and Cox, M.M. (2004) The single-stranded DNA-binding protein of *Deinococcus radiodurans*. *BMC Microbiol.*, **4**, 2.
97. Southworth, M.W. and Perler, F.B. (2002) Protein splicing of the *Deinococcus radiodurans* strain R1 Snf2 intein. *J. Bacteriol.*, **184**, 6387-6388.
98. Dronkert, M.L. and Kanaar, R. (2001) Repair of DNA interstrand cross-links. *Mutat. Res.*, **486**, 217-247.
99. Mendonca, V.M., Kaiser-Rogers, K. and Matson, S.W. (1993) Double helicase II (*uvrD*)-helicase IV (*helD*) deletion mutants are defective in the recombination pathways of *Escherichia coli*. *J. Bacteriol.*, **175**, 4641-4651.
100. Mendonca, V.M., Klepin, H.D. and Matson, S.W. (1995) DNA helicases in recombination and repair: construction of a *ΔuvrD ΔhelD ΔrecQ* mutant deficient in recombination and repair. *J. Bacteriol.*, **177**, 1326-1335.
101. Heinz, K. and Marx, A. (2007) Lesion bypass activity of DNA polymerase A from the extremely radioresistant organism *Deinococcus radiodurans*. *J. Biol. Chem.*, **282**, 10908-10914.
102. Biswas, E.E. and Biswas, S.B. (1999) Mechanism of DnaB helicase of *Escherichia coli*: structural domains involved in ATP hydrolysis, DNA binding, and oligomerization. *Biochemistry*, **38**, 10919-10928.
103. Biswas, S.B., Chen, P.H. and Biswas, E.E. (1994) Structure and function of *Escherichia coli* DnaB protein: role of the N-terminal domain in helicase activity. *Biochemistry*, **33**, 11307-11314.
104. Wood, E.R. and Matson, S.W. (1987) Purification and characterization of a new DNA-dependent ATPase with helicase activity from *Escherichia coli*. *J. Biol. Chem.*, **262**, 15269-15276.

105. Lovett, S.T. and Kolodner, R.D. (1989) Identification and purification of a single-stranded-DNA-specific exonuclease encoded by the *recJ* gene of *Escherichia coli*. *Proc. Natl. Acad. Sci. U S A*, **86**, 2627-2631.
106. Dianov, G., Sedgwick, B., Daly, G., Olsson, M., Lovett, S. and Lindahl, T. (1994) Release of 5'-terminal deoxyribose-phosphate residues from incised abasic sites in DNA by the *Escherichia coli* RecJ protein. *Nucleic. Acids. Res.*, **22**, 993-998.
107. Cooper, D.L., Lahue, R.S. and Modrich, P. (1993) Methyl-directed mismatch repair is bidirectional. *J. Biol. Chem.*, **268**, 11823-11829.
108. Courcelle, J. and Hanawalt, P.C. (1999) RecQ and RecJ process blocked replication forks prior to the resumption of replication in UV-irradiated *Escherichia coli*. *Mol. Gen. Genet.*, **262**, 543-551.
109. Burdett, V., Baitinger, C., Viswanathan, M., Lovett, S.T. and Modrich, P. (2001) In vivo requirement for RecJ, ExoVII, ExoI, and ExoX in methyl-directed mismatch repair. *Proc. Natl. Acad. Sci. U S A*, **98**, 6765-6770.
110. Pfaffl, M.W. (2001) A new mathematical model for relative quantification in real-time RT-PCR. *Nucleic. Acids. Res.*, **29**, e45.
111. Stoscheck, C.M. (1990) Quantitation of protein. *Methods. Enzymol.*, **182**, 50-68.
112. Mossessova, E. and Lima, C.D. (2000) Ulp1-SUMO crystal structure and genetic analysis reveal conserved interactions and a regulatory element essential for cell growth in yeast. *Mol. Cell.*, **5**, 865-876.
113. Yamagata, A., Masui, R., Kakuta, Y., Kuramitsu, S. and Fukuyama, K. (2001) Overexpression, purification and characterization of RecJ protein from *Thermus thermophilus* HB8 and its core domain. *Nucleic. Acids. Res.*, **29**, 4617-4624.
114. Voet, D., Voet, JG. (2004) *Biochemistry*. third ed. John Wiley and Sons, INC.
115. Arnau, J., Lauritzen, C., Petersen, G.E. and Pedersen, J. (2006) Current strategies for the use of affinity tags and tag removal for the purification of recombinant proteins. *Protein. Expr. Purif.*, **48**, 1-13.
116. Butt, T.R., Edavettal, S.C., Hall, J.P. and Mattern, M.R. (2005) SUMO fusion technology for difficult-to-express proteins. *Protein. Expr. Purif.*, **43**, 1-9.
117. Han, E.S., Cooper, D.L., Persky, N.S., Sutera, V.A., Jr., Whitaker, R.D., Montello, M.L. and Lovett, S.T. (2006) RecJ exonuclease: substrates, products and interaction with SSB. *Nucleic. Acids. Res.*, **34**, 1084-1091.
118. Eggington, J.M., Kozlov, A.G., Cox, M.M. and Lohman, T.M. (2006) Polar destabilization of DNA duplexes with single-stranded overhangs by the *Deinococcus radiodurans* SSB protein. *Biochemistry*, **45**, 14490-14502.
119. Omelchenko, M.V., Wolf, Y.I., Gaidamakova, E.K., Matrosova, V.Y., Vasilenko, A., Zhai, M., Daly, M.J., Koonin, E.V. and Makarova, K.S. (2005) Comparative genomics of *Thermus thermophilus* and *Deinococcus radiodurans*: divergent routes of adaptation to thermophily and radiation resistance. *BMC Evol. Biol.*, **5**, 57.
120. Markillie, L.M., Varnum, S.M., Hradecky, P. and Wong, K.K. (1999) Targeted mutagenesis by duplication insertion in the radioresistant bacterium *Deinococcus radiodurans*: radiation sensitivities of catalase (*katA*) and superoxide dismutase (*sodA*) mutants. *J. Bacteriol.*, **181**, 666-669.

121. Xu, Z.J., Tian, B., Xu, G.Z. and Hua, Y.J. (2006) Construction and functional analysis of the crtl gene disruptant in *Deinococcus radiodurans*. *Wei Sheng Wu Xue Bao*, **46**, 210-213.
122. Lipton, M.S., Pasa-Tolic, L., Anderson, G.A., Anderson, D.J., Auberry, D.L., Battista, J.R., Daly, M.J., Fredrickson, J., Hixson, K.K., Kostandarithes, H. *et al.* (2002) Global analysis of the *Deinococcus radiodurans* proteome by using accurate mass tags. *Proc. Natl. Acad. Sci. U S A*, **99**, 11049-11054.
123. Shereda, R.D., Bernstein, D.A. and Keck, J.L. (2007) A central role for SSB in *Escherichia coli* RecQ DNA helicase function. *J. Biol. Chem.*, **282**, 19247-19258.
124. Courcelle, J. and Hanawalt, P.C. (2001) Participation of recombination proteins in rescue of arrested replication forks in UV-irradiated *Escherichia coli* need not involve recombination. *Proc. Natl. Acad. Sci. U S A*, **98**, 8196-8202.
125. Lovett, S.T. and Clark, A.J. (1984) Genetic analysis of the *recJ* gene of *Escherichia coli* K-12. *J. Bacteriol.*, **157**, 190-196.
126. Sargentini, N.J. and Smith, K.C. (1986) Quantitation of the involvement of the *recA, recB, recC, recF, recJ, recN, lexA, radA, radB, uvrD,* and *umuC* genes in the repair of X-ray-induced DNA double-strand breaks in *Escherichia coli*. *Radiat. Res.*, **107**, 58-72.
127. Singleton, M.R., Dillingham, M.S., Gaudier, M., Kowalczykowski, S.C. and Wigley, D.B. (2004) Crystal structure of RecBCD enzyme reveals a machine for processing DNA breaks. *Nature*, **432**, 187-193.
128. Cline, G.W. and Hanna, S.B. (1987) The aminolysis of N-hydroxysuccinimide esters. A structure-reactivity study. *J. Am. Chem. Soc.*, **109**, 3087-3091.
129. Cuatrecasas, P. and Parikh, I. (1972) Adsorbents for affinity chromatography. Use of N-hydroxysuccinimide esters of agarose. *Biochemistry*, **11**, 2291-2299.
130. Burgess, R.R. and Jendrisak, J.J. (1975) A procedure for the rapid, large-scall purification of *Escherichia coli* DNA-dependent RNA polymerase involving Polymin P precipitation and DNA-cellulose chromatography. *Biochemistry*, **14**, 4634-4638.
131. Fu, H. (2004) *Protein-Protein Interactions: Method and Application*. Humana Press, Totowa, New Jersey.
132. Formosa, T., Barry, J., Alberts, B.M. and Greenblatt, J. (1991) Using protein affinity chromatography to probe structure of protein machines. *Methods. Enzymol.*, **208**, 24-45.
133. Wittmeyer, J. and Formosa, T. (1995) Identifying DNA replication complex components using protein affinity chromatography. *Methods. Enzymol.*, **262**, 415-430.
134. Phizicky, E.M. and Fields, S. (1995) Protein-protein interactions: methods for detection and analysis. *Microbiol. Rev.*, **59**, 94-123.
135. Mellon, I. (2005) Transcription-coupled repair: a complex affair. *Mutat. Res.*, **577**, 155-161.
136. Svejstrup, J.Q. (2007) Contending with transcriptional arrest during RNAPII transcript elongation. *Trends. Biochem. Sci.*, **32**, 165-171.

137. Wu, Y., Li, Q. and Chen, X.Z. (2007) Detecting protein-protein interactions by Far western blotting. *Nat. Protoc.*, **2**, 3278-3284.
138. Mimitou, E.P. and Symington, L.S. (2009) Nucleases and helicases take center stage in homologous recombination. *Trends. Biochem. Sci.*, **34**, 264-272.